PB81-150310

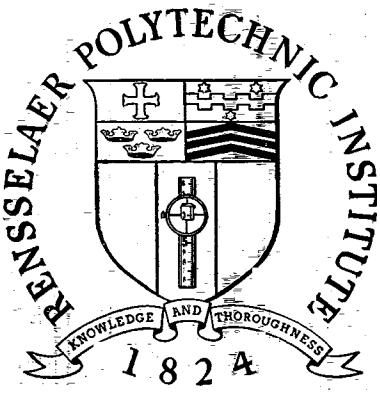

REPRODUCED BY
NATIONAL TECHNICAL
INFORMATION SERVICE
U.S. DEPARTMENT OF COMMERCE
SPRINGFIELD, VA 22161

Rensselaer Polytechnic Institute

Troy, New York 12181

EAS INFORMATION RESOURCES
NATIONAL SCIENCE FOUNDATION

A STUDY OF THE ENGINEERING CHARACTERISTICS OF THE 1971 SAN FERNANDO EARTHQUAKE RECORDS USING TIME DOMAIN TECHNIQUES

by

William E. Bond
Ricardo Dobry
Michael J. O'Rourke

Report No. CE-80-1

Sponsored by National Science Foundation

Directorate for Applied Science and

Research Application (ASRA)

Grant No. PFR-7902871

Any opinions, findings, conclusions or recommendations expressed in this publication are those of the author(s) and do not necessarily reflect the views of the National Science Foundation.

Department of Civil Engineering
Rensselaer Polytechnic Institute
Troy, New York 12181

June 1980

REPRODUCED BY
NATIONAL TECHNICAL
INFORMATION SERVICE
U.S. DEPARTMENT OF COMMERCE
SPRINGFIELD, VA 22161

CONTENTS

LIST OF TABLES

LIST OF FIGURES

ACKNOWLEDGEMENTS

This report is identical with the doctoral dissertation of William E. Bond. It is the first report of a research project sponsored by the Earthquake Engineering Program of NSF-ASRA under Grant No. PFR-7902871 in which Dr. William Hakala is the Program Manager. In the first phase of this work, William E. Bond was supported by an NSF fellowship. This overall support given by the National Science Foundation is gratefully acknowledged.

Doctor D. Harkrider of Caltech kindly performed the calculations summarized in Table 12.

ABSTRACT

The accelerograms recorded at ground elevation during the 1971 San Fernando Earthquake are examined through the use of time domain techniques. These techniques are the buildup of the Arias Intensity with time, the variation with time of the root mean square acceleration, the variation with time of the principal planes of ground motion, and the change in the response envelope of a single degree of freedom system with time. These techniques exclude consideration of the physics of the earthquake source or seismic wave propagation.

Through the use of these techniques, a part of the accelerograms that includes the arrival of direct S-waves from the source is computationally identified. This strong part is characterized by two parameters, the duration and the level of shaking. Horizontal plane root mean square acceleration is used to provide a measure of the level of shaking which is independent of the orientation of the recording devices. The attenuation of the root mean square acceleration with distance is generally consistent with an equation recently developed by Hanks which relates root mean square acceleration with the earthquake's source parameters. However, no significant decrease in the scatter of the

attenuation relation was found when root mean square acceleration was used instead of the peak acceleration. Conversely, it was found that root mean square and peak accelerations were closely correlated.

A traveling Rayleigh wave is identified at two deep soil sites located in the San Fernando Valley. The speed, direction, and frequency of the Rayleigh wave are estimated and compared with theoretical calculations. This information and the proximity of the surface faulting suggest this wave may have been caused by the shallowness of the faulting process.

PART 1

INTRODUCTION

The reduction of the hazards caused by earthquake shaking is related to the ability to forecast the expected intensity of the ground shaking. Through the use of this information, the engineer may ensure that his structures are adequately designed against earthquake forces. Thus it becomes necessary for the engineer to examine past earthquake events to gain insight into future events. From an engineering viewpoint, the measure of intensity associated with recorded ground motions at a site should be an easily determined number or set of numbers which indicates the destructiveness or severity of those motions. In the past, the intensity (Housner, 1975) has been linked with the level of horizontal shaking and has been characterized by a single parameter, such as peak ground acceleration, peak ground velocity, Spectral Intensity, Arias Intensity, or Modified Mercalli Intensity (MMI).

It has been shown (Husid, 1967; Housner, 1970) that the duration of shaking, in addition to its level, is an important factor in determining the amount of damage or the collapse of a yielding structure subjected to the combined action of earthquake shaking and gravity. This has

also been verified by the low failure rate of structures for earthquakes of short duration even though both maximum acceleration and response spectrum ordinates were very large. Duration is also important in determining the potential of liquefaction for saturated sand deposits. Therefore, Housner (1975) has proposed defining the intensity of earthquake motion by a combination of two parameters, one describing the level and the other the duration of the motion. A third parameter determining the failure potential of many civil engineering structures, such as multistory buildings and dams, is the frequency content of the motion. A definition of the motion by its level, duration, and frequency content parameters should be sufficient for many earthquake engineering purposes.

Dobry, Idriss and Ng (1978) have indicated that accelerograms at both rock and soil sites in the epicentral region seem to exhibit three distinguishable parts for earthquakes up to magnitude 7. In rock the three parts are:

1) Initial weak part
2) Strong high frequency part
3) Final weak part

In soil the three parts are:

1) Initial weak part
2) Strong high frequency part

3) Final part, which can be either weak or a moderately strong low frequency part

The first part at both rock and soil sites corresponds to P-wave arrivals while the second corresponds mainly to the arrival of S-waves along a direct path from the source to the site. The third part which causes different responses at rock and soil sites seems to correspond to the arrival of both indirect body waves and surface waves.

The rest of this work attempts to characterize the second and third parts of the accelerograms for basement, first floor, and free field sites that were subjected to shaking from the February 9, 1971 San Fernando, California Earthquake. This characterization excludes consideration of the physics of the earthquake source or seismic wave propagation.

The second high frequency part, which usually contains the highest accelerations, is studied here using time domain techniques developed by the author. The level of shaking defined using root mean square acceleration and the duration of this second part are determined to characterize the motion. Finally, this characterization is compared against the conventional measure of peak acceleration. It is believed that root mean square acceleration will provide a more stable measure of the level of shaking than peak

acceleration. Specific characteristics of the high frequency part which are related to the San Fernando faulting mechanism are also explored.

The third low frequency part is examined for the five soil sites in the San Fernando Valley for which records are available. Using the techniques developed in this thesis it was possible to distinguish phases in which specific surface waves are prevalent. Estimates of the speed, direction, and frequency of these surface waves are made.

The time domain techniques developed here should provide engineers with new methods of studying earthquake strong motion accelerograms. These methods require a minimum number of assumptions and therefore are convenient to use in practical applications. The application of these techniques to the accelerograms recorded during the San Fernando Earthquake serves as an illustration of the methods and also provides insight into the characteristics of those records.

PART 2

TIME DOMAIN TECHNIQUES

This part develops the time domain techniques that will be utilized in this investigation. Information about the background of these methods is also discussed. Examples are given demonstrating the unique contribution each technique makes to the characterization of earthquake strong motion accelerograms.

Four basic time domain techniques were used. They are the following:

1) Husid plot of energy buildup
2) Root mean square acceleration
3) Principal planes of ground motion
4) Response envelope

The following will describe each technique in detail. Typical plots of the four methods are shown in Figures 1, 2, 5, and 7.

2.1 Husid Plot of Energy Buildup

Arias (1969) assumed that the amount of damage experienced by a structure was proportional to the energy dissipated by the structure per unit weight during the overall duration of the motion induced by an earthquake. This concept was generalized by Arias by considering a

collection of structures whose undamped circular frequencies, w, are uniformly distributed in the interval $(0, \infty)$ and which all have the same damping ratio, n. E is the energy dissipated per unit weight by a structure of frequency w as a result of the motion caused by the earthquake. Thus Arias defined the intensity of the earthquake as:

$$(1) \qquad I_A = \int_0^{\infty} E\,dw$$

Arias assumed that all the structures could be modeled as simple linear oscillators with viscous damping. He also showed that the results are still generally applicable if the oscillators are nonlinear or elasto-plastic (Arias, 1969). After considerable manipulation it may be shown that:

$$(2) \qquad I_{A(n)} = \frac{\arccos n}{g\sqrt{1-n^2}} \int_0^{t_f} a^2(t)\,dt$$

where I_A = Arias Intensity

n = damping ratio of a collection of simple linear oscillators

g = acceleration of gravity

t_f = total duration of the earthquake

$a(t)$ = ground acceleration time history

Note that Eqn. 2 is a product of two factors, with the first factor being dependent on the structures considered, while

the second factor is dependent only on the ground motion. It can be shown that for the range of damping values associated with real structures, the factor outside the integral is practically a constant. Therefore a value of n=0 was chosen to standardize the process. The Arias Intensity then becomes:

$$I_A = \frac{\pi}{2g}\int_0^{t_f} a^2(t)dt \tag{3}$$

This provides a single number as a measure of earthquake intensity for the event described by the acceleration time history.

It should be noted that Arias Intensity can be related to the Fourier amplitude spectrum of the acceleration time history by the use of Parseval's theorem:

$$f(w) = \left| \int_0^{t_f} a\,(t)e^{-iwt}dt \right| \tag{4}$$

$$\int_0^{t_f} a^2(t)dt = \frac{1}{\pi}\int_0^{\infty} f^2(w)dw \tag{5}$$

where $f(w)$ = Fourier amplitude spectrum

w = frequency of vibration

t_f = total duration of the earthquake record

$a(t)$ = acceleration time history

Recorded ground accelerograms normally consist of three orthogonal components, $a_X(t)$, $a_Y(t)$, and $a_Z(t)$, where

$a_X(t)$ and $a_Y(t)$ are the horizontal components and $a_Z(t)$ is the vertical component. The time t is the same for all three components and is measured from the moment the recording device is triggered. The triggering time is generally not known on an absolute scale and thus usually varies from station to station for the same earthquake event. In calculating the Arias Intensity for horizontal ground motions a(t), may be taken to be either one of the individual horizontal components, $a_X(t)$ and $a_Y(t)$, or the horizontal plane acceleration, $a_H(t)$.

$$a_H^2(t) = a_X^2(t) + a_Y^2(t) \tag{6}$$

The advantage of the horizontal plane acceleration is that it provides a measure of ground acceleration which is independent of the orientation of the recording device.

Husid (1967) chose to plot the buildup of Arias Intensity as a function of time.

$$h(t) = \frac{I_A(t)}{I_A(t_f)} = \frac{\int_0^t a^2(\tau)d\tau}{\int_0^{t_f} a^2(\tau)d\tau} \tag{7}$$

The function varies from h=0 at t=0 to h=1 (100%) at $t=t_f$. The Husid plot is an indicator of how rapidly energy is being dissipated by structures during the various parts or

sections of the accelerogram. It also has been noted (Husid, 1967; Housner, 1975) that the slope of the Husid plot versus time is a measure of the level of shaking or the rate at which the accelerogram energy is built up. This slope or the power, P, of the motion is defined during the interval Δ:

$$P = \frac{1}{\Delta}\int_{t_1}^{t_1+\Delta} a^2(t)dt \tag{8}$$

By examining the slope of h(t), an indication of the severity of ground shaking may be obtained. A constant slope indicates a constant energy input while an increase or decrease in the slope indicates respectively an increase or decrease in the energy input. Figure 1 shows the NS component of ground accelerogram as well as the Husid plot calculated for the motion recorded during the 1971 San Fernando Earthquake at 3838 Lankershim Boulevard. The central portion in Figure 1 having a steep slope corresponds to a high level of shaking. A Husid plot may be calculated for either an individual acceleration component or for the horizontal plane acceleration.

2.2 Root Mean Square Acceleration

By taking the square root of the slope of the Husid plot the root mean square acceleration is obtained. It is defined as:

$$(9) \qquad \bar{a} = \sqrt{P} = \sqrt{\frac{1}{\Delta}\int_{t_1}^{t_1+\Delta} a^2(t)dt}$$

where $\bar{a}$ = root mean square acceleration in the interval t_1 to $t_1 + \Delta$

Δ = size of the time interval

t_1 = beginning of the time interval

It is this measure of the level of shaking which will be used in this thesis.

Hanks (1979) lists several seismological and engineering reasons why using root mean square (rms) acceleration should be superior to the use of peak acceleration for characterization purposes. First, as the result of integration, the root mean square could be expected to be a more stable measure of high frequency ground motion than an individual amplitude measurement. Second, for many earthquakes the time interval of large accelerations is much shorter than the duration of strong shaking. Thus these intervals are not indicative of the gross source properties (see also Seekins and Hanks, 1978). Third, at close distances to the source the peak acceleration is only weakly dependent on the the magnitude of the earthquake (see also Hanks and Johnson, 1976). Finally, the amplitude of the peak acceleration values could

be reduced in most accelerograms with little change in the response of many structures (see also Schnabel and Seed, 1973; Donovan, Bolt and Whitman, 1976).

Hanks (1979) has also shown that the rms acceleration can be predicted theoretically from a simple model of the earthquake source. He points out that rms acceleration does not quantify the intensity of the ground motion by itself. It must be accompanied by a definition of the duration.

The following equation results from the consideration of a simple model suggested originally by Brune (1970) and later developed by Hanks which calculates the rms acceleration for an individual horizontal component.

$$\bar{a} = 0.85 \frac{\sqrt{2}\,(2\pi)^2}{106} \frac{\Delta s}{\rho R^{1.5}} \sqrt{\frac{QB}{\pi f_o}} \tag{10}$$

where Δs = earthquake stress drop

$f_o = 1/T_d$ = spectral corner frequency

T_d = faulting duration of the earthquake

R = distance to hypocenter

ρ = density of the medium

B = shear wave velocity of the medium

Q = quality factor of the medium

Thus using the rms acceleration, an engineering measure of

the level of shaking can be related to a simple earthquake source model.

It is especially useful to investigate the variation of the rms acceleration as a function of time. This can be done by employing a moving time window as follows:

$$\bar{a}(t) = \sqrt{\frac{1}{\delta}\int_{t-0.5\delta}^{t+0.5\delta} a^2(\tau)d\tau} \tag{11}$$

where δ = width of the moving time window

During those parts of the accelerogram where there is severe ground shaking the value of $\bar{a}(t)$ will increase accordingly. Figure 2 presents the moving time window rms acceleration calculated for the NS component of ground acceleration recorded at 3838 Lankershim Boulevard. It should be noted that $\bar{a}(t)$ values such as those in Figure 2 are highly dependent upon the size of the moving time window. The time window has the effect of "smoothing" energy arrivals over a period of time with the smoothing becoming more pronounced as δ increases. Thus the usefulness of the numeric values obtained for moving time window root mean square acceleration is questionable. The examination of the shape of the $\bar{a}(t)$ graph, however, is helpful in determining, in a simple way, intervals of strong and weak levels of shaking.

Trifunac and Brune (1970) examined the accelerograms recorded at El Centro for the May 18, 1940 Imperial Valley, California Earthquake and determined that the earthquake consisted of multiple events at the source. They could distinguish four clear events occurring during the first 25 seconds of the record. Figure 3 is the moving time window horizontal plane rms acceleration plot of that record. The wave arrivals determined by Trifunac and Brune are also indicated on the plot. In all cases these arrivals correspond directly with an increase in the rms acceleration plot. This confirms the usefulness of the moving time window rms acceleration plot in identifying significant wave arrivals at a recording station.

2.3 Principal Planes of Ground Motion

The ability to distinguish between the types of seismic waves which arrive at a site simplifies the characterization of the ground motion at that site. With this in mind, it is possible to define a moving time window intensity tensor, $[G(t)]$, for a set of ground accelerations, $a_X(t)$, $a_Y(t)$, and $a_Z(t)$, known along three mutually perpendicular axes:

$$(12) \qquad [G(t)] = \begin{vmatrix} g_{XX} & g_{XY} & g_{XZ} \\ g_{YX} & g_{YY} & g_{YZ} \\ g_{ZX} & g_{ZY} & g_{ZZ} \end{vmatrix}$$

$$\text{where} \quad g_{ij} = g_{ij}(t) = \int_{t-0.5\delta}^{t+0.5\delta} a_i(\tau) a_j(\tau) d\tau$$

δ = width of moving time window

The diagonal terms of the tensor have the form:

$$g_{XX}(t) = \int_{t-0.5\delta}^{t+0.5\delta} a_X^2(\tau) d\tau$$

While the off-diagonal terms have the form:

$$g_{XY}(t) = \int_{t-0.5\delta}^{t+0.5\delta} a_X(\tau) a_Y(\tau) d\tau$$

This definition of [G(t)] is similar to that proposed by Arias (1969) and Penzien (Penzien and Watabe, 1975; Kubo and Penzien, 1976; Kubo and Penzien, 1977). Penzien used his procedure to determine the types of seismic waves arriving at a site and their approximate direction of travel at the site.

The eigenvalues and eigenvectors of the tensor [G(t)] may be found as a function of time. The eigenvectors correspond to the principal directions of the moving time window intensity while the eigenvalues correspond to the

principal values of the moving time window intensity. This is analogous to the determination of the principal stress planes and the principal stresses for a continuum mechanics or elasticity problem. The principal directions of intensity correspond to the direction of principal earth ground motions. Thus the maximum principal plane should be indicative of the direction of the predominant ground motion at time t. This information will be helpful in distinguishing phases in which different types of seismic waves and directions of travel at the recording site are prevalent.

In order to simplify the interpretation, the eigenvectors (x,y,z) are converted using the procedure shown in Figure 4. The value of theta is with respect to the EAST while phi is relative to UP. By varying t in the tensor and calculating the corresponding values of phi and theta for each principal plane, the time variation of the direction of the ground motions may be obtained. The values corresponding to the major principal plane are usually the most helpful.

Seismic body waves traveling from the fault to the surface usually become more vertical in their travel paths due to refraction occurring as they go from stiff to softer rock and soil materials. Thus it could be expected that a P-wave incident at a site should produce motions

predominantly in the vertical direction corresponding to a phi of 0 degrees. S-waves on the other hand should exhibit motions predominantly in the horizontal plane corresponding to a phi of 90 degrees. Thus it would be reasonable to expect a shift in the phi angle of the maximum principal plane from 0 degrees to 90 degrees at the initial arrival of S-waves at a site (this presupposes that the recording device was triggered by one of the initial P-wave arrivals). This hypothesis has been confirmed by the work performed by Kubo and Penzien (1976). It must be noted that Kubo and Penzien used a very wide time window with a width of 5 seconds. This investigation utilizes a time window width of 0.5 seconds. This allows a much sharper determination of the first S-wave arrivals. Figure 5 is a plot of the phi angle for the maximum principal plane for 3838 Lankershim Boulevard. A time window width of 0.5 seconds was used. This method provides an accurate and easy to use procedure for determining the time of initial S-wave arrival. It also has the advantage of not requiring additional assumptions or special training.

An excellent check of this method of processing accelerograms was obtained by an examination of the acceleration data recorded at San Francisco Golden Gate Park during the March 22, 1957 San Francisco Earthquake. Figure 6

is a plot of the phi angle for the maximum principal plane for this site. An aftershock occurred approximately 28 seconds after the initial shock while the recorder was still running. The phi plot dips toward 0 degrees at the first P-wave arrival corresponding to the aftershock. Phi returns to approximately 90 degrees when the S-waves from the aftershock arrive.

The theta plot for the maximum principal plane does not prove as easy to interpret. Figure 5 shows the theta plot of the maximum principal plane for 3838 Lankershim Boulevard using a time window width of 0.5 seconds. The angle changes rapidly making conclusions hard to draw. The fact that phi can be interpreted successfully demonstrates that S-waves arrive almost vertically at a site. The variation of theta, however, suggests that this technique can not be used to determine the polarization, if any, in a specific horizontal direction.

A precaution must be observed when employing this procedure. Phi and theta are calculated through the use of a time window. Thus estimates of the exact time of a wave arrival are accurate to within about one half of the time window size or $\pm$0.25 seconds for a time window of 0.5 seconds.

2.4 Response Envelope

It is also useful to examine how the frequency content of the individual acceleration components change with time. A moving time window procedure was used to calculate the Fourier amplitude spectrum as a function of time by Kubo and Penzien (1976; 1977). They found that the value of the dominant frequency generally decreased with time. In some cases the dominant frequency changed its value suddenly at a fixed time. It was concluded that this may indicate the arrival of a different type of seismic wave. This method, however, contains some serious drawbacks because of the use of a time window. The time window must be large, several seconds in length, in order to properly sample the low frequency content of the record. Conversely, it would be desireable to use a small time window so that the variation of the high frequency components can be observed. Thus the moving time window approach has obvious limitations.

This method can, however, be successfully applied to a specific segment of acceleration data. The equivalent frequency of a stationary random process is usually defined as (Clough and Penzien, 1975):

$$(13) \qquad \nu = \frac{1}{2\pi}\left[\frac{\int_{-\infty}^{\infty} w^2 S(w)dw}{\int_{-\infty}^{\infty} S(w)dw}\right]^{1/2}$$

where w = angular frequency

$S(w)$ = power spectral density of the process

ν = equivalent frequency

For a deterministic signal, such as an accelerogram, $S(w)$ can be defined in terms of the Fourier amplitude spectrum of the accelerogram (Bendat, 1958):

$$(14) \qquad S(w) = \frac{1}{\Delta\pi} f^2(w)$$

where Δ = time interval considered of the acceleration time history

$f(w)$ = Fourier amplitude spectrum

The above equation assumes that during a limited duration, the accelerogram is a random process with a constant average frequency content. The Fourier amplitude spectrum can easily be calculated for a set of discrete data by employing the Fast Fourier Transform method. Combining both equations results in the following:

$$(15) \qquad \nu = \frac{1}{2\pi}\left[\frac{\int_0^\infty w^2 f^2(w)dw}{\int_0^\infty f^2(w)dw}\right]^{1/2}$$

The equivalent frequency is used for probabilistic studies which require an equivalent number of cycles.

Following a similar procedure, Liu (1970) divided an accelerogram into contiguous segments, calculating the power spectral density for each segment. This method represents approximately the evolution of the frequency content with time.

Kameda (1975) made use of a technique developed by Priestley to calculate approximately an evolutionary power spectrum. This is a multifilter technique which employs a single degree of freedom linear oscillator to filter the input accelerogram. A modification of Kameda's work was used in this thesis. The equation of motion of a single degree of freedom linear oscillator subjected to a base acceleration is:

$$(16) \qquad \ddot{d}(t) + 2nw_o\dot{d}(t) + w_o^2 d(t) = -a(t)$$

where $d(t)$ = relative displacemnt of the oscillator

n = damping ratio of the oscillator

w_o = natural frequency of the oscillator

a(t) = base acceleration time history

The energy of the oscillator is proportional to the response envelope, e(t):

$$e(t) = [d(t)]^2 + \left[\frac{\dot{d}(t)}{w_o}\right]^2 \tag{17}$$

The first term represents the potential energy stored in the spring while the second term represents the kinetic energy resulting from motion of the mass of the system. When the value of the damping ratio is small the oscillator acts as a narrow band filter responding primarily to frequencies close to its own natural frequency. The response envelope indicates how the energy of the acceleration time history varies as a function of time for a specific individual frequency. By varying the natural frequency of the filter it is possible to determine what frequencies are prevalent during various parts of the ground motion. A damping ratio of 0.05 was used in this study following Kameda's suggestion that the damping should be in the range 0.05 to 0.2. Figure 7 shows the response envelopes resulting from the use of 5 and 10 Hz filters on the NS component recorded at 3838 Lankershim Boulevard. Kameda modified the response envelope by the natural frequency and damping ratio of the filter to

obtain the evolutionary power spectral density of the accelerogram.

This method eliminates the problems associated with the use of a time window. However, the user must select a value for the frequency of the filter that corresponds to the frequency of the seismic waves of interest. To determine the parts of an accelerogram in which the energy at the filter frequency is prevalent, a comparison of the relative magnitudes found in the response envelope plot should be made.

2.5 Computer Programs

Following the definition of the above techniques, a computer program was written to allow their application to corrected accelerograms which were obtained from Caltech, and which are described in Volume II of the series, Strong Motion Earthquake Accelerograms (Hudson et. al., 1971). This program was labeled SMAP (Strong Motion Analysis Program) and is described in Appendix 1.

It is possible to substitute velocity for acceleration in Husid, rms, and principal plane calculations. These substitutions were made and another program was written to perform these procedures for velocity time histories.

Both computer programs were used to process the

records obtained during the 1971 San Fernando Earthquake. The results are presented in Part 3. Some applications of an earlier version of the accelerogram processing program were reported by Dobry, Singh and Bond (1978).

PART 3

CHARACTERIZATION OF THE SAN FERNANDO EARTHQUAKE

Several procedures have been suggested by other researchers to characterize and represent ground motions in both frequency and time domains. Shoja-Taheri and Bolt (1977) proposed the use of a spectrally maximized record. This record is obtained by combining the Fourier spectra of both horizontal components in order to maximize the resultant spectrum. The record resulting from this combination is independent of azimuthal orientation. The spectrally maximized record may be used for engineering analysis. Seed and Idriss (1971) evaluated the liquefaction potential of saturated sand deposits through the use of a peak acceleration and an equivalent number of cycles. This method of characterization has been used primarily to study the response of soils. Perez (1973) has defined a graph called the time duration spectrum. A response spectrum is a plot of the maximum response of a single degree of freedom system subjected to a particular acceleration time history, for a specific damping factor and for a range of frequencies. However, the use of this maximum value does not indicate the duration of time that a specified level is exceeded. For that purpose, Perez calculated the velocity

response of a single degree of freedom system versus time for a given damping ratio and for a range of system frequencies. These results produce the velocity response envelope spectrum. By plotting the cumulative total time that the velocity response envelope spectrum equals or exceeds a given level, the time duration spectrum is obtained. Thus, a level of response and an associated duration become available for design purposes.

This study will characterize ground motions using a procedure suggested by Housner (1975). The intensity will be defined by a combination of two parameters, one describing the level of shaking and the other the duration of the shaking. The level of shaking will be measured by the horizontal plane rms acceleration which is defined as follows:

$$\bar{a}_H = \sqrt{\frac{1}{\Delta}\int_{t_1}^{t_1+\Delta} \left[a_x^2(t) + a_y^2(t)\right] dt} \tag{18}$$

where t_1 = time corresponding to the beginning of strong high frequency shaking

Δ = duration of strong shaking (this is in principle identical with the duration of the second part of the accelerogram record defined in

Part 1)

$a_X(t)$, $a_Y(t)$ = orthogonal acceleration time histories recorded in the horizontal plane

As discussed in Part 2, rms acceleration is used as a measure of the level of shaking for several reasons. One of these reasons is the expectation that a reduction of scatter will be realized over the more conventional measure of peak acceleration. The horizontal plane definition used provides results which are independent of the orientation of the recording device.

3.1 Definition of the Duration of Strong Shaking

Methods used in the past for the determination of the duration of strong shaking will be examined first. The first definition, bracketed duration (Bolt, 1973; Cloud and Perez, 1969; Cloud, 1973), is the time interval during which the acceleration amplitude equals or exceeds a specified level. This level is usually specified as 0.05 g or 0.10 g. This method has been found useful due to its approximate correspondence with the strong part of ground shaking and is generally applied to the individual acceleration components. It should be noted that for a given earthquake event, the duration by this definition decreases with an increase in distance from the source, with the duration becoming zero

when the peak acceleration at a site is less than the specified level (Chang and Krinitzsky, 1977).

The second method for determining duration examines the Husid plot of energy buildup versus time (Trifunac and Brady, 1975). The duration using this second method is the time interval required to accumulate a prescribed fraction of the total Arias Intensity. Thus the time interval between two arbitrary levels, for instance, 5% and 95% of the total Arias Intensity would be defined as the duration. This methods eliminates, at least partially, the beginning and end of the accelerogram which represent a low energy input.

Another method (Vanmarcke and Lai, 1977) assumes that an acceleration time history is a stationary Gaussian process with the expected peak acceleration occurring once during the duration of motion. Under this assumption the peak acceleration is related to the rms acceleration by the following equation:

$$\frac{a_p}{b_o} = \sqrt{2\ln(2s_o/T_o)} \tag{19}$$

The rms acceleration, b_o, may be related to the Arias Intensity, I_A (see Eqn. 3), by the following equation:

$$\frac{2g}{\pi} I_A = I_o = s_o b_o^2 \tag{20}$$

Combining these equations yields:

$$(21) \qquad s_o = [2\ln(2s_o/T_o)](I_o/a_p^2)$$

where $I_o = (2g/\pi)I_A$

s_o = strong motion duration

b_o = rms acceleration

a_p = peak acceleration

T_o = predominant period of the motion

Knowing I_A, a_p, and T_o it is possible to calculate b_o and s_o. This method essentially replaces the accelerogram by a sample of a Gaussian stationary process whose total Arias Intensity and expected peak value match those of the record.

McCann and Shah (1979) have determined the duration of strong shaking through the use of the cumulative rms acceleration which is defined as:

$$(22) \qquad \mathrm{crms}(t) = \sqrt{\frac{1}{t}\int_0^t a^2(\tau)\,d\tau}$$

where crms(t) = cumulative rms acceleration from the beginning of the record to time t

a(t) = acceleration time history

This is equivalent to obtaining the square root of the slope

of a line drawn from the origin to the point on the Husid plot corresponding to time t. The time after which the cumulative rms acceleration is always decreasing is assumed by McCann and Shah to correspond to the end of strong shaking since the accumulated accelerogram energy per unit time has reached its highest level and is now decreasing. By reversing the acceleration time history and again determining the time after which the cumulative rms acceleration is always decreasing, the time at the beginning of the record where significant energy begins to arrive may be determined. The time interval between these points is defined as the interval of strong shaking. In this indirect way, the method attempts to determine the portion of the record where the average rate of energy arriving is increasing or at a constant level.

The above procedures are related only in an indirect manner to the underlying seismological cause of the strong shaking part, the arrival of direct S-waves. It is desirable to define an engineering approximation which corresponds more closely to the actual seismological phases observed. Also, serious problems may arise when the definitions proposed by Trifunac-Brady, Vanmarcke-Lai, and McCann-Shah are used for soil records, as these definitions will tend to lump together the strong, high frequency and

the moderate, low frequency parts of the accelerogram without considering their different freguency content.

Hanks (1979) has suggested that the fault rupture duration should indicate the duration of shaking experienced at sites. This definition makes use of a seismological parameter. Unfortunately, no account is taken of how the energy is modified during its travel to the considered site.

As discussed in Part 1, Dobry, Idriss and Ng (1978) have indicated that three distinct parts may be seen in the accelerogram recorded at a rock site. These three parts can be more clearly defined by examining the slope of the Husid plot. These parts are related to three different sets of wave arrivals at the site and to different slopes in the Husid plot. They are as follows (see Figure 8):

1) Initial weak part, corresponding to P-wave arrivals, and to the initial flat slope of the Husid plot.

2) Intermediate strong part, corresponding mainly to the arrival of S-waves following a direct path between the earthquake source and the recording station. This strong part corresponds to the steep slope of the Husid plot.

3) Final weak part, corresponding to the arrival of indirect body waves and surface waves.

The significant duration of the record is defined for the purposes of this thesis as the duration of the intermediate

strong part of the record which corresponds to the steep slope of the Husid plot. This duration will hopefully also correspond to the time interval which contains the arrival of S-waves following a direct path between the earthquake source and the recording station. This time interval may be difficult to identify in the accelerograms recorded at soil sites. The third part of the record obtained at soil sites is moderately strong, making it difficult to distinguish from the second part.

Two times, t_1 and t_2, will be defined as corresponding respectively to the first and last times of direct S-wave arrival. The Husid plot, moving time window rms acceleration, and the principal planes of ground motion techniques described in Part 2 are directly applicable to the determination of t_1. As a check, t_1 calculated by these methods for the San Fernando Earthquake records will be compared to t_{1B}, the time of first S-wave arrival estimated by Berrill (1975). Berrill calculated this time by the use of a technique described by Hanks (1975) which requires the computation of a set of rotated horizontal accelerograms parallel and perpendicular to the source-station direction. For the 1971 San Fernando Earthquake, Berrill's value, t_{1B}, was 1.8 ± 0.2 seconds at the 3838 Lankershim Boulevard station. Figures 8 and 9 are plots of the NS accelerogram,

horizontal plane Husid plot, horizontal plane rms acceleration, and maximum principal plane phi for 3838 Lankershim Boulevard. Note that the beginning of the steep slope in the Husid plot corresponds approximately to the value t_{1B} calculated by Berrill. An examination of the moving time window root mean square acceleration plot at 1.8 seconds also indicates that the energy input is increasing. However, the sudden jump in acceleration corresponding to the initial S-wave arrival evident in the accelerogram is not found in the moving time window rms acceleration plot. This is because the time window size smooths the transition from low to high levels of acceleration when it calculates an average value for the width of the time window. The maximum principal plane phi plot is also in transition at 1.8 seconds from a value of approximately 10 to 80 degrees. This indicates a change from predominantly vertical motion corresponding to P-waves to predominantly horizontal motion corresponding to S-waves. This transition is also gradual due to the smoothing effect of the width of the time window. The use of the Husid plot in conjunction with the moving time window rms acceleration and maximum plane phi plots provide a good estimate of t_1. The value t_1 = 1.6 seconds obtained from these techniques for the Lankershim record is indicated in Figures 8 and 9.

The determination of t_2, the time corresponding to the arrival of the last direct waves proves to be more difficult. The Husid plot is normally "rounded" in shape during the transition from direct to indirect wave arrivals. This is demonstrated by the Husid plot found in Figure 8 for the time interval from about 7.0 to 8.0 seconds. The maximum principal plane phi plot shown in Figure 9 makes no dramatic changes in value comparable to the P to S-wave transition at t_1. Hence the Husid and maximum principal plane phi plots offer little insight into the determination of t_2. However, the moving time window rms acceleration plot values found in Figure 9 drop in the time interval from 7.0 to 8.0 seconds. An examination of the accelerogram in Figure 8 indicates that this time interval corresponds approximately with the termination of large amplitude high frequency acceleration pulses at the site. Thus, for the San Fernando records, t_2 will be defined as the time at which the moving time window rms acceleration values are in transition from the high values experienced following the initial S-wave arrivals to a final lower level. The value t_2 = 7.5 seconds obtained from the rms acceleration for the Lankershim station is also indicated in Figures 8 and 9. Figures 10 and 11 show the t_1 and t_2 values determined for four San Fernando sites on plots of moving time window rms acceleration. Thus strong

shaking is defined to occur in the time interval from t_1 to t_2 and the duration of the strong shaking equals $\Delta = t_2 - t_1$.

3.2 Moving Time Window RMS Acceleration Plot

As previously mentioned, this study examined the accelerograms which were recorded at free field, basement, and ground floor sites that recorded shaking from the February 9, 1971 San Fernando Earthquake. Altogether, 97 sets of accelerograms, each consisting of three individual components (2 horizontal, 1 vertical) were considered. The list of stations studied is presented in Table 1. A map of the area of strong shaking is contained in Figure 12. The map explicitly locates each recording station for which a plot is presented in this thesis.

Several reports have provided information about the source characteristics of the 1971 San Fernando Earthquake (Bolt, 1972; Mikumo, 1973; Trifunac, 1974; Hanks, 1974; Boore and Zoback, 1974; Niazy, 1975; Bouchon and Aki, 1977; Bouchon, 1978; Heaton and Helmberger, 1978). The thrust fault produced an earthquake with a local magnitude, $M_L = 6.3$ (Kanamori and Jennings, 1978). Figure 12 shows the location of the surface trace of the fault. Figure 13 shows the approximate geometry of the fault with depth. The causative fault which dips to the northeast ruptured along a

total length of 15 to 23 km. The rupture started at the hypocenter, located to the north of the ground surface trace and at a depth of 10 to 15 km, and propagated up and south until it reached the ground surface. The rupture velocity at the fault was estimated to be between 2 and 3 km/sec. Values estimated for the total rupture duration are from 9 to 10 seconds (Bouchon, 1978; Heaton and Helmberger, 1978).

Horizontal plane Husid, horizontal plane moving time window rms acceleration, and maximum principal plane phi plots were produced for each station. A moving time window width of 0.5 seconds was used when obtaining the moving time window rms acceleration and maximum principal plane phi plots.

An examination of the moving time window rms acceleration plots produced for sites within several kilometers of each other produced interesting results. A distinct shape of the moving time window rms acceleration values is evident. This fact is illustrated in Figures 14 through 17 which show plots for four pairs of adjacent sites, whose locations are indicated in Figure 12. These figures indicate that stations located in a small area experienced the same sequence of energy arrivals regardless of local site conditions.

Figure 14 shows the moving time window rms

acceleration plots at Hollywood Storage Basement and Hollywood Storage P.E. Lot. These stations are located within several hundred feet of each other. The shapes of the plots are similar, indicating the same sequence of arrivals, but with different absolute amplitudes, probably due to the influence of local conditions. The Hollywood Storage Basement site has lower absolute rms acceleration values than the Hollywood Storage P.E. Lot site which is located in the free field.

The azimuth of the sites with respect to the epicenter (north or south) also affects the resulting moving time window root mean square acceleration shape. Figures 14, 15, and 16 contain plots from sites located to the south of the epicenter while Figure 17 shows the plots from two northern sites. The northern sites in Figure 17 have one short duration jump in the moving time window rms acceleration while the southern sites exhibit more numerous jumps with a greater total duration. The consistency of duration characteristics for stations south of the fault is illustrated by Figure 18, which shows horizontal plane Husid plots for four stations. All four sites are located in the Santa Monica Mountains (see Figure 12). In Figure 18, all four time scales have been shifted so that t_1 occurs at 2.0 seconds for all of the plots. This difference between

northern and southern sites, which was also true for other stations, must be related to the directionality of the faulting and wave radiation process which has also been observed by other researchers (Hanks, 1974; Heaton and Helmberger, 1978).

3.3 Probabilistic Model of the San Fernando Earthquake

The similarity of moving time window rms acceleration plots for specific areas and azimuths suggests that the shape may be related to definite wave arrivals which adjacent sites experienced. Thus, to characterize the strong part of ground shaking experienced at a site and obtain good results, a nonstationary model would be required.

A plot representing the average moving time window rms acceleration for a set of 11 sites south of the epicenter was produced. Table 2 identifies the 11 locations. The moving time window rms accelerations computed for 22 horizontal components, recorded at 11 different locations were normalized and averaged. The individual components were shifted by the time of initial S-wave arrival determined by Berrill, t_{1B} . This aligns the initial S-wave arrivals at all the sites. Then the average, $[S_a(t)]_{ave}$, was computed as:

$$(23) \qquad [S_a(t)]_{ave} = \sqrt{\frac{1}{(22)(0.5)} \sum_{i=1}^{22} \frac{1}{(\bar{s}_a)_i^2} \int_{t-0.25}^{t+0.25} a_i^2(\tau) d\tau}$$

where t varies from 0.0 to 6.2 seconds

$$(24) \qquad \bar{s}_{ai} = \sqrt{\frac{1}{6.2} \int_0^{6.2} a_i^2(t) dt}$$

$a_i(t)$ = ith acceleration time history shifted by t_{1B}

A duration of 6.2 seconds was assumed since this value is representative of the strong motion duration of the 11 stations listed in Table 2. $[S_a(t)]_{ave}$ has an average value of 1 since each individual moving time window root mean square acceleration plot has been normalized by $(\bar{s}_a)_i^2$. Figure 19a gives the resulting $[S_a(t)]_{ave}$ plot. Figure 19a shows the same two main peaks that are present in moving time window rms acceleration plots for most stations south of the epicenter (see Fig. 11). A simple nonstationary model, $\phi_n(t)$, consisting of two peaks of equal height and two valleys of equal height was fitted to $[S_a(t)]_{ave}$ as shown in Figure 19a. Therefore, for computational purposes, $\phi_n(t)$ can be divided into two succesive stationary segments of durations d_1 and d_2 with $d_1 + d_2 = d = 6.2$ seconds. The segment of height ϕ_1 represents the peaks, while the second

segment of height ϕ_2 represents the valleys. It should be noted that $1/d(\ \phi_1^2 d_1 + \phi_2^2 d_2\ ) = 1$. Then the normalized nonstationary model $\phi_n(t)$ was used to predict the times of occurrence, t_p, of peak accelerations for the ground motion during the San Fernando Earthquake.

For a stationary model, the probability density function of the time of peak acceleration, t_p, is:

$$(25) \qquad PDF(t_p - t_1) = \frac{1}{d}$$

Thus with a stationary model, the peak acceleration has an equal chance of occurring anytime during the strong motion duration d. The probability density function of the nonstationary model can be calculated by assuming independence between the two stationary segments ϕ_1 and ϕ_2.

$$(26) \qquad m_1 = PDF(t_p - t_1) =$$

$$\frac{1}{d_1}\int_0^{\infty}\left\{1-\exp\left[-vd_1\exp\left(-\frac{1}{2}n_1^2\right)\right]\right\}\frac{d}{dn_1}\left\{\exp\left[-vd_2\exp\left(-\frac{1}{2}n_1^2\frac{\phi_1^2}{\phi_2^2}\right)\right]\right\}dn_1$$

$$m_2 = PDF(t_p - t_1) = \frac{1 - m_1 d_1}{d_2}$$

where v = equivalent frequency (This quantity is calculated using Eqn. 15, An average value of 4.5 cps was calculated for the 22 components)

By multiplying m_1 and m_2 by the total number of actual cases (108), a theoretical histogram was obtained. This histogram is included in Figure 19b. The theoretical histogram shows the same peaks and valleys observed in Figure 19a. Figure 19b compares the theoretical histogram with one obtained by plotting the number of actual cases of component peak accelerations which correspond to a value of $t_p - t_{1B}$ for 108 horizontal components recorded at 54 stations south of the epicenter during the San Fernando Earthquake. The time scales of the individual components were shifted by the corresponding value of t_{1B} . The shape indicates that there were two intervals of strong horizontal shaking lasting about 1 second each, occurring at about 2.5 and 5 seconds after the first S-wave arrival. Most of the recorded peak accelerations occurred within these intervals. The shapes of the theoretical and observed histograms in Figure 19b show very good agreement. It should be noted that the histogram resulting from a stationary model would plot in Figure 19b as a horizontal line with a constant uniform distribution and a height of 8.7 cases. Thus, the strong shaking part experienced to the south of the epicenter can not be accurately modeled using a stationary process. This probabilistic model was also presented in a previously published paper (Dobry, Bond and O'Rourke, 1979).

Perhaps the observed moving time window rms acceleration plots can be related to the process which occurred at the fault. The differences observed between moving time window rms acceleration plots from the north and the south of the epicenter may possibly be explained by the directionality of the faulting process which has been noted by other researchers (Hanks, 1974; Heaton and Helmberger, 1978). Additionally, as shown in Figure 13, the faulting occurred on two planes separated by a bend at a depth of about 5 km (Hanks, 1974; Bouchon and Aki, 1977; Bache and Barker, 1978; Bouchon,1978). Archambeau (1978) and Heaton and Helmberger (1978) have found it necessary to include both directionality and fault plane irregularities in their San Fernando fault models in order to obtain good results at various azimuths between predicted and recorded ground motions. Bouchon (1978) provides an explanation of the distinct shape found for certain areas and azimuths for the moving time window rms acceleration plots. He has introduced a San Fernando rupture model which contains barriers or high strength materials. As the propagating rupture encounters these barriers, high localized stress drops and high frequency acceleration pulses result. Archambeau (1978) proposed that two high stress drop "events" occurred during the fault rupture. One event occurred at the hypocenter at a

depth of about 14 km while the second occurred at the fault bend at a depth of about 5 km. Thus, the moving time window rms acceleration shape may be related to acceleration and deceleration pulses which resulted from the faulting process. The consistency in the shapes of the moving time window rms acceleration plots and in the time of the peak accelerations, illustrated by Figures 19a and 19b , could then be explained by body wave phases related to these barriers. For example, based on the work Bouchon and Aki (1977) and Bouchon (1978), it could be speculated that the first peak at about 2.5 seconds in Figures 19a and 19b may be associated with S-wave arrivals from the fault plane below the fault bend, while the second peak at about 5 seconds could be associated with S-waves generated at the area between the fault bend and the fault tip.

3.4 Duration of the San Fernando Earthquake Strong Shaking

Using the procedure described at the end of Part 3.1, records from 97 sites from the 1971 San Fernando Earthquake were examined to determine t_1 and t_2. It was possible to determine t_1 and t_2 for 68 of the 97 sites. Those sites for which a t_1 or t_2 value could not be determined along with a possible explanation are contained in Table 3. t_1 could not be calculated for those sites where the accelerograph triggered late. A late triggering

recording device produces accelerograms which show no characteristics of the transition from P to S-wave arrivals. In these cases, the moving time window rms acceleration plot has high values at the beginning of the plot indicating that the typical initial low level part corresponding to P-wave arrivals was not recorded. Additionally, the maximum principal plane phi plot has values of approximately 90 degrees at the start confirming that the S-wave arrivals had started before the beginning of the recording. Certain soil sites also introduced problems. The determination of t_2 for these soil sites is difficult because the transition from high to low levels of moving time window rms acceleration values is gradual with no distinct separation. This problem will be investigated further in Part 4 for the sites C048, I137, and J145. Sites located in close proximity to the Pacific Ocean and at large distances from the epicenter demonstrated no discernible strong part. This is probably due to the increased importance of surface waves relative to body waves with increasing distance from the source (the shoreline sites were 50 to 100 km from the epicenter).

Table 4 contains the values of t_1, t_2, and $\Delta = t_2 - t_1$ for the 68 stations. Also included in Table 4 is t_{1B}, the time of initial S-wave arrivals estimated by Berrill (1975). Figure 20 demonstrates that t_1 calculated by

this study is in good agreement with t_{1B} calculated by Berrill for most of the stations. Berrill's method seems to produce better results for distant records than the method used in this thesis.

Figures 21 and 22 present plots of the duration of strong shaking, Δ, versus distance to the hypocenter and azimuth from the epicenter respectively. The value of duration does not seem to be related to distance. This result may appear at first sight inconsistent with studies made by other researchers (Trifunac and Brady, 1975; Dobry, Idriss and Ng, 1978; Hays, King and Park, 1978) where duration was found to increase with distance from the source. These other studies, however, calculated significant duration using the Trifunac-Brady procedure described in Part 3.1 where the duration is defined as the time interval required to accumulate between 5% and 95% of the total Arias Intensity of the record. The Trifunac-Brady procedure includes in the computed duration, in addition to the strong shaking part, some of the indirect, reflected, and surface wave arrivals contained in the third weak part of the record. These wave types increase in importance with distance from the source thus increasing the Trifunac-Brady duration. The method used in this thesis to compute duration attempts to eliminate this effect by considering only the

strong shaking part and thus shows no influence of distance on duration.

A correlation exists between the duration and the azimuth from the epicenter as seen in Figure 22. Azimuth is measured clockwise with respect to north which is 0 degrees. Sites north of the epicenter have a duration, Δ, of 3 to 4 seconds while sites south of the epicenter have a duration of 5 to 8 seconds. The total rupture duration for the San Fernando Earthquake has been estimated as 9 to 10 seconds (Bouchon, 1978; Heaton and Helmberger, 1978). However, the San Fernando Earthquake fault process was directional with the thrust fault rupture propagating in a southernly direction. This effect causes recording stations to see different apparent durations depending on their azimuth. Heaton and Helmberger (1978) found the shear wave radiation time to be approximately 8 seconds for the sites south of the epicenter and 12 seconds for the sites north of the epicenter. Thus, the method used in this thesis shows good agreement for the southern sites and bad agreement for the northern sites. Evidently for the northern sites, the procedure only identified the time interval corresponding to the strong rupture which occurred at the hypocenter.

The determination of duration at soil sites is clearly more complex than at rock sites. The time domain and

duration characterization at soil sites should consist of two parts. The first part is the strong, high frequency part of the accelerogram which is also evident at adjacent rock sites. This part has a duration Δ. The second part is the moderate, longer period part found only at some soil sites. These parts together determine the motion experienced at a site. Thus, for practical purposes it may be reasonable to separate the duration experienced at rock and soil sites and to define them as two distinct entities in future studies.

3.5 Level of Strong Shaking of the San Fernando Earthquake

Using the values of t_1 and Δ determined in Part 3.4, the horizontal plane rms acceleration, $\bar{a}_H$ defined by Eqn. 18 was determined for the 68 sites listed in Table 4. Table 4 contains the values calculated for $\bar{a}_H$. Two other quantities were also calculated for comparison, $\bar{a}_{HB}$ and a_{pH}. $\bar{a}_{HB}$ is the horizontal plane rms acceleration calculated by using Berrill's estimate of the first S-wave arrivals, t_{1B}, as the beginning of the strong part coupled with a constant duration, Δ, of 6.0 seconds. A duration of 6.0 seconds was used for two reasons. First, it corresponds closely to the value of duration found for sites south of the epicenter in Part 3.4. Second, it is better to underestimate the duration in the calculation of $\bar{a}_H$ than to overestimate it. By overestimating the duration, the low level shaking following

the strong part is included in the calculation of $\bar{a}_H$, resulting in an underestimated value of $\bar{a}_H$. By underestimating the duration, only the strong shaking part is included. This produces a more realistic value for $\bar{a}_H$. The values of $\bar{a}_{HB}$ for the 97 sites have been included in Table 4.

a_{pH} is the horizontal plane peak acceleration. This measure of the peak acceleration is independent of the orientation of the recording devices and is determined as follows:

$$a_H(t) = \sqrt{a_X^2(t) + a_Y^2(t)} \tag{27}$$

$$a_{pH} = \left| a_H(t) \right|_{max}$$

where $a_H(t)$ = horizontal plane acceleration

$a_X(t)$, $a_Y(t)$ = horizontal plane acceleration components

Table 5 contains the values calculated for a_{pH}. a_{pH} is closely related to a_{pX} and a_{pY}, the peak acceleration values of the horizontal components. This is illustrated by the plot of a_{pH} versus the maximum of a_{pX} and a_{pY} in Figure 23.

In the calculation of $\bar{a}_H$, it was observed that some small geographic areas contained stations with comparable values of $\bar{a}_H$ (example - C051:534, C054:575,

E078:554, K157:598, Q241:538, R244:589). In other small areas, dissimilar values of $\bar{a}_H$ were obtained. This lack of similarity was prominent at the Hollywood Storage Basement and Hollywood Storage P.E. Lot stations where $\bar{a}_H$ was calculated to be 672 and 937 mm/sec/sec respectively. These stations are within several hundred feet of each other. Crouse and Turner (1978) and Shakal and Toksoz (1978) have noted a difference in the Fourier amplitude spectra of these accelerograms for frequencies higher than 5 Hz. The P.E. Lot station is a free field site and its Fourier amplitude spectrum contains more energy above 5 Hz than the basement station. Newmark et. al. (1977) and Crouse and Turner (1978) have explained this by suggesting that the large building foundation filtered out the high frequencies and thus averaged the ground motions at the building site. In an effort to assess the effect of this difference and to simulate crudely the filtering effect of large buildings, the Hollywood Storage accelerograms as well as the other accelerograms in Table 4 were band pass filtered with only frequencies below 5 Hz passed. The horizontal plane rms acceleration was then recalculated using the filtered accelerograms. The filtered horizontal plane rms acceleration, $\bar{a}_{HF}$, may be found in Table 4 for the 68 stations. The results at the Hollywood Storage sites are

encouraging. $\bar{a}_{HF}$ is 637 and 743 mm/sec/sec for Hollywood Storage Basement and Hollywood Storage P.E. Lot respectively. The free field site root mean square acceleration value decreases more than the basement value confirming what was observed in the Fourier amplitude spectrum. In most other areas, however, the band pass filtered values of $\bar{a}_{HF}$ did not show a reduction of scatter compared with the unfiltered values of $\bar{a}_H$. This suggests that other effects besides the filtering of high frequencies by massive foundations of multistory buildings influence the scatter of rms acceleration.

$\bar{a}_H$, $\bar{a}_{HB}$, and a_{PH} were plotted versus the hypocentral and epicentral distances to the recording stations to determine the attenuation of these values with distance. The distances of the stations from the hypocenter and epicenter were obtained from Berrill (1975). Figures 24 through 30 present the plots of a_{PH}, $\bar{a}_{HB}$, and $\bar{a}_H$ versus distance to the hypocenter. Plots of a_{PH}, $\bar{a}_{HB}$, and $\bar{a}_H$ versus epicentral distance may be found in Appendix 2.

A least squares analysis was performed assuming an equation of the form $y = cx^d$ where y represents the acceleration quantity at a distance x from the source. The numerical values for the parameters c and d are found in Table 6. The curves resulting from the least squares

analysis are plotted in Figures 24 through 27 for the 97 sites of Table 4, Figures 28 and 29 for 68 sites, and Figure 30 for rock sites only. The acceleration data fits the least squares curves well with the coefficient of correlation, r, ranging from 0.83 to 0.89 (see Table 6). However, the scatter of $\bar{a}_{HB}$ and $\bar{a}_{H}$ values measured by the value of r in Table 6 is not significantly less than the scatter of a_{PH} values. This result was not expected and tends to discourage the use of $\bar{a}_{HB}$ or $\bar{a}_{H}$ over a_{PH} for characterization purposes. The equations for $\bar{a}_{HB}$ (97 sites) and $\bar{a}_{H}$ (68 sites) in Table 6 are very similar, if x = hypocentral distance, $\bar{a}_{HB} = 1.17*10^{5}x^{-1.46}$ and $\bar{a}_{H} = 1.20*10^{5}x^{-1.43}$. The equation for a_{PH} (97 sites) is $a_{PH} = 4.22*10^{5}x^{-1.54}$. This confirms that $\bar{a}_{H}$ is approximately equal to $\bar{a}_{HB}$ and suggests that on the average a_{PH} is about three times larger than $\bar{a}_{H}$. The curve calculated for rock sites only contains too few sites to draw any definitive conclusions.

Figure 31 is a plot of $\bar{a}_{H}$ versus $\bar{a}_{HB}$. $\bar{a}_{HB}$ calculated using a constant duration, Δ, of 6.0 seconds produces results which are comparable to $\bar{a}_{H}$ which was calculated using a duration, $\Delta = t_2 - t_1$ except for sites north of the epicenter. At these northern sites 6.0 seconds overestimates the duration experienced resulting in an underestimated value of rms acceleration. This conclusion

probably applies also to the values of rms acceleration computed by Hanks (1979) using a constant duration of 10.0 seconds for the San Fernando Earthquake. Figures 32 and 33 are plots of a_{PH} versus $\bar{a}_{HB}$ and $\bar{a}_H$ respectively. a_{PH} is closely related to both $\bar{a}_{HB}$ and $\bar{a}_H$ as shown in these plots with $a_{PH} \cong 2.55\bar{a}_H \cong 2.7\bar{a}_{HB}$. This result together with the values of r in Table 6 suggests that for a given earthquake event such as San Fernando, a_{PH} is as suitable as $\bar{a}_{HB}$ or $\bar{a}_H$ for earthquake characterization. This conclusion should be verified, however, for other earthquake events. It is also possible that the factor 2.7 may change for other earthquakes.

The regressions summarized in Table 6 suggest that a_{PH}, $\bar{a}_{HB}$, and $\bar{a}_H$ are similarly attenuated with distance as (hypocentral distance)$^{-1.5}$. This is exactly what is predicted by the Brune-Hanks model of Eqn. 10. Therefore, it was decided to compare the attenuation curve predicted by this model for the San Fernando Earthquake with the empirical attenuation curves from the regression found in Table 6. Figures 34 and 35 include these comparisons for $\bar{a}_{HB}$ and $\bar{a}_H$. In order to convert from component to horizontal plane rms acceleration, Equation 10 was multiplied by a factor of $\sqrt{2}$:

$$(28) \qquad \bar{a}_H = 1.20 \frac{\sqrt{2}\,(2\pi)^2}{106} \frac{\Delta s}{\rho R^{1.5}} \sqrt{\frac{QB}{\pi f_o}}$$

where the symbols are the same as Eqn. 10

The following estimates of the San Fernando parameters used in Figures 34 and 35 were made by Hanks (1979):

Δs = 50 bars

T_d = 10 seconds

ρ = 2.8 gm/cubic cm

B = 3.2 km/sec

Q = 300

The observed curves are greater than the theoretical curve by a factor of about 1.9 with all three curves being similarly attenuated by distance. Hanks has assumed a faulting duration of 10 seconds for calculating the theoretical curve while 6 seconds was used here for the calculation of $\bar{a}_{HB}$. If the faulting duration was taken to be 6 seconds, the ratio between the theoretical and the actual curves would increase to a factor of about 2.5.

Hanks (1979) also noticed this discrepency between the predicted and observed values of rms acceleration for the San Fernando Earthquake and offers two possible explanations. First, the data includes all azimuths and thus

samples different parts of the irregular focal sphere which concentrated its energy mainly to the south. Second, Hanks believes that the event was more energetic than the theoretical parameters suggest. A larger value of stress drop, Δs, in Eqn. 28 would improve the agreement between the theoretical and observed values.

3.6 Examination of Velocity as a Strong Shaking Parameter

It was shown in the previous section that rms acceleration was not significantly superior to peak acceleration as a ground motion parameter. Thus the decision was made to attempt to characterize the level of strong shaking by rms velocity. Velocity was chosen because it represents longer wavelength motions, which are hopefully more consistent over a wider area than the shorter wavelength motions represented by the acceleration. The horizontal plane rms velocity, $\bar{v}_H$, is defined as:

$$\bar{v}_H = \sqrt{\frac{1}{\Delta}\int_{t_1}^{t_1+\Delta} \left[v_X^2(t)+v_Y^2(t)\right]dt} \tag{29}$$

where t_1 = time corresponding to the beginning of strong shaking

Δ = duration of strong shaking

$v_X(t)$, $v_Y(t)$ = velocity time histories in the horizontal plane

The time interval corresponding to the strong shaking is assumed to be $\Delta = t_2 - t_1$. The values of t_1 and Δ found in Table 4 were used to calculate $\bar{v}_H$.

The horizontal plane peak velocity, v_{PH}, was also calculated for comparison purposes. v_{PH} is defined as follows:

$$(30) \qquad v_H(t) = \sqrt{v_X^2(t) + v_Y^2(t)}$$

$$v_{PH} = \left| v_H(t) \right|_{max}$$

where $v_H(t)$ = horizontal plane velocity

$v_X(t)$, $v_Y(t)$ = horizontal plane velocity components

Table 5 contains the calculated values of v_{PH} and $\bar{v}_H$.

Figures 36 and 37 are plots of v_{PH} and $\bar{v}_H$ versus distance to the hypocenter respectively. Appendix 2 has these values plotted versus the distance to the epicenter. A least squares analysis was performed assuming an equation of the form $y = cx^d$ where y represents the velocity quantity at a distance x from the source. The numerical values for the paramters c and d are found in Table 6. The coefficient of correlation, r, for acceleration versus distance for both soil and rock sites ranged from 0.83 to 0.89 while the range for velocity versus distance for the same sites ranged from

0.73 to 0.80. The fit of data points to the curves in Figures 36 and 37 indicates that the scatter is larger for velocity than for acceleration. Therefore, the expectation of decreasing the scatter by utilizing velocity was not realized. Boore et. al. (1978) have concluded that for the San Fernando Earthquake, peak acceleration is not significantly modified by soil sites. Velocity, however, was amplified at soil sites. This may help explain the larger scatter found when plotting velocity instead of acceleration versus distance.

The time at which v_{pH} occurred was also determined. Table 5 indicates which records had v_{pH} occur during the interval from t_1 to t_2. 50 of the 68 stations (78%) have v_{pH} occurring in the strong shaking part. Hence the arrival of direct body waves and not surface waves seems to be responsible for approximately 75% of the v_{pH} values.

PART 4

ANALYSIS OF SURFACE WAVE MOTION IN THE SAN FERNANDO VALLEY

This part describes a detailed analysis of five San Fernando Valley records using the time domain techniques of Part 2. These sites are:

Caltech number	Location
C048	8244 Orion Blvd., Los Angeles
H115	15250 Ventura Blvd., Los Angeles
I137	15910 Ventura Blvd., Los Angeles
J145	15107 Vanowen Street, Los Angeles
Q233	14724 Ventura Blvd., Los Angeles

Figure 12 is a map which gives the approximate locations of these sites in the San Fernando Valley. C048 and J145 are located near the center of the valley. H115, I137, and Q233 are located at the southern end of the valley close to the boundary of the valley and the Santa Monica Mountains.

The San Fernando Valley is a broad, fairly flat plain bounded on the north by the San Gabriel and Santa Susana Mountains, on the west by the Simi Hills, to the south by the Santa Monica Mountains and on the east by the Verdugo Mountains. Tables 9, 10, and 11 summarize subsurface information for the San Fernando Valley presented by Duke et. al. (1971). Table 9 corresponds to station C048 which is

located near the center of the valley. Table 10 corresponds to station J145 which is more to the south. Table 11 corresponds to the three Venture stations (H115, I137, and Q233) which are close to the southern edge of the valley (see also Figure 12). These tables show that the valley geology consists essentially of a layer of alluvium followed by sedimentary rock, both underlaid by basement rock. The thickness of the alluvium is about 1000 feet at C048 and decreases to the south being about 80 feet at the Ventura stations (see also Shannon and Wilson, 1978; Arango and Clayton, 1978). The combined thickness of the alluvium and the sedimentary layers also decreases rapidly to the south, being 13900 feet at C048, 9500 feet at J145 and 6000 feet at the Ventura stations. The P-wave velocities, V_p , in Tables 9, 10 , and 11 are field measurements. The S-wave velocities, V_S , are field measurements only at shallow depths (0 to 100-300 feet). The S-wave velocities at greater depths are estimated from P-wave velocities.

Hanks (1975) and Dobry, Idriss and Ng (1978) have indicated that the San Fernando Valley structure contributed to the number of indirect, reflected, and surface waves which stations located in the valley experienced. The resulting ground motions in the valley were considerably different from those experienced in the neighboring hills.

Figure 38 compares the horizontal plane Husid and moving time window rms acceleration plots at one of the San Fernando Valley sites (I137) with those those of the Lankershim station (L166). The time scale of I137 has been shifted so that t_1 of both records corresponds to 1.6 seconds. The motions experienced at Lankershim are representative of the motions experienced by stations located in the Santa Monica Mountains. This can be verified by comparing the moving time window rms acceleration plot for Lankershim with Figure 19a which represents the average moving time window acceleration found in the Santa Monica Mountains. The shape of the moving time window rms acceleration plots is similar during the strong part of shaking which corresponds to the time period from about 1.5 to 7.5 seconds. At 7.5 seconds the level of shaking at the Lankershim site drops rapidly while the level of shaking at the Ventura site maintains a high level. This continued high level confirms the existence of wave arrivals unique to the San Fernando Valley. Table 7 gives specific information describing the five stations which recorded motions during the San Fernando Earthquake.

Stations C048 and J145 will be considered in more detail first. In the preceding section, it was not possible to determine a t_2 value for these sites. The reason why can

be seen by examining Figures 39 and 40 which contain the horizontal plane Husid and rms acceleration plots for the two sites. The Husid plots exhibit no distinct changes in slope after the end of the direct S-wave arrivals and the rms acceleration values remain at a high level for a considerable portion of the record. This increase in the interval of strong shaking can be attributed to the arrival of indirect, reflected, or surface waves at these stations. Additional details become evident when an examination is made of the vertical rms acceleration, obtained using Eqn. 11 with the vertical ground acceleration, $a_Z(t)$, and maximum principal plane phi plots contained in Figures 41 and 42. An unusual phenomenon is found in the plots of the C048 site starting at about 18.0 seconds and the J145 site starting at about 23.0 seconds. The vertical rms acceleration values oscillate between high and low levels while the phi angle oscillates between 10 and 90 degrees. The meaning of this periodic behavior becomes clear when the definition of the phi angle is examined. The phi angle indicates on which plane the predominant ground motions are occurring. The periodic change in the direction of predominant ground motions evident in Figures 41 and 42 is consistent with the passage of a Rayleigh surface wave. The ground particle motion of a Rayleigh wave is elliptical in a vertical plane.

This hypothesis would explain the periodic variation of the phi angle. The phi angle is determined by sampling a 0.5 second portion of the accelerogram and then calculating the principal direction of ground motion for that portion. If a Rayleigh wave were passing the site, a different phi angle would be determined depending upon which portion of the Rayleigh cycle was sampled. When the motion is predominantly vertical phi will be approximately 0 degrees while phi will be approximately 90 degrees when the motion is predominantly horizontal. Thus the phi angle of the maximum principal plane will be constantly changing as the ground particle motion traverses an elliptical path, with phi going from 0 to 90 degrees or vice versa every quarter of a cycle. It should be noted that the time window size must be considerably smaller than the period of the Rayleigh wave in order that the sampling will produce this effect on the phi angle. This suggests that if the wave arriving at the two sites after 18.0 and 23.0 seconds respectively is a Rayleigh wave, the period of this wave is considerably larger than 0.5 seconds.

The vertical moving time window rms acceleration plots contained in Figures 41 and 42 also support the Rayleigh wave hypothesis. A Rayleigh wave would produce periodic changes in the vertical rms acceleration as the

acceleration alternated from predominantly horizontal to predominantly vertical. In Figures 41 and 42 a peak in the vertical rms acceleration plots corresponds to a valley in the principal plane phi plots. The greatest vertical rms acceleration is experienced when phi is approximately 0 degrees, implying motion predominantly in the vertical plane. A valley in the vertical rms acceleration plots corresponds to a peak in the principal plane phi plots. Low values of vertical rms acceleration are experienced when phi is approximately 90 degrees, implying motion predominantly in the horizontal plane. Figure 43 shows the plots of the vertical moving time window rms acceleration experienced at the C048 and J145 sites superimposed. The time scales of both plots have been shifted. The time of 2.0 seconds in this plot corresponds to 18.6 and 23.0 seconds in the plots of the C048 and J145 sites respectively. There is very good agreement between the acceleration experienced at both sites between 2.0 and 6.0 seconds in this graph. A consistent pattern of energy arrivals is evident. Thus it will be assumed that 18.6 seconds at the C048 site record and 23.0 seconds at the J145 site record represent approximately the same point in the Rayleigh wave train at both sites. Table 8 presents the minimum and maximum values of vertical rms acceleration and phi for the time period of 18.5 to 22.5

seconds for the C048 station and 23.0 to 27.0 seconds for the J145 station.

An estimate of the period of the Rayleigh motion may be obtained by determining the times at which the minimum and maximum values of vertical rms acceleration and phi occur. By finding the time between every other minimum or maximum, the time to complete an entire period may be determined. The period estimated for these portions of the suspected Rayleigh wave train for both stations is approximately 2.5 seconds or a frequency of 0.4 Hz.

An estimate of the frequency allows the use of the response envelope technique to verify the existence of the Rayleigh wave train. The response envelope for the vertical component at each site defined by Eqns. 16 and 17 is calculated by obtaining the response of a single degree of freedom system having a natural period of 2.5 seconds and a damping ratio of 0.05. Figure 44 illustrates the 0.4 Hz vertical response envelope plots for two stations not in the San Fernando Valley, specifically 445 Figuroa Street and 3838 Lankershim Boulevard. Figures 45 and 46 contain the 0.4 Hz vertical response envelope plots for the C048 and J145 sites respectively. The vertical response envelope increases rapidly during the 18 to 24 second period at the C048 site and the 23 to 28 second period at the J145 site. The

response at C048 and J145 is more than 25 times greater than the response at 445 Figueroa Street and 3838 Lankershim Boulevard. This high response in the San Fernando Valley could most likely be explained by a low frequency Rayleigh wave having a large vertical amplitude.

Additional confirmation is obtained by examining the locus of surface ground particle displacement as it varies during time. Figures 47, 48, and 49 contain the ground particle motions experienced at the C048 site from 18.5 to 22.5 seconds projected on the horizontal and two vertical planes. Figures 50, 51, and 52 contain the the same information at the J145 site from 23.0 to 27.0 seconds. The ground particle motions in the vertical planes are elliptical. This is characteristic of Rayleigh wave motion.

Assuming that 18.6 seconds in the C048 site record and 23.0 seconds in the J145 site record represent approximately the same point in the Rayleigh wave train, the direction of the wave train may be estimated. An examination of the particle displacements in the horizontal plane demonstrates that both sites exhibit the majority of their motion in a predominantly northeast-southwest line. This is seen in Figures 47 and 50. This is reasonable since the area of surface faulting is located approximately northeast of the two stations (see Figure 12). A more exact measure is

obtained by finding the value of theta for the maximum principal plane that corresponds to a phi value of 90 degrees for the ground accelerations during the Rayleigh motion. When phi is approximately 90 degrees, both acceleration and displacement are predominantly in the horizontal plane and the theta angle indicates the orientation of the motions in the horizontal plane. Table 8 contains the values of theta corresponding to phi values of about 90 degrees during the assumed Rayleigh wave motion. These values also indicate particle motion along a northeast-southwest line.

The solution of a ideal elastic halfspace model demonstrates that the particle motion of a Rayleigh wave describes a retrograde ellipse, in contrast to the prograde ellipse motion associated with water waves (Richart, Woods and Hall, 1970). Using this information the particle displacement found at these sites indicates that the wave front originated in the northeast which is consistent with the location of the fault shown in Figure 12. This conclusion is also supported by considering the time of the slower Rayleigh wave arrival minus the time of first S-wave arrivals for each site. This time difference for the C048 and J145 sites is 15.9 and 21.4 seconds respectively. Thus the Rayleigh wave front passed by C048 first and then by

J145 as it moved southwest away from the fault.

The shallow faulting which occurred along the upper thrust fault plane (see Figure 13) is probalbly responsible for generating the strong response in the San Fernando Valley which caused the Rayleigh waves. Mal (1972) modeled the Rayleigh wave motion resulting from a thrust fault inclined at an arbitrary angle with the surface. He found that the Rayleigh wave amplitude ahead of the fault break is considerably higher than that behind the epicentral region and that the amplification depends only on the orientation of the fault. The San Fernando Valley lies ahead of the shallow faulting which occurred during the San Fernando Earthquake.

It has been shown in Table 8 that the period of the suspected Rayleigh wave is approximately 2.5 seconds for the portions identified at stations C048 and J145. The group velocity is the speed at which a specific group of similar frequencies travel (Officer, 1958). It is also the speed at which the energy associated with that group travels. Thus, by estimating the difference in distance and time between 18.6 seconds in the record of the C048 site and 23.0 seconds in the record of the J145 site, an estimate of the group velocity may be determined. This calculation assumes that it is possible to accurately determine the proper times in both

wave trains. This is not the case and thus these calculations serve only as an approximation. The Rayleigh wave front is assumed to move in a direction away from but parallel to the surface fault (see Figure 53). The group velocity may be calculated from the following equation:

$$(31) \qquad V_G = \frac{d_{(J145)} - d_{(C048)}}{[(t_{R(J145)} - t_{1(J145)}) - (t_{R(C048)} - t_{1(C048)})] + t_d}$$

where v_G = group velocity

$d_{(J145)} - d_{(C048)}$ = distance from C048 to J145

t_R = time of Rayleigh wave arrival

t_1 = time of initial S-wave arrival

t_d = difference between the times of the initial S-wave arrivals at C048 and J145 (it is assumed that they arrive first at C048)

The difference in the times of the initial S-wave arrivals must be included because each site's instrument triggered independently. The values substituted into the equation are:

$d_{(J145)} - d_{(C048)}$ = 1.45 km

$t_{R(J145)}$ = 23.0 seconds

$t_{R(C048)}$ = 18.6 seconds

$t_{1(J145)}$ = 1.6 seconds

$t_{1(C048)}$ = 2.7 seconds

The distance between the sites was calculated along a northeast-southwest line since this was determined to be the approximate direction of wave travel (see Figure 53). If t_d is assumed to be zero (initial S-waves assumed to arrive simultaneously at both stations), the group velocity is calculated to be 0.26 km/sec or 860 ft/sec. This value will increase or decrease depending upon the value of t_d. In deriving Equation 31, it was assumed that the initial S-waves arrived at the C048 site first because it is nearer to the surface fault. However, the depth to the basement rock is greater at the C048 site than it is at the J145 site (13,900 feet versus 9,500 feet). To obtain an approximation for t_d, it is assumed that the S-wave arrived simultaneously to the basement rock at a depth of 13,900 feet under both stations, and that it propagated between this depth and the ground surface. With this assumption, the V_S profiles in Tables 9 and 10 were used to calculate t_d = -0.57 seconds. The corresponding Rayleigh wave group velocity changes from 860 ft/sec to 970 ft/sec. Therfore, about 1000 ft/sec seems to be a reasonable estimate of the group velocity obtained from the recorded motions.

Doctor David Harkrider of Caltech computed the theoretical phase and group velocities corresponding to the fundamental mode of Rayleigh waves for the three geologic

profiles of Tables 9 through 11. These values have been included in Table 12 for a period, T = 2.5 seconds. The theoretical group velocities at the C048 and J145 sites are 2,900 and 3,400 ft/sec, respectively, or about three times larger than the value of 1000 ft/sec estimated from the records. The high values of phase velocity computed by Harkrider and included in Table 12 are consistent with the phase velocities from a finite element model of the San Fernando Valley reported by Drake (1972) and Drake and Mal (1972). They are also consistent with the results of some simplified calculations performed by the author, based on the profiles of Tables 9 and 10 and using the charts provided by Mooney and Bolt (1968) for Rayleigh waves in two-layer systems.

Therefore, a large difference exists between the group velocity estimated from the records and the theoretical group velocity computed from the subsurface profiles of Tables 9 and 10. Several reasons may possibly explain this difference. First, the assumption of a plane Rayleigh wave front made in Equation 31 may not be correct. This assumption may be important considering the geometry of stations C048 and J145. Second, the shape of the San Fernando Valley may be important (one dimensional models were used to calculate Table 12). Third, the subsurface

profile of the valley used for the theoretical calculations may be in error. Fourth, this amy be an air coupled Rayleigh wave resulting from the air compression caused by the thrust fault. This would account for the low velocity calculated. Finally, the procedure used may have failed to identify the proper times necessary to calculate the velocity.

The Ventura (H115, I137, and Q233) sites were also examined. Another study (Lanners, 1978) had suggested that a correlation exists between the velocity time histories experienced at these sites following the direct body wave arrivals. The accelerogram time domain processing, however, did not reveal any clear distinguishing features to link these sites with the accelerograms recorded at the C048 and J145 sites. Figures 54, 55, and 56 are the ground particle displacement plots for the I137 site for times between 20.0 and 30.0 seconds. The displacement describes a flat elliptical motion suggesting Rayleigh wave motion. The thickness of alluvium and the depth to basement rock in the San Fernando Valley decreases as the distance from the center of the valley increases. This is associated with the flattening of the displacement curves evident when comparing Figures 47 through 56. This flattening of the Rayleigh wave elliptical surface ground motion from north to south is not predicted by the theoretical model, as indicated by the

ratios between horizontal and vertical displacement of Table 12.

PART 5

DISCUSSION AND CONCLUSIONS

The accelerograms recorded at ground elevation during the 1971 San Fernando Earthquake were examined by four time domain techniques. These techniques are the Husid plot, the moving time window root mean square acceleration, the variation of the principal planes of ground motion with time, and the response envelope of a single degree of freedom system.

Two of these techniques were especially useful. The moving time window rms acceleration is a good indicator of the level of shaking experienced at a site for a specified interval of the accelerogram. Knowledge about the level of shaking is useful for determining which parts of an accelerogram correspond to high levels of shaking or specific wave arrivals. The vertical component of the eigenvector corresponding to the maximum principal plane of ground motions indicates on which plane the predominant ground motions are occurring. A change in the plane of the predominant ground motions occurs when the seismic waves incident at a site change from predominantly P-waves to predominantly S-waves.

Using the Husid, moving time window rms

acceleration, and maximum principal plane phi plots of each station which recorded the 1971 San Fernando Earthquake, a part of each accelerogram corresponding to strong shaking was identified. The moving time window root mean square acceleration plots of stations located in small geographic areas exhibited distinct shapes. These shapes were different for each area and thus seem to be related to the sequence of energy arrivals a specific area experienced. A nonstationary model of the strong shaking part of the San Fernando Earthquake was constructed for stations south of the epicenter. The model predictions of the time of peak acceleration correlated well with the actual times of peak acceleration south of the epicenter. The model demonstrated that sites south of the epicenter received a similar sequence of energy arrivals and that a nonstationary model was necessary to characterize the process.

The duration and the level of shaking of each accelerogram strong part was determined. The duration of strong shaking for sites south of the epicenter was 5 to 8 seconds while sites north of the epicenter had a duration of 3 to 4 seconds. The level of shaking at each site was characterized by peak and rms acceleration. The use of rms acceleration did not reduce the scatter of resultant data values compared to peak acceleration. This result was

disappointing. The rms acceleration of the strong shaking part is closely related to the peak acceleration by a ratio of 2.6 for the San Fernando Earthquake. Root mean square acceleration seems to offer little advantage over peak acceleration. Both peak and rms acceleration are attenuated similarly with distance. They attenuate with distance as approximately (hypocentral distance)$^{-1.5}$. This attenuation is identical to that predicted by the Brune-Hanks model.

Velocity was also investigated as a measure of the level of strong shaking. Correlations of rms velocity with distance were not as good as those obtained for rms acceleration due to the possible amplification of ground velocity at soil sites.

The accelerograms of five stations located in the San Fernando Valley were examined for the presence of surface waves. A Rayleigh wave train was identified at two sites by the distinct trace the wave makes in a maximum principal plane phi plot. The maximum principal plane phi plot oscillates because of the variation in the predominant ground motions caused by the Rayleigh surface wave. The locus of ground particle motion describes a retrograde elliptical motion in the vertical plane further confirming the presence of the surface wave. It was estimated from the record that the Rayleigh wave train had a frequency of 0.4

Hz and propagated away from the fault trace in a NE-SW direction with a group velocity of about 1000 ft/sec. The calculated group velocity, however, does not agree with theoretical calculations made for the area. The available information suggests that the surface wave resulted from the shallow faulting associated with the San Fernando Earthquake.

The time domain techniques presented in this thesis have demonstrated their usefulness in characterizing the San Fernando Earthquake motions for engineering purposes. Their use in the future should provide additional insight into other earthquake records. It is recommended that root mean square acceleration be investigated for other earthquake records to confirm the conclusions drawn for the 1971 San Fernando Earthquake accelerograms.

PART 6

LITERATURE CITED

Arias, A. (1969)"A Measure of Earthquake Intensity", Seismic Design for Nuclear Power Plants, Robert Hansen, Editor, Massachusetts Institute of Technology Press, Cambridge, Massachusetts.

Archambeau, C.B. (1978)"Recent Developments and Applications of Deterministic Earthquake Models: Prediction of Near and Far Field Ground Motion", Seminar-Workshop on Strong Motions, Rancho Santa Fe.

Bache, T.C. and Barker, T.G. (1978)"The San Fernando Earthquake-A Model Consistent with Near-field and Far-field Observations at Long and Short Periods (abs)", U.S. Geological Survey, Summaries of Technical Reports, Vol. 5, National Earthquake Hazards Reduction Program.

Bendat, J.S. (1958)Principles and Applications of Random Noise Theory, John Wiley and Sons, Inc., New York.

Berrill, J.B. (1975)"A Study of Hgh-Frequency Strong Ground Motion from the San Fernando Earthquake", Thesis, California Institute of Technology, Pasadena, California.

Bolt, B.A. (1972)"San Fernando Rupture Mechanism and the Pacoima Strong-Motion Record", Bulletin of the Seismological Society of America, Vol. 62, No. 4, August.

Bolt, B.A. (1973)"Duration of Strong Ground Motion", Proceedings, 5th World Conference on Earthquake Engineering, Rome, Italy.

Boore, D.M. and Zoback, M.D. (1974)"Two-Dimensional Kinematic Fault Modeling of the Pacoima Dam Strong-Motion Recordings of the February 9, 1971, San Fernando Earthquake", Bulletin of the Seismological Society of America, Vol. 64, No. 3, June.

Boore, D.M., Joyner, W.B., Oliver, A.A. and Page, R.A. (1978)"Estimation of Ground Motion Parameters", Geological Survey Circular 795.

Bouchon, M. and Aki, K. (1977)"Discrete Wave-Number

Representation of Seismic-Source Wave Fields", Bulletin of the Seismological Society of America, Vol. 67, No. 2, April.

Bouchon, M. (1978)"A Dynamic Source Model for the San Fernado Earthquake", Bulletin of the Seismological Society of America, Vol. 68, No. 6, December.

Brune, J.N. (1970)"Tectonic Stress and the Spectra of Seismic Shear Waves", Journal of Geophysical Research, Vol. 75.

Chang, F.K. and Krinitzsky, E.L. (1977)"Duration, Spectral Content and Predominant Period of Strong Earthquake Records from the Western United States", Miscellaneous Paper S-73-1, Soils and Pavements Laboratory, U.S. Army Waterways Experiment Station, Vicksburg, Mississippi.

Cloud, W.K. and Perez, V. (1969)"Strong Motion-Records and Acceleration", Proceedings, 4th World Conference on Earthquake Engineering, Santiago, Chile.

Cloud, W.K. (1973)"Strong Motion During Earthquakes", Proceedings, 5th World Conference on Earthquake Engineering, Rome, Italy.

Clough, R.W. and Penzien, J. (1975)Dynamics of Structures, McGraw-Hill, Inc., New York, New York.

Crouse, C.B. and Turner, B.E. (1978)"Analysis of Ground Motion Spectra", Proceedings of the Second International Conference on Microzonation, San Francisco, California.

Dobry, R., Idriss, I.M. and Ng, E. (1978)"Duration Characteristics of Horizontal Components of Strong Motion Earthquake Records", Bulletin of the Seismological Society of America, Vol. 68, No. 5, October.

Dobry, R., Singh, S. and Bond, W.E. (1978)"Study of Ground Motions at Soil Sites During Two California Earthquakes", Report No. CE-78-8, Rensselaer Polytechnic Institute, Troy, New York.

Dobry, R., Bond, W.E. and O'Rourke, M. (1979)"Probabilistic Model for Earthquake Accelerations", Proceedings, ASCE Specialty Conference on Probabilistic Mechanics and Structural Reliability, Tucson, Arizona.

Donovan, N.C., Bolt, B.A. and Whitman, R.V.

(1976)"Developments of Expectancy Maps and Risk Analysis", Preprint 2805, ASCE Annual Convention and Exposition, Philadelphia, Pennsylvania.

Drake, L.A. (1972)"Love and Rayleigh Waves in Nonhorizontally Layered Media", Bulletin of the Seismological Society of America, Vol. 62, No. 5, October.

Drake, L.A. and Mal, A.K. (1972)"Love and Rayleigh Waves in the San Fernando Valley", Bulletin of the Seismological Society of America, Vol. 62, No. 6, December.

Duke, C.M., Johnson, J.A., Kharraz, Y., Campbell, K.W. and Malpiede, N.A. (1971)"Subsurface Site Conditions and Geology in the San Fernando Earthquake Area", UCLA-ENG-7206, University of California, Los Angeles, December.

Grant, W.P., Arango, I. and Clayton, D.N. (1978)"Geotechnical Data at Selected Strong Motion Accelograph Station Sites", Proceedings of the Second International Conference on Microzonation, San Francisco, California.

Hanks, T.C. (1974)"The Faulting Mechanism of the San Fernando Earthquake", Journal of Geophysical Research, Vol. 79, No. 8.

Hanks, T.C. (1975)"Strong Ground Motion of the San Fernando, California, Earthquake: Ground Displacements", Bulletin of the Seismological Society of America, Vol. 65, No. 1, February.

Hanks, T.C. and Johnson, D.A. (1976)"Geophysical Assessment of Peak Accelerations", Bulletin of the Seismological Society of America, Vol. 66, No. 3, June.

Hanks, T.C. (1979)"b Values and $w^{-\gamma}$ Seismic Source Models: Implications for Tectonic Stress Variations Along Active Crustal Fault Zones and the Estimation of High-Frequency Strong Ground Motion", Journal of Geophysical Research, Vol. 84, No. B5, May.

Hays, W.W., King, K.W. and Park, R.B. (1978)"Duration of Nuclear Explosion Ground Motion", Bulletin of the Seismological Society of America, Vol. 68, No. 4, August.

Heaton, T.H. and Helmberger, D.V. (1978)"Synthesis of San Fernando Strong-Motion Records",Seminar-Workshop on Strong

Grounds, Rancho Santa Fe.

Housner, G.W. (1970)"Design Spectrum", Earthquake Engineering, Robert Wiegel, Editor, Prentice-Hall, Englewood Cliffs, New Jersey.

Housner, G.W. (1975)"Measures of Severity of Earthquake Ground Shaking", Proceedings, U.S. National Conference on Earthquake Engineering, Ann Arbor, Michigan.

Hudson, D.E., Brady, A.G., Trifunac, M.D. and Vijayaraghavan, A. (1971)Strong Motion Earthquake Accelerograms - Volume II, Corrected Accelerograms and Integrated Ground Velocity and Displacement Curves, Earthquake Engineering Research Laboratory, California Institute of Technology, Pasadena, California.

Husid, R. (1967)"Gravity Effects on the Earthquake Response of Yielding Structures", Report of Earthquake Engineering Research Laboratory, California Institute of Technology, Pasadena, California.

Idriss, I.M. and Power, M.S. (1978)"Peak Horizontal Accelerations, Velocities and Displacements on Rock and Stiff Soil Sites for Moderately Strong Earthquakes", Submitted for publication to the Bulletin of the Seismological Society of America.

Kameda, H. (1975)"Evolutionary Spectra of Seismogram by Multifilter", Journal of the Engineering Mechanics Division, Proceedings of the American Society of Civil Engineers, Vol. 101, No. EM6, December.

Kanamori, H. and Jennings, P.C. (1978)"Determination of Local Magnitude, M_L, from Strong Motion Accelerograms, Bulletin of the Seismological Society of America, Vol. 68, No. 2, April.

Kubo, T. and Penzien, J. (1976)"Time and Frequency Domain Analysis of Three-Dimensional Ground Motions, San Fernando Earthquake", EERC 76-6, University of California, Berkeley, California.

Kubo, T. and Penzien, J. (1977)"Characteristics of Three-Dimensional Ground Motions Along Principal Axes, San Fernando Earthquake", Proceedings, 6th World Conference on Earthquake Engineering, New Delhi, India.

Lanners, C.L. (1978)"The 1971 San Fernando Valley Earthquake: Analysis of the Long Period Motion in Soil", Master's Project, Rensselaer Polytechnic Institute, Troy, New York.

Liu, S.C. (1970)"Evolutionary Power Spectral Density of Strong-Motion Earthquakes", Bulletin of the Seismological Society of America, Vol. 60, No. 3, June.

McCann, M.W. and Shah, H.C. (1979)"Determining Strong-Motion Duration of Earthquakes", Bulletin of the Seismological Society of America, Vol. 69, No. 4, August.

Mal, A.K. (1972)"Rayleigh Waves From a Moving Thrust Fault", Bulletin of the Seismological Society of America, Vol. 62, No. 3, June.

Mikumo, T. (1973)"Faulting Process of the San Fernando Earthquake of February 9, 1971, Inferred from Static and Dynamic Near-Field Displacements", Bulletin of the Seismological Society of America, Vol. 63, No. 1, February.

Mooney, H.M. and Bolt, B.A. (1966)"Dispersive Characteristics of the First Three Rayleigh Modes for a Single Surface Layer", Bulletin of the Seismological Society of America, Vol. 56, No.1, February.

Newmark, N.M. et. al. (1977)"Comparison of Building Response and Free Field Motion in Earthquakes", Proceedings, 6th World Conference on Earthquake Engineering, New Delhi, India.

Niazy, A. (1975)"An Exact Solution for a Finite, Two-Dimensional Moving Dislocation in an Elastic Half-Space with Application to the San Fernando Earthquake of 1971", Bulletin of the Seismological Society of America, Vol. 65, No. 6, December.

Officer, C.B. (1958)Introduction to the Theory of Sound Transmission with Application to the Ocean, McGraw-Hill, Inc., New York, New York.

Penzien, J. and Watabe, M. (1975)"Characteristics of 3-Dimensional Earthquake Ground Motions", International Journal of Earthquake Engineering and Structural Dynamics, Vol. 3.

Perez, V. (1973)"Velocity Response Envelope Spectrum as a

Function of Time, for Pacoima Dam, San Fernando Earthquake, February 9, 1971", Bulletin of the Seismological Society of America, Vol. 63, No. 1, February.

Richart, F.E., Woods, R.D. and Hall, J.R. (1970)Vibrations of Soils and Foundations, Prentice-Hall, Inc., Englewood Cliffs, New Jersey.

Schnabel, P.B. and Seed, H.B. (1973)"Accelerations in Rock for Earthquakes in the Western United States", Bulletin of the Seismological Society of America, Vol. 63, No. 2, April.

Seed, H.B. and Idriss, I.M. (1971)"A Simplified Procedure for Evaluating Soil Liquefaction Potential", Journal of the Soil Mechanics and Foundations Division, Proceedings of the American Society of Civil Engineers, Vol. 97, No. SM9, September.

Seed, H.B., Murarka, R., Lysmer, J. and Idriss, I.M. (1976)"Relationships of Maximum Acceleration, Maximum Velocity, Distance from Source and Local Site Conditions for Moderately Strong Earthquakes", Bulletin of the Seismological Society of America, Vol. 66, No. 4, August.

Seekins, L.C. and Hanks, T.C. (1978)"Strong Motion Accelerograms of the Oroville Aftershocks and Peak Acceleration Data", Bulletin of the Seismological Society of America, Vol. 68, No. 3, June.

Shakal, A.F. and Toksoz, M.N. (1978) "Analysis of Source and Medium Effects on Strong Motion Observations", Proceedings of the Second International Conference on Microzonation, San Francisco, California.

Shannon and Wilson, Inc. and Agbabian Associates (1978)"Data from Selected Accelerograph Stations at Wilshire Blvd., Century City, and Ventura Blvd., Los Angeles, California", Report NUREG/CR-0074, NRC-6A, U.S. Nuclear Regulatory Commission.

Shoja-Taheri, J. and Bolt, B.A. (1977)"A Generalized Strong-Motion Accelerogram Based on Spectral Maximization From Two Horizontal Components", Bulletin of the Seismological Society of America, Vol. 67, No. 3, June.

Trifunac, M.D. and Brune, J.H. (1970)"Complexity of Energy Release During the Imperial Valley, California, Earthquake of 1940", Bulletin of the Seismological Society of America,

Vol. 60, No. 1, February.

Trifunac, M.D. (1974)"A Three-Dimensional Dislocation Model for the San Fernando, California, Earthquake of February 9, 1971, Bulletin of the Seismological Society of America, Vol. 64, No. 1, February.

Trifunac, M.D. and Brady, A.G. (1975)"A Study of the Duration of Strong Earthquake Ground Motion", Bulletin of the Seismological Society of America, Vol. 65, No. 3, June.

Vanmarcke, E.H. and Lai, S.P. (1977)"Strong-Motion Duration of Earthquakes", Evaluation of Seismic Safety of Buildings, Report No. 10, Massachusetts Institute of Technology, Cambridge, Massachusetts.

Table 1

Accelerograph Stations and Numbers
San Fernando Earthquake

Caltech Number	Location in California	Rock Site*
C041	Pacoima Dam	x
C048	8244 Orion Blvd. 1st Floor, LA	
C051	250 E. First Street Basement, LA	
C054	445 Figueroa Street, Sub-basement, LA	
D056	Castaic Old Ridge Route	
D057	Hollywood Storage Basement, LA	
D058	Hollywood Storage P.E. Lot, LA	
D059	1901 Ave. of the Stars Sub-basement, LA	
D062	1640 S. Marengo Street 1st Floor, LA	
D065	3710 Wilshire Blvd. Basement, LA	
D068	7080 Hollywood Blvd. Basement, LA	
E071	Wheeler Ridge	
E072	4680 Wilshire Blvd. Basement, LA	
E075	3470 Wilshire Blvd. Sub-basement, LA	
E078	Water and Power Building Basement, LA	x
E081	Santa Felicia Dam Outlet Works	x
E083	3407 6th Street Basement, LA	
F086	Vernon, CMD Building	
F087	Engineering Building, Santa Ana	
F088	633 E. Broadway, Glendale	
F089	808 S. Olive Street, Street Level, LA	
F092	2011 Zonal Avenue Basement, LA	x
F095	120 N Robertson Blvd. Sub-basement, LA	
F098	646 S. Olive Avenue Basement, LA	
F101	Edison Company, Colton	
F102	Ft. Tejon, Tejon	x
F103	Pumping Plant, Pearblossom	
F104	Oso Pumping Plant, Gorman	
F105	UCLA Reactor Laboratory, LA	
G106	Caltech Seismological Lab., Pasadena	x
G107	Caltech Athenaeum, Pasadena	
G108	Caltech Millikan Library Basement, Pasadena	
G110	Jet Propulsion Lab. Basement, Pasadena	
G112	611 W. Sixth Street Basement, LA	
G114	Palmdale Fire Station, Palmdale	
H115	15250 Ventura Blvd. Basement, LA	
H118	8639 Lincoln Avenue Basement, LA	
H121	900 S. Fremont Avenue Basement, Alhambra	
H124	2600 Nutwood Avenue Basement, Fullerton	

Caltech Number	Location in California	Rock Site*
I128	435 N. Oakhurst Ave. Basement, Beverly Hills	
I131	450 N. Roxbury Dr. First Floor, Beverly Hills	
I134	1800 Century Park East Basement (P-3), LA	
I137	15910 Ventura Blvd. Basement, LA	
J141	Lake Hughes, Array Station 1	
J142	Lake Hughes, Array Station 4	x
J143	Lake Hughes, Array Station 9	x
J144	Lake Hughes, Array Station 12	x
J145	15107 Vanowen Street Basement, LA	
J148	616 S. Normandie Avenue Basement, LA	
K157	420 S. Grand Avenue Second Floor, LA	
L166	3838 Lankershim Blvd. Basement, LA	x
L171	S. Calif. Edison Power Plant, San Onofre	
M176	1150 S. Hill Street Sub-basement, LA	
M179	Tehachapi Pumping Plant, Grapevine	x
M180	4000 W. Chapman Avenue Basement, Orange	
M183	6074 Park Drive Ground Level, Wrightwood	
M184	6074 Park Drive Ground Level, Wrightwood	
N185	Carbon Canyon Dam	
N186	Whittier Narrows Dam	
N187	San Antonio Dam	
N188	1880 Century Park East 1st Level Parking, LA	
N191	2516 Via Tejon, Palos Verdes Estates	
N192	2500 Wilshire Blvd. Basement, LA	
N195	San Juan Capistrano	
N196	Long Beach State College, Long Beach	
N197	Anza Post Office, Anza	
O198	Griffith Park Observatory, LA	x
O199	1625 Olympic Blvd. Ground Floor, LA	
O204	215 West Broadway, Long Beach	
O205	Terminal Island, Long Beach	
O206	Hall of Records, San Bernardino	
O207	Reservoir, Fairmont Reservoir	x
O208	University of California, Santa Barbara	
O210	Hemet Fire Station, Hemet	
P214	4867 Sunset Blvd. Basement, LA	
P217	3345 Wilshire Blvd. Basement, LA	
P220	666 W. 19th Street Ground Floor, Costa Mesa	
P221	Santa Anita Reservoir, Arcadia	x
P222	Port Hueneme, Navy Laboratory	
P223	Puddingstone Reservoir, San Dimas	x
P231	9841 Airport Blvd. Basement, LA	
Q233	14724 Ventura Blvd. First Floor, LA	
Q236	1750 N. Orchid Avenue Ground Floor, Hollywood	
Q239	9100 Wilshire Blvd. Basement, Beverly Hills	

Caltech Number	Location in California	Rock Site*
Q241	800 W. First Street First Floor, LA	
R244	222 Figueroa Street First Floor, LA	
R246	6464 Sunset Blvd. Basement, LA	
R249	1900 Avenue of the Stars Basement, LA	
R251	234 Figueroa Street Basement, LA	
R253	535 S. Fremont Avenue Basement, LA	
S255	6200 Wilshire Blvd. Ground Floor, LA	
S258	3440 University Avenue Basement, LA	
S261	1177 Beverly Drive Basement, LA	
S262	5900 Wilshire Blvd. 'B' Lot, LA	
S265	3411 Wilshire Blvd. 5th Basement, LA	
S266	3550 Wilshire Blvd. Basement, LA	
S267	5260 Century Blvd. First Floor, LA	

* Determined from the following sources:
a) Trifunac and Brady (1975)
b) Seed, Murarka, Lysmer and Idriss (1976)
c) Boore, Joyner, Oliver and Page (1978)
d) Grant, Arango and Clayton (1978)
e) Idriss and Power (1978)

Note: The decision about a site being rock is not always an obvious one. The references listed above disagreed about several of the stations considered here. The rock sites included in this table were obtained mainly from references d and e above. Reference d, in particular, contains recent subsurface information and also evaluates work done by other researchers on the subject of site conditions at recording stations.

Table 2

Accelerograms Used to Generate the Probabilistic Model
San Fernando Earthquake

Caltech Number	Location in California
C041	Pacoima Dam
C048	8244 Orion Blvd. 1st Floor, LA
C054	455 Figueroa Street, Sub-basement, LA
E078	Water and Power Building Basement, LA
H115	15250 Ventura Blvd. Basement, LA
I137	15910 Ventura Blvd. Basement, LA
J145	15107 Vanowen Street Basement, LA
K157	420 S. Grand Avenue Second Floor, LA
L166	3838 Lankershim Blvd. Basement, LA
0198	Griffith Park Observatory, LA
9233	14724 Ventura Blvd. First Floor, LA

Table 3

Accelerograms Demonstrating No Discernable Strong Part
San Fernando Earthquake

Caltech Number	Possible reason for failure to identify strong part
C048	Deep soil site
E072	Late triggering of recording device
E081	Late triggering of recording device
F087	88.5 km from epicenter
F092	Late triggering of recording device
F101	107.6 km from epicenter
F102	Late triggering of recording device
F103	Late triggering of recording device
F104	Late triggering of recording device
H118	Proximity of shoreline
H124	76.2 km from epicenter
I137	Deep soil site
J145	Deep soil site
L171	139.8 km from epicenter
M179	Late triggering of recording device
N187	72.1 km from epicenter
N191	Proximity of shoreline
N195	122.6 km from epicenter
N196	Proximity of shoreline
N197	185.7 km from epicenter
O204	Proximity of shoreline
O205	Proximity of shoreline
O206	108.2 km from epicenter
O208	133.4 km from epicenter
P220	Proximity of shoreline
P222	79.3 km from epicenter
P231	Proximity of shoreline
S261	Late triggering of recording device
S267	Proximity of shoreline

Table 4

Characterization Results
San Fernando Earthquake
(see units at end of table)

Caltech Number	t_1	t_1	t_2	Δ	$\bar{a}_{HB}$	$\bar{a}_H$	$\bar{a}_{HF}$
C041	1.7	2.3	8.8	6.5	3033.4	3636.7	3172.6
C048	2.8	2.7			865.8		
C051	0.0	0.0	7.0	7.0	540.5	533.6	474.6
C054	1.8	1.8	7.7	5.9	573.6	575.1	531.3
D056	0.8	0.8	4.7	3.9	1098.4	1280.7	1147.3
D057	1.5	1.4	7.4	6.0	673.0	671.8	637.3
D058	1.5	1.4	7.4	6.0	939.4	936.5	742.7
D059	0.0	0.0	6.6	6.6	572.6	575.3	419.1
D062	4.4	4.4	11.3	6.9	660.5	656.9	598.8
D065	0.0	0.0	6.2	6.2	663.7	661.4	624.0
D068	0.0	0.0	5.5	5.5	437.7	447.3	402.1
E071	0.0	0.0	3.1	3.1	100.5	123.2	80.3
E072	2.6				480.8		
E075	1.3	1.3	7.6	6.3	641.2	637.0	591.7
E078	1.3	1.3	7.4	6.1	561.3	558.5	468.3
E081	0.0				667.8		
E083	1.1	1.2	7.8	6.6	784.2	775.5	641.5
F086	1.7	1.7	7.6	5.9	429.7	432.7	407.1
F087	0.0				133.8		
F088	1.2	1.2	7.2	6.0	1263.6	1263.6	1184.7
F089	4.6	4.6	10.6	6.0	627.4	627.4	532.3
F092	0.0				358.9		
F095	2.5	2.7	9.0	6.3	453.1	480.4	435.7
F098	4.9	4.9	10.9	6.0	800.1	800.1	608.3
F101	1.3				172.3		
F102	0.0				103.3		
F103	0.2				495.2		
F104	0.0				304.8		
F105	2.3	2.6	8.6	6.0	394.2	398.4	329.0
G106	2.9	3.0	9.5	6.5	633.5	617.1	527.1
G107	5.0	5.0	11.9	6.9	491.4	484.0	447.4
G108	4.5	4.3	12.2	7.9	743.3	688.5	655.3
G110	1.8	1.8	8.2	6.4	680.0	670.8	629.8
G112	2.0	2.2	8.0	5.8	431.2	437.8	382.0
G114	1.1	0.9	6.7	5.8	582.0	595.2	476.8
H115	4.1	4.1	9.7	5.6	896.7	897.6	819.6
H118	1.0				130.7		
H121	6.0	6.0	13.2	7.2	569.6	555.3	469.4

Caltech Number	t_{1B}	t_1	t_2	Δ	$\bar{a}_{HB}$	$\bar{a}_H$	$\bar{a}_{HF}$
H124	8.8	8.6			159.4		
I128	5.1	5.1	13.0	7.9	370.0	362.2	332.1
I131	6.4	6.6	12.8	6.2	694.1	712.0	621.1
I134	6.0	6.2	13.0	6.8	449.5	459.8	424.8
I137	4.9	4.8			591.2		
J141	2.1	2.0	5.4	3.4	557.5	696.2	663.5
J142	2.0	2.0	5.2	3.2	589.2	734.9	475.6
J143	0.0	0.0	3.6	3.6	432.6	530.3	340.6
J144	0.8	0.8	3.8	3.0	1208.1	1584.8	1172.7
J145	1.5	1.6			542.0		
J148	5.6	5.6	13.2	7.6	600.6	570.2	507.6
K157	-	2.9	8.7	5.8	595.0	598.2	539.1
L166	1.8	1.6	7.5	5.9	641.8	642.6	578.0
L171	2.4				66.4		
M176	2.5	2.4	10.2	7.8	457.3	460.5	403.3
M179	0.0				136.2		
M180	1.3	1.5	7.8	6.3	141.0	147.1	142.2
M183	6.7	6.7	13.4	6.7	212.1	212.1	183.0
M184	4.1	4.1	10.8	6.7	215.9	217.3	187.7
N185	1.1	1.3	8.1	6.8	339.0	344.0	294.3
N186	0.3	0.0	6.3	6.3	439.7	430.9	327.5
N187	0.0				283.6		
N188	5.7	5.7	12.8	7.1	592.2	607.7	560.3
N191	0.6				137.5		
N192	4.1	4.1	11.0	6.9	477.6	484.0	395.2
N195	9.7	9.7			158.7		
N196	1.4	1.0			194.7		
N197	8.3				144.7		
O198	3.5	3.5	10.0	6.5	828.3	818.1	747.8
O199	6.3	6.5	12.9	6.4	748.6	768.5	657.4
O204	0.0				101.1		
O205	1.8				124.5		
O206	6.5	5.9			172.0		
O207	0.0	0.0	2.9	2.9	296.4	401.9	366.0
O208	2.7				85.4		
O210	2.2	4.2	10.3	6.1	159.8	169.9	139.0
P214	1.0	1.1	7.2	6.1	823.9	824.1	770.2
P217	1.1	1.2	7.9	6.7	489.0	490.1	449.1
P220	0.0				140.9		
P221	0.6	0.0	4.6	4.6	639.6	677.6	333.6
P222	0.5				123.9		
P223	2.5	0.0	5.3	5.3	246.4	263.2	206.9
P231	0.0				156.4		
Q233	4.9	4.9	10.8	5.9	1123.1	1125.5	930.2
Q236	4.6	4.8	10.7	5.9	643.3	649.2	503.9

Caltech Number	t_{1B}	t_1	t_2	Δ	$\bar{a}_{HB}$	$\bar{a}_H$	$\bar{a}_{HF}$
♀239	4.8	5.0	12.2	7.2	631.6	641.9	553.8
♀241	6.2	6.3	12.4	6.1	535.0	538.2	494.7
R244	5.2	5.5	11.2	5.7	575.7	588.5	561.7
R246	5.0	5.1	10.8	5.7	553.8	559.1	501.7
R249	5.0	5.1	11.8	6.7	422.8	427.7	376.0
R251	2.9	3.2	10.2	7.0	779.2	785.4	752.1
R253	5.9	5.9	12.1	6.2	821.3	845.0	744.8
S255	1.0	1.1	7.0	5.9	588.8	593.6	542.0
S258	4.8	6.6	12.0	5.4	317.3	377.4	363.8
S261	0.0				473.2		
S262	-	2.0	8.7	6.7	339.6	423.5	419.5
S265	5.9	5.9	12.5	6.6	526.9	519.5	390.7
S266	5.6	5.6	13.1	7.5	651.1	620.1	560.8
S267	6.2	6.3			229.8		

units:
t_{1B} - sec
t_1 - sec
t_2 - sec
Δ - sec
$\bar{a}_{HB}$ - mm/sec/sec
$\bar{a}_H$ - mm/sec/sec
$\bar{a}_{HF}$ - mm/sec/sec

Table 5

Characterization Results
San Fernado Earthquake
(see units at end of table)

Caltech Number	a_{PH}	v_{PH}	$\bar{v}_H$	*	d_H	d_E	azimuth
C041	13563.0	121.4	42.0	x	15.9	9.1	159.6
C048	2709.0	31.6			25.9	22.4	199.6
C051	1230.0	21.9	8.5	x	44.7	42.8	159.6
C054	1500.0	17.4	7.6		43.9	41.9	161.5
D056	3331.0	28.9	10.6	x	31.4	28.6	305.9
D057	1592.0	21.2	9.7	x	39.3	37.1	168.7
D058	2112.0	21.6	9.8		39.3	37.1	168.7
D059	1623.0	18.1	8.1	x	41.8	39.8	184.0
D062	1482.0	19.6	9.4	x	44.8	42.8	155.6
D065	1617.0	22.4	9.0		42.0	40.0	166.3
D068	985.0	14.5	7.1		37.3	35.0	169.6
E071	271.0	2.5	1.1	x	87.0	86.0	321.6
E072	1177.0	23.9			41.6	39.5	169.3
E075	1456.0	24.1	10.0	x	42.1	40.1	165.9
E078	1736.0	23.4	8.8	x	44.5	42.5	160.5
E081	2556.0	10.1			35.3	32.9	279.8
E083	1703.0	18.5	9.5	x	42.1	40.0	165.4
F086	1050.0	18.1	5.7		51.1	49.4	157.5
F087	293.0	9.0			89.4	88.5	145.9
F088	3053.0	33.1	16.7	x	36.5	34.1	154.9
F089	1645.0	21.6	9.2		45.9	44.0	161.4
F092	801.0	13.8			45.0	43.1	154.7
F095	1022.0	19.1	9.6		39.6	37.4	175.5
F098	2420.0	21.8	9.2	x	44.6	42.7	161.1
F101	402.0	3.1			108.4	107.6	111.0
F102	257.0	1.4			69.7	68.5	317.7
F103	1492.0	5.6			47.2	45.4	76.2
F104	1032.0	8.6			53.6	52.2	325.6
F105	996.0	9.7	5.1	x	40.8	38.7	188.3
G106	1888.0	11.6	4.9	x	38.4	36.1	143.8
G107	1126.0	14.6	5.9	x	41.8	39.8	139.4
G108	1980.0	16.7	7.5	x	41.8	39.8	140.0
G110	2082.0	15.1	6.4	x	34.1	31.5	138.0
G112	1146.0	17.2	7.2	x	44.5	42.5	160.9
G114	1362.0	14.1	7.1	x	34.8	32.3	55.2
H115	2210.0	30.2	5.9		32.1	29.3	193.0
H118	381.0	14.4			51.9	50.2	183.9
H121	1446.0	20.0	7.2	x	45.0	43.1	147.1

Caltech Number	a_{PH}	v_{PH}	$\bar{v}_H$	*	d_H	d_E	azimuth
H124	362.0	5.9			77.3	76.2	140.9
I128	950.0	16.6	7.9	x	39.3	37.1	175.7
I131	1843.0	17.3	7.5	x	40.3	38.2	184.4
I134	1054.0	17.2	7.8	x	41.0	38.9	174.5
I137	1580.0	24.0			31.8	29.0	195.9
J141	1480.0	18.6	9.4	x	32.3	29.6	350.8
J142	1698.0	9.8	4.2	x	29.8	26.8	342.5
J143	1275.0	5.7	2.8	x	29.6	26.6	325.2
J144	3911.0	19.3	6.9	x	26.7	23.3	319.7
J145	1179.0	32.8			28.0	24.7	193.3
J148	1328.0	19.2	8.7	x	42.0	39.9	166.1
K157	1807.0	18.8	7.9	x	43.1	41.1	161.3
L166	1780.0	15.0	6.6	x	33.4	30.8	170.9
L171	161.0	3.0			140.4	139.8	145.8
M176	1170.0	21.2	9.6		44.8	42.9	161.7
M179	480.0	2.8			71.9	70.7	326.4
M180	332.0	8.5	1.4		85.3	84.3	146.0
M183	568.0	4.0	1.6	x	72.0	70.8	94.3
M184	575.0	4.9	1.6	x	72.0	70.8	94.3
N185	757.0	4.5	2.0	x	76.7	75.6	136.7
N186	1161.0	10.0	3.7		55.6	54.1	143.4
N187	763.0	3.7			73.3	72.1	112.8
N188	1314.0	18.4	8.1	x	41.0	38.9	183.2
N191	401.0	5.4			69.1	67.8	177.7
N192	1184.0	19.6	7.9	x	42.7	40.7	163.6
N195	418.0	5.0			123.2	122.6	146.4
N196	410.0	10.1			76.5	75.4	159.1
N197	363.0	2.8			186.1	185.7	120.3
O198	1932.0	20.2	9.4	x	36.4	34.0	163.1
O199	2393.0	21.5	9.4		43.9	42.0	163.2
O204	271.0	10.3			74.9	73.8	164.8
O205	313.0	10.5			74.8	73.6	167.0
O206	444.0	4.3			109.0	108.2	108.0
O207	1167.0	9.1	3.4	x	35.3	32.8	355.1
O208	196.0	3.7			134.0	133.4	270.5
O210	397.0	3.3	1.4		152.0	151.4	119.6
P214	1906.0	24.3	10.2	x	38.5	36.2	163.6
P217	1200.0	17.0	8.1	x	42.1	40.0	165.4
P220	344.0	7.7			96.7	95.8	152.6
P221	1943.0	7.6	4.0	x	45.2	43.3	125.4
P222	343.0	7.9			80.3	79.3	248.8
P223	698.0	4.6	2.0	x	66.2	65.0	123.4
P231	484.0	13.5			53.3	51.7	176.6
Q233	2767.0	34.3	8.5		32.1	29.3	191.3
Q236	1719.0	14.6	6.9	x	37.3	34.9	168.9

Caltech Number	a_{PH}	v_{PH}	$\overline{v}_H$	*	d_H	d_E	azimuth
Q239	1638.0	21.2	9.4	x	40.5	38.4	176.2
Q241	1418.0	19.9	8.0	x	43.8	41.8	160.1
R244	1504.0	19.1	8.2		43.8	41.9	160.0
R246	1263.0	18.7	8.6	x	38.0	35.7	167.9
R249	952.0	18.0	8.5	x	41.3	39.2	184.7
R251	2125.0	19.8	9.3	x	43.8	41.8	160.9
R253	2796.0	19.4	9.0	x	44.0	42.0	161.4
S255	1306.0	24.0	8.6		41.0	38.9	175.5
S258	844.0	19.4	8.3	x	46.5	44.6	165.3
S261	1130.0	19.3			41.7	39.6	175.4
S262	945.0	28.3	11.1	x	39.9	37.7	174.9
S265	1328.0	19.5	7.7		42.0	39.9	166.1
S266	1595.0	22.3	8.8		42.1	40.0	165.9
S267	694.0	14.0			53.6	52.0	175.0

* v_{PH} in interval t_1 to t_2

units:
a_{PH} - mm/sec/sec
v_{PH} - cm/sec
$\overline{v}_H$ - cm/sec
d_H - distance to hypocenter - km
d_E - distance to epicenter - km
azimuth - measured clockwise with respect to the north - deg

Table 6

Results of Least Squares Analysis
San Fernando Earthquake
($y = cx^d$)

Graph			c	d	r
a_{PH}	vs	distance to hypocenter	4.22*10**5	-1.54	.86
a_{PH}	vs	distance to epicenter	2.42*10**5	-1.41	.86
$\bar{a}_{HB}$	vs	distance to hypocenter	1.17*10**5	-1.46	.85
$\bar{a}_{HB}$	vs	distance to epicenter	6.67*10**4	-1.33	.85
$\bar{a}_H$	vs	distance to hypocenter	1.20*10**5	-1.43	.83
$\bar{a}_H$	vs	distance to hypocenter*	2.80*10**5	-1.68	.87
$\bar{a}_H$	vs	distance to epicenter	5.67*10**4	-1.25	.84
$\bar{a}_H$	vs	distance to epicenter*	5.44*10**4	-1.26	.89
v_{PH}	vs	distance to hypocenter	3.01*10**3	-1.40	.80
v_{PH}	vs	distance to epicenter	1.76*10**3	-1.28	.80
$\bar{v}_H$	vs	distance to hypocenter	2.03*10**3	-1.52	.74
$\bar{v}_H$	vs	distance to epicenter	8.16*10**2	-1.30	.73

* Rock sites only (see Table 1)
r = coefficient of correlation

Table 7

San Fernando Valley Accelerograph Site Characteristics
San Fernando Earthquake

Caltech Number	C048	H115	I137	J145	Q233
Station Location	34.22 N 118.47 W	34.15 N 118.46 W	34.16 N 118.48 W	34.20 N 118.46 W	34.15 N 118.46 W
Distance to Hypocenter (km)	25.9	32.1	31.8	28.0	32.1
Distance to Epicenter (km)	22.4	29.3	29.0	24.7	29.3
Distance to Fault* (km)	7.7	15.0	14.8	10.7	15.4
Azimuth (deg)	199.6	193.0	195.9	193.3	191.3
Building Type	7-story RC	12-story RC	17-story Steel	7-story RC	12-story RC
Depth of Alluvium** (ft)	1000	80	80	1000	80
Depth to Basement Rock** (ft)	13900	6000	6000	9500	6000

* From Boore, Joyner, Oliver and Page (1978)
** From Duke et. al. (1971)

Table 8

Minimum and Maximum Values of Phi and Z Rms
During Rayleigh Wave Motion
San Fernando Earthquake

Caltech Number	Phi (deg)	Theta (deg)	Time (sec)	Wave Period (sec)	
C048	9.8		18.53		
	89.3	47.2	19.05		
	4.3		19.53	2.26	(20.79-18.53)
	89.8	29.9	20.57	2.72	(21.77-19.05)
	14.5		20.79	2.82	(22.35-19.53)
	88.2	40.7	21.77		
	23.0		22.35		
J145	9.2		23.09		
	89.9	29.2	23.57		
	17.8		24.03	2.08	(25.17-23.09)
	88.3	52.5	24.77	2.50	(26.07-23.57)
	14.3		25.17	2.74	(26.77-24.03)
	89.3	78.2	26.07		
	23.6		26.77		

Caltech Number	Z Rms Acc (mm/sec/sec)	Time (sec)	Wave Period (sec)	
C048	623.4	18.61		
	353.1	19.05		
	569.5	19.55	2.42	(21.03-18.61)
	240.3	20.43	2.74	(21.79-19.05)
	558.9	21.03	2.72	(22.27-19.55)
	191.4	21.79		
	426.9	22.27		
J145	441.5	23.01		
	164.6	23.59		
	465.1	24.19	2.32	(25.33-23.01)
	171.0	24.77	2.50	(26.09-23.59)
	345.7	25.33	2.66	(26.85-24.19)
	111.8	26.09		
	231.1	26.85		

Table 9

Geologic Structure at 8244 Orion Boulevard (C048)
San Fernando Valley
(from Duke et. al., 1971)

Layer Number	Geologic Unit	Thickness (ft)	V_P (ft/sec)	V_S (ft/sec)	Unit Weight (cu ft)
1		40	1410	635	105
2		60	3300	1485	111
3		100	4680	2100	113
4	Alluvium	100	5355	2400	114
5		100	5760	2590	115
6		200	6190	2785	119
7		200	6590	2965	120
8	_____	200	6900	3100	123
9		340	7220	3610	126
10		720	7610	3805	128
11		900	7741	3870	129
12		220	8679	4335	133
13		400	9114	4557	134
14		460	8308	4154	145
15		1340	10331	5165	144
16	Sedimentary	320	9060	4983	147
17	Rock	640	9790	5385	146
18		660	8850	4868	152
19		1000	9950	5375	155
20		1000	10400	5690	155
21		1000	10800	6480	156
22		1000	11150	6690	161
23		1000	11550	6930	167
24	_____	1900	11890	7130	172
25	Basement Rock		17000	11050	172

Table 10

Geologic Structure at 15107 Vanowen Street (J145)
San Fernando Valley
(from Duke. et. al., 1971)

Layer Number	Geologic Unit	Thickness (ft)	V_P (ft/sec)	V_S (ft/sec)	Unit Weight (cu ft)
1		10	1270	570	107
2		15	1730	780	107
3		50	3180	1430	117
4		25	3710	1670	124
5		100	4100	1850	137
6	Alluvium	100	5100	2300	137
7		100	5840	2630	137
8		100	6350	2960	137
9		100	7000	3160	137
10		100	7800	3520	137
11	_____	300	8600	3880	148
12		1000	9000	4500	148
13		1000	9950	4980	148
14		1000	10600	5300	148
15	Sedimentary	1000	10850	5420	148
16	Rock	1000	11500	6320	148
17		1000	11700	6440	148
18		1000	12000	6600	148
19	_____	1500	12600	7310	152
20	Basement Rock		16000	10400	170

Table 11

Geologic Structure at Ventura Stations (H115, I137 and Q233)
San Fernando Valley
(from Duke et. al., 1971)

Layer Number	Geologic Unit	Thickness (ft)	V_P (ft/sec)	V_S (ft/sec)	Unit Weight (cu ft)
1	Alluvium	40	1300	620	112
2		40	5280	1180	124
3		20	5560	2500	148
4		100	6100	2740	148
5		100	6580	2960	148
6		100	7000	3150	148
7		200	7420	3440	148
8	Sedimentary	200	7850	3530	148
9	Rock	200	8260	3720	148
10		1000	9000	4500	148
11		1000	10000	5000	148
12		1000	10600	5300	152
13		1000	11140	5570	152
14		1000	11600	6370	152
15	Basement Rock		16000	10400	166

Table 12

Velocity of the Fundamental Rayleigh Mode
For a Period of 2.5 Seconds
San Fernando Valley
(courtesy of Dr. D. Harkrider of Caltech)

Caltech Number	C048	J145	H115 I137 Q233
Profile Used	Table 9	Table 10	Table 11
Phase Velocity (ft/sec)	4100	5200	6300
Group Velocity (ft/sec)	2900	3400	3000
Hor/Vert Displacement at Surface	1.0	1.1	0.9

LIST OF SYMBOLS

$a(t)$	accleration time history
$a_H(t)$	horizontal plane acceleration
$\bar{a}(t)$	moving time window rms acceleration
$\bar{a}_H$	horizontal plane rms acceleration
$\bar{a}_{HB}$	horizontal plane rms acceleration (Berrill)
a_{PH}	peak horizontal plane acceleration
$d(t)$	displacement time history
$e(t)$	response envelope
$f(w)$	Fourier amplitude spectrum
$[G(t)]$	moving time window intensity tensor
$h(t)$	Husid plot
I_A	Arias Intensity
n	damping ratio
r	correlation coefficient
$S(w)$	power spectral density
t_f	total earthquake duration
t_1	beginning of strong earthquake shaking
t_2	end of strong earthquake shaking
t_{1B}	beginning of strong earthquake shaking (Berrill)
v	equivalent frequency
$v(t)$	velocity time history
$\bar{v}_H$	horizontal plane rms velocity
v_{PH}	peak horizontal plane velocity
V_P	P-wave velocity
V_S	S-wave velocity
w	frequency
Δ	duration of strong earthquake shaking
δ	width of moving time window

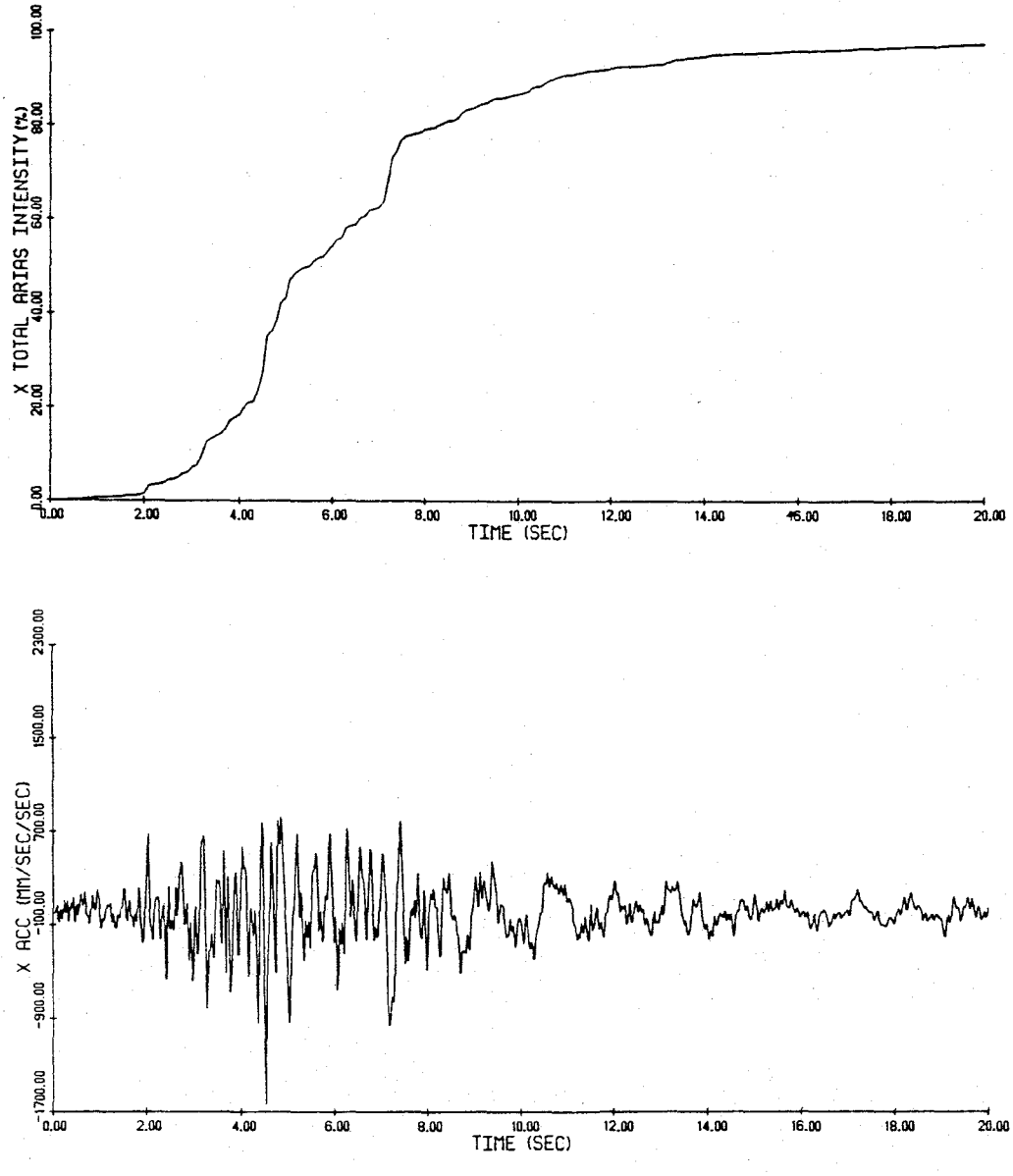

Figure 1 - Husid and ground acceleration plots, NS component, 3838 Lankershim Boulevard (L166)

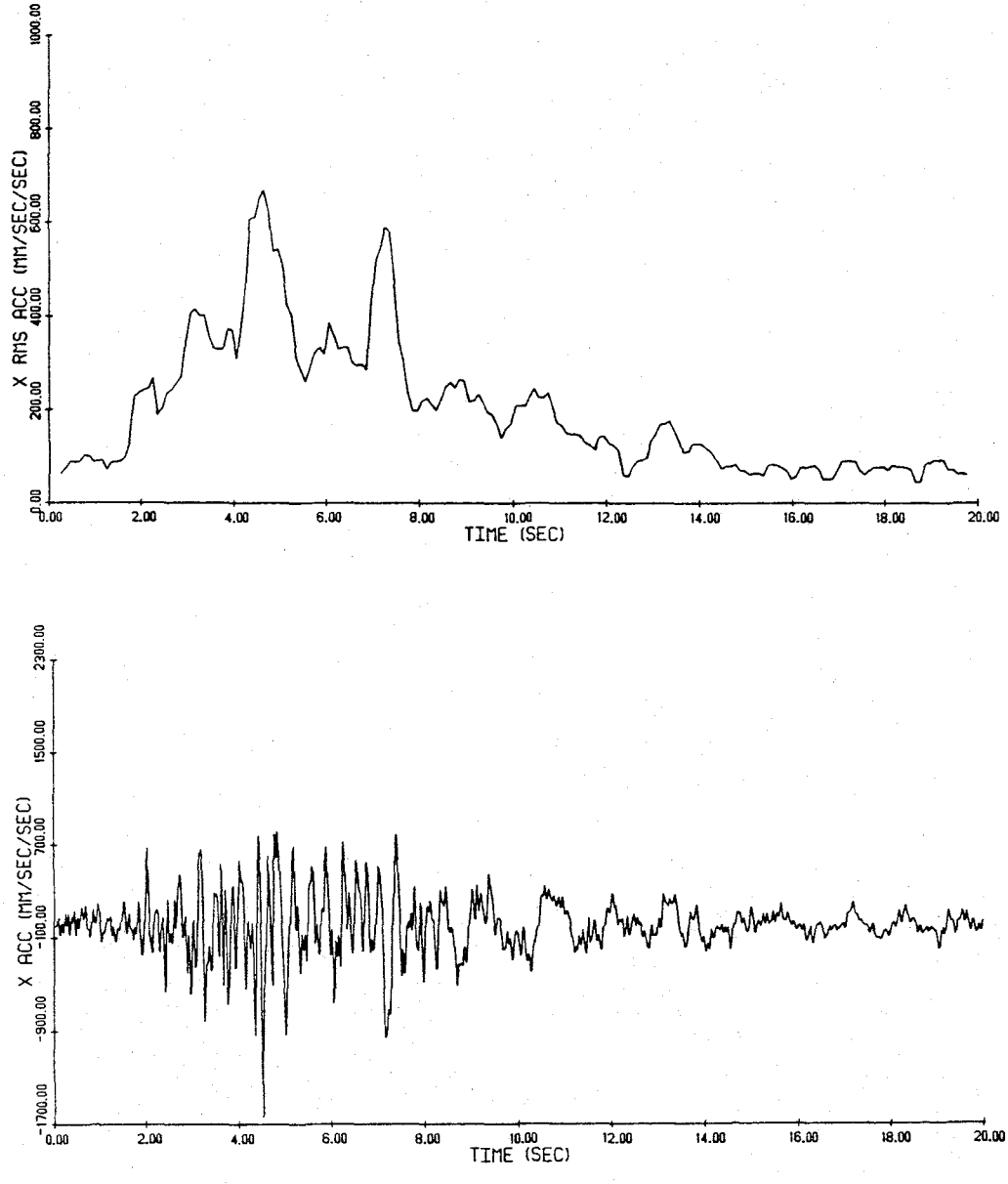

Figure 2 - Moving time window rms acceleration and ground acceleration plots, NS component, 3838 Lankershim Boulevard (L166)

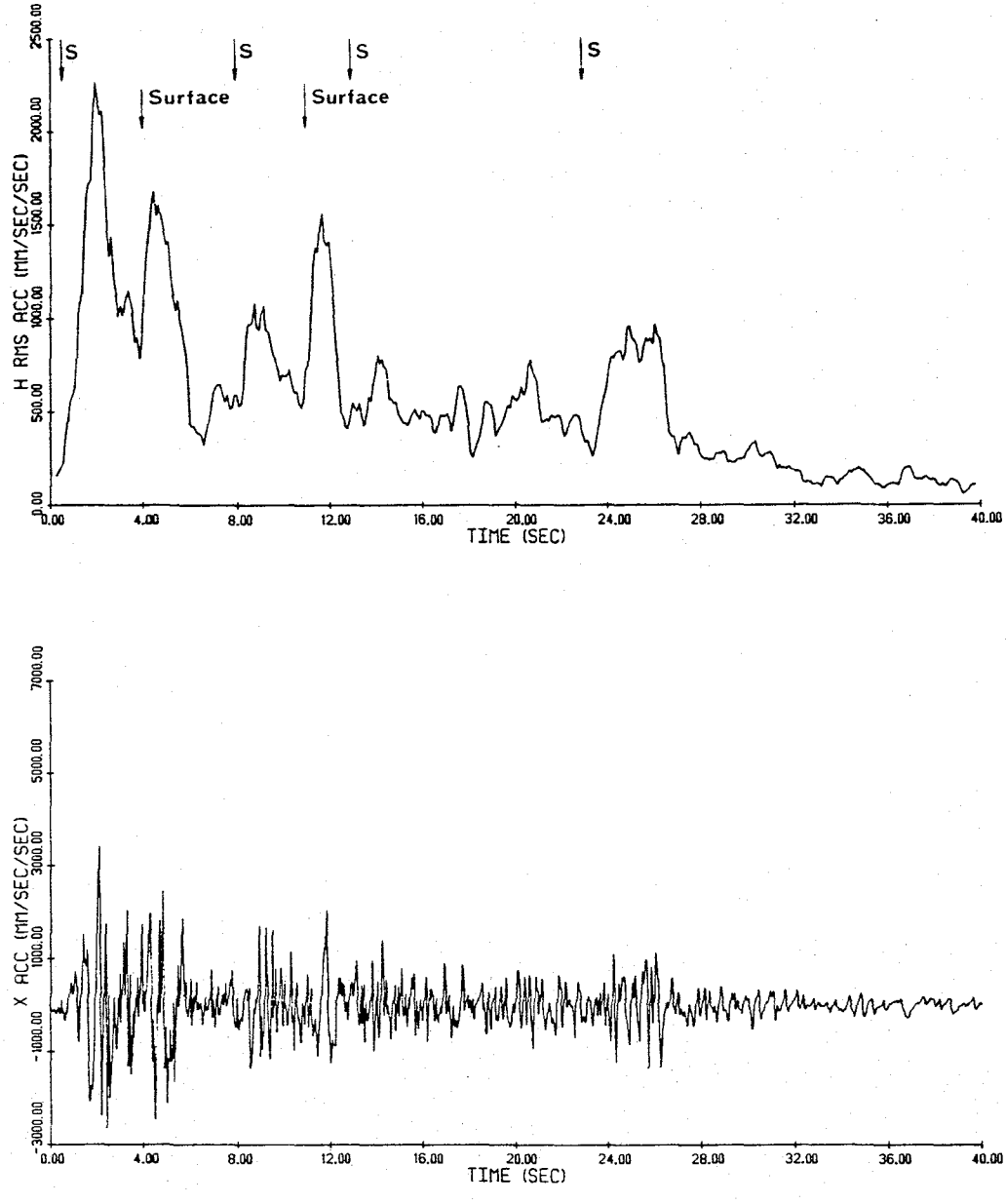

Figure 3 - Horizontal moving time window rms acceleration and NS ground acceleration plots, El Centro, 1940

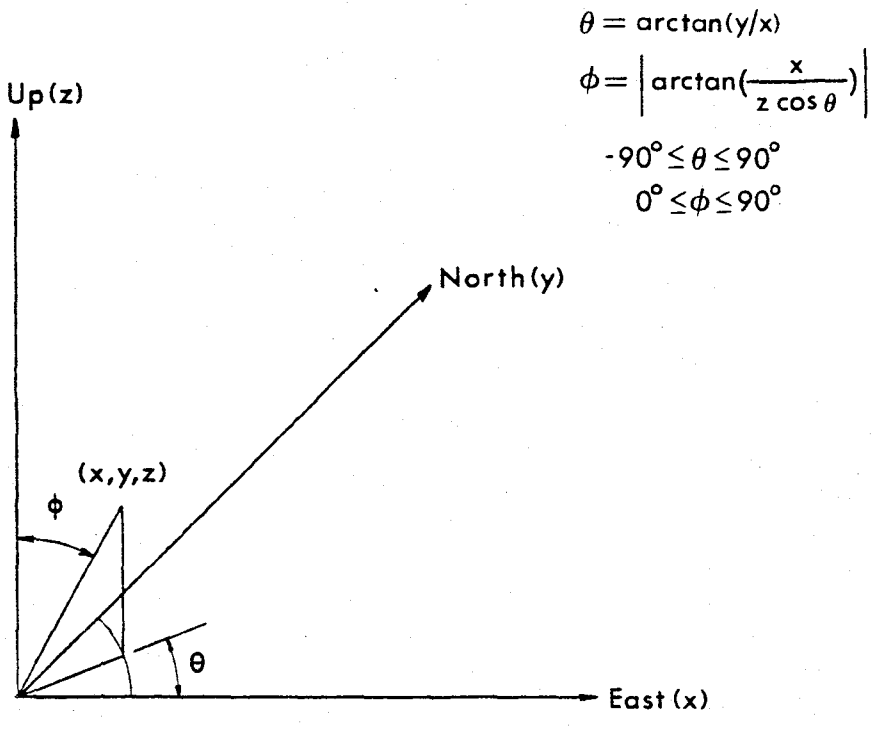

Figure 4 - Definition of phi and theta angles

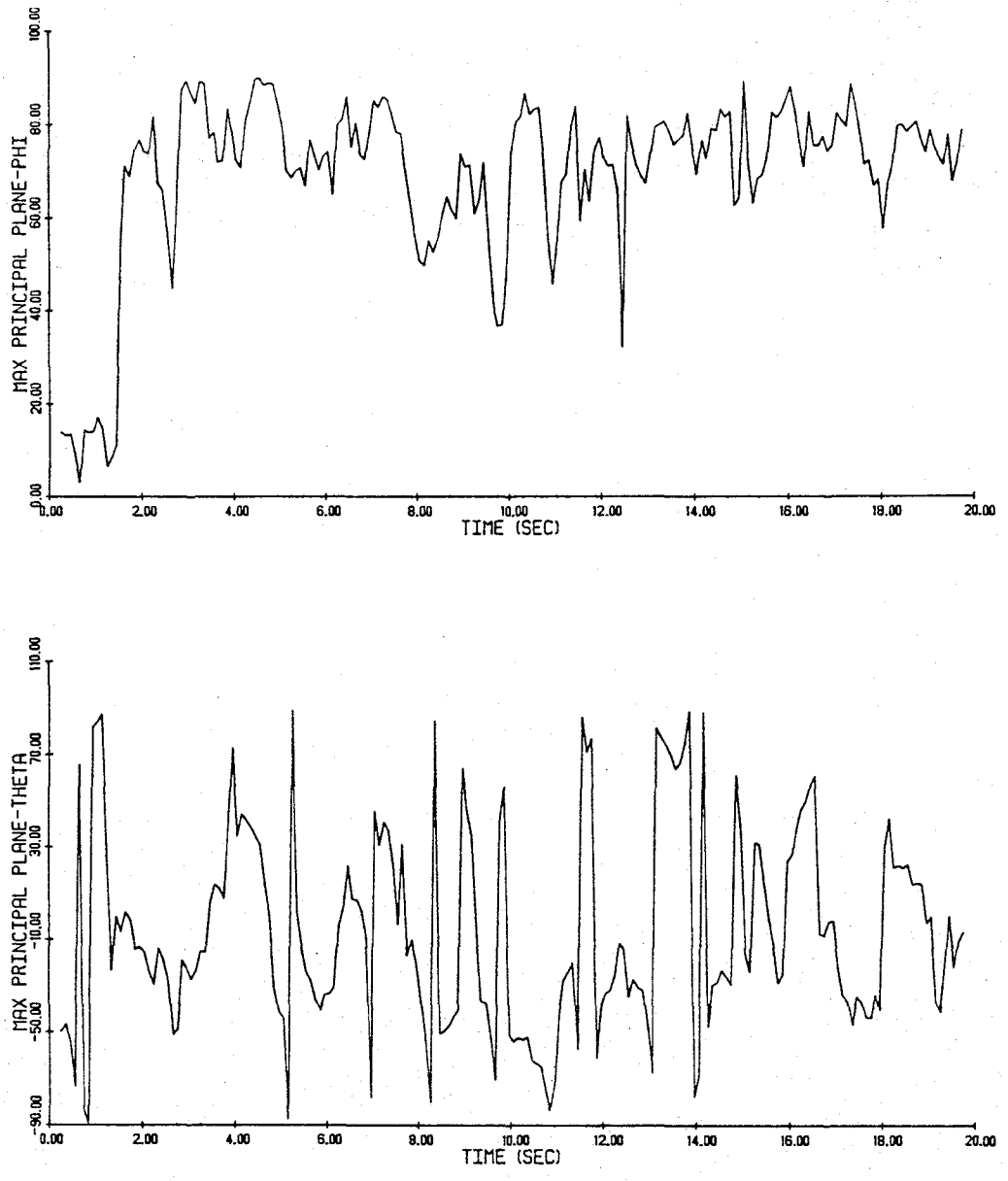

Figure 5 - Phi and theta angle maximum principal plane plots, 3838 Lankershim Boulevard (L166)

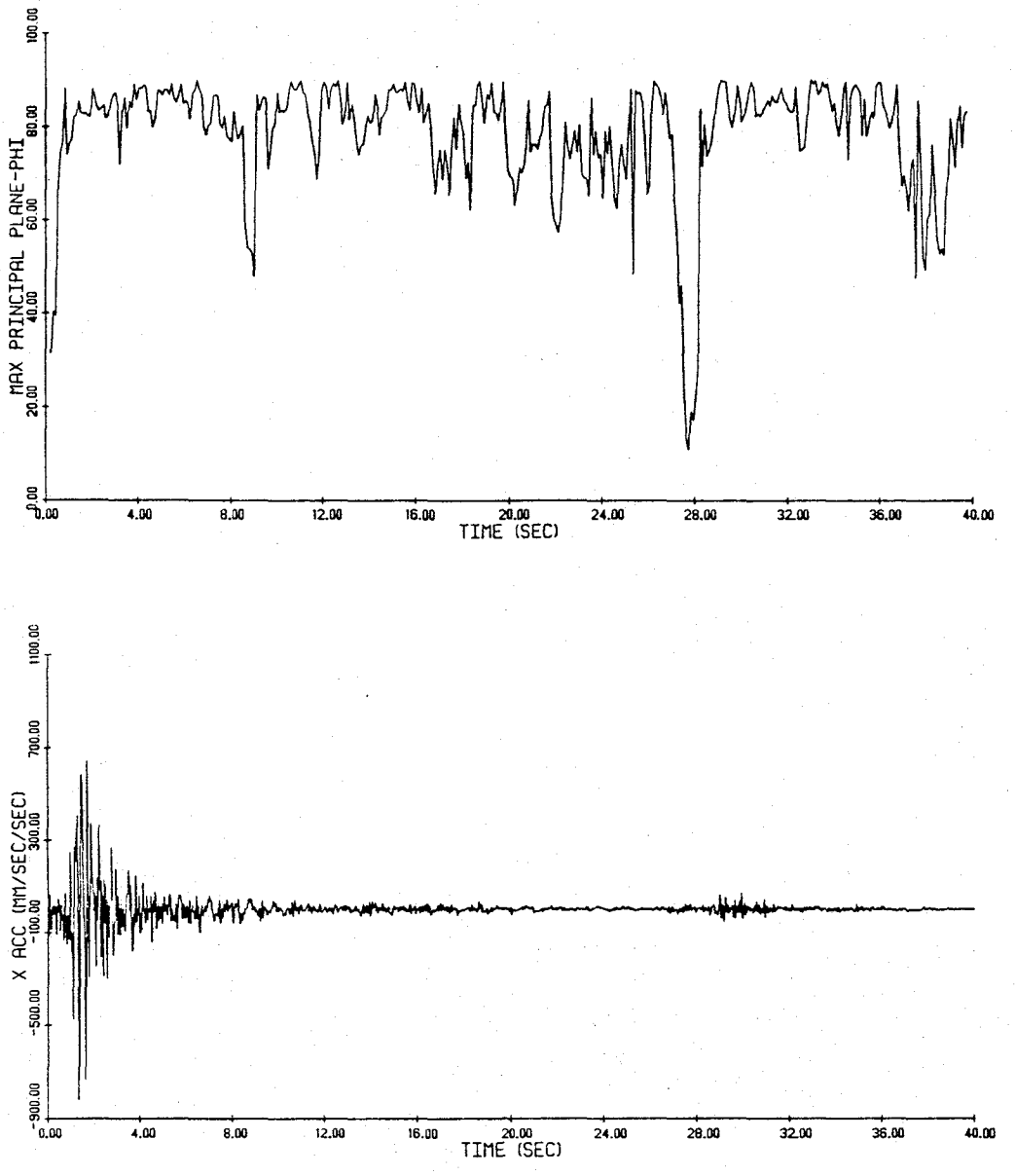

Figure 6 - Maximum principal plane phi and N10E ground acceleration plots, Golden Gate Park, 1957 San Francisco Earthquake

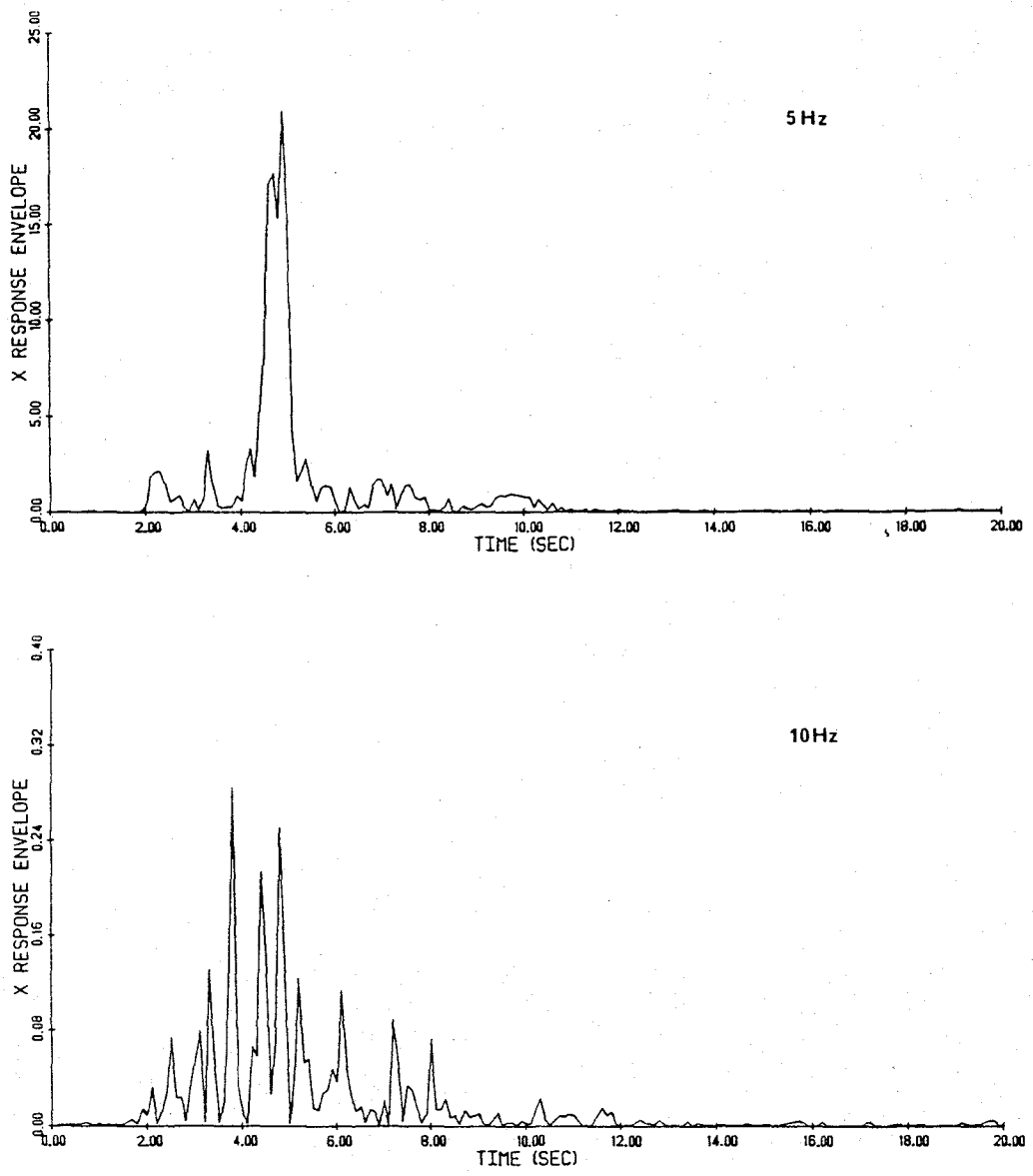

Figure 7 - 5 and 10 Hz response envelope plots, 3838 Lankershim Boulevard (L166)

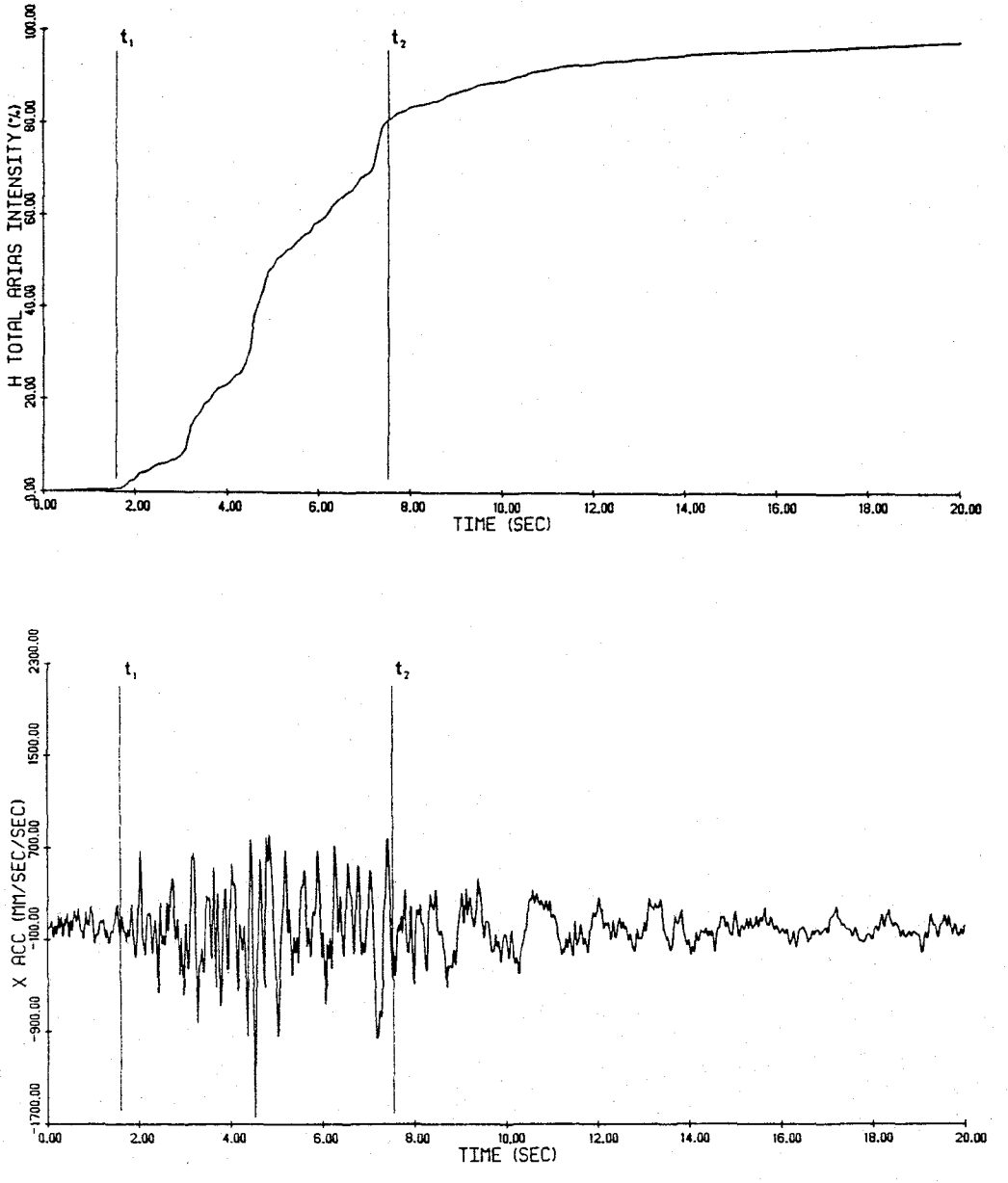

Figure 8 - Horizontal Husid and NS ground acceleration plots, 3838 Lankershim Boulevard (L166)

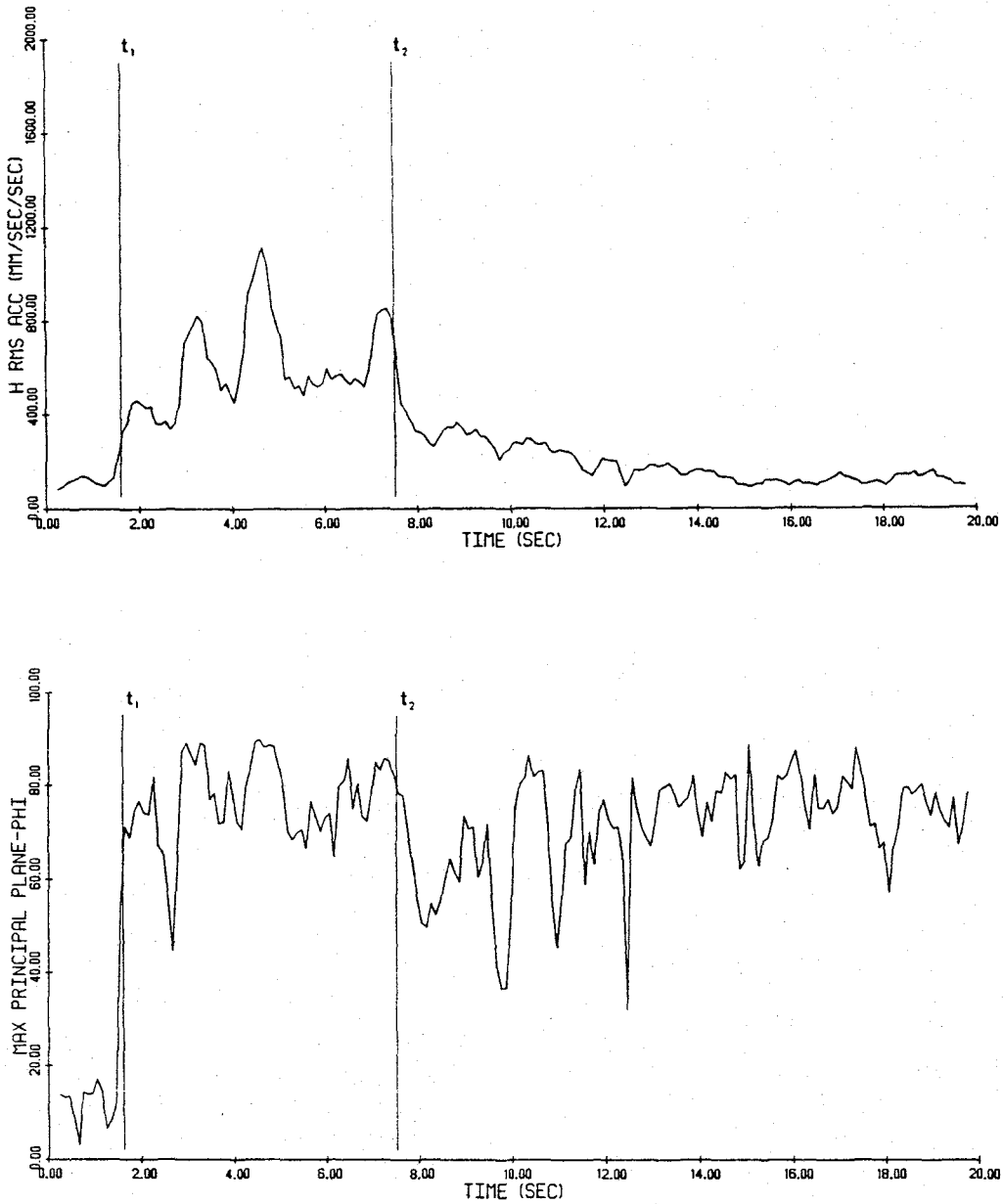

Figure 9 - Horizontal moving time window rms acceleration and maximum principal plane phi plots, 3838 Lankershim Blvd. (L166)

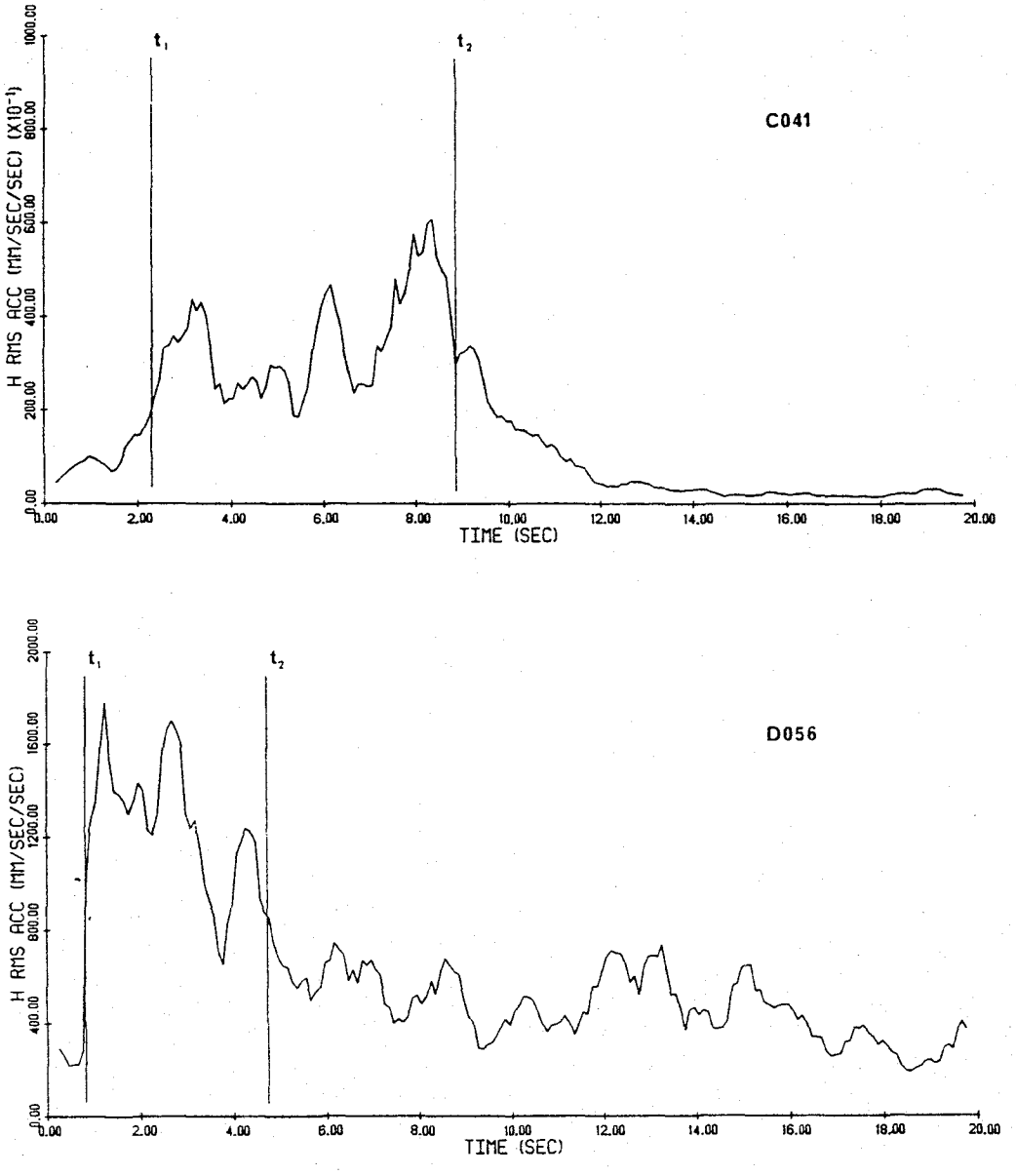

Figure 10 - Horizontal moving time window rms acceleration plots at Pacoima Dam (C041) and Castaic Old Ridge Route (D056)

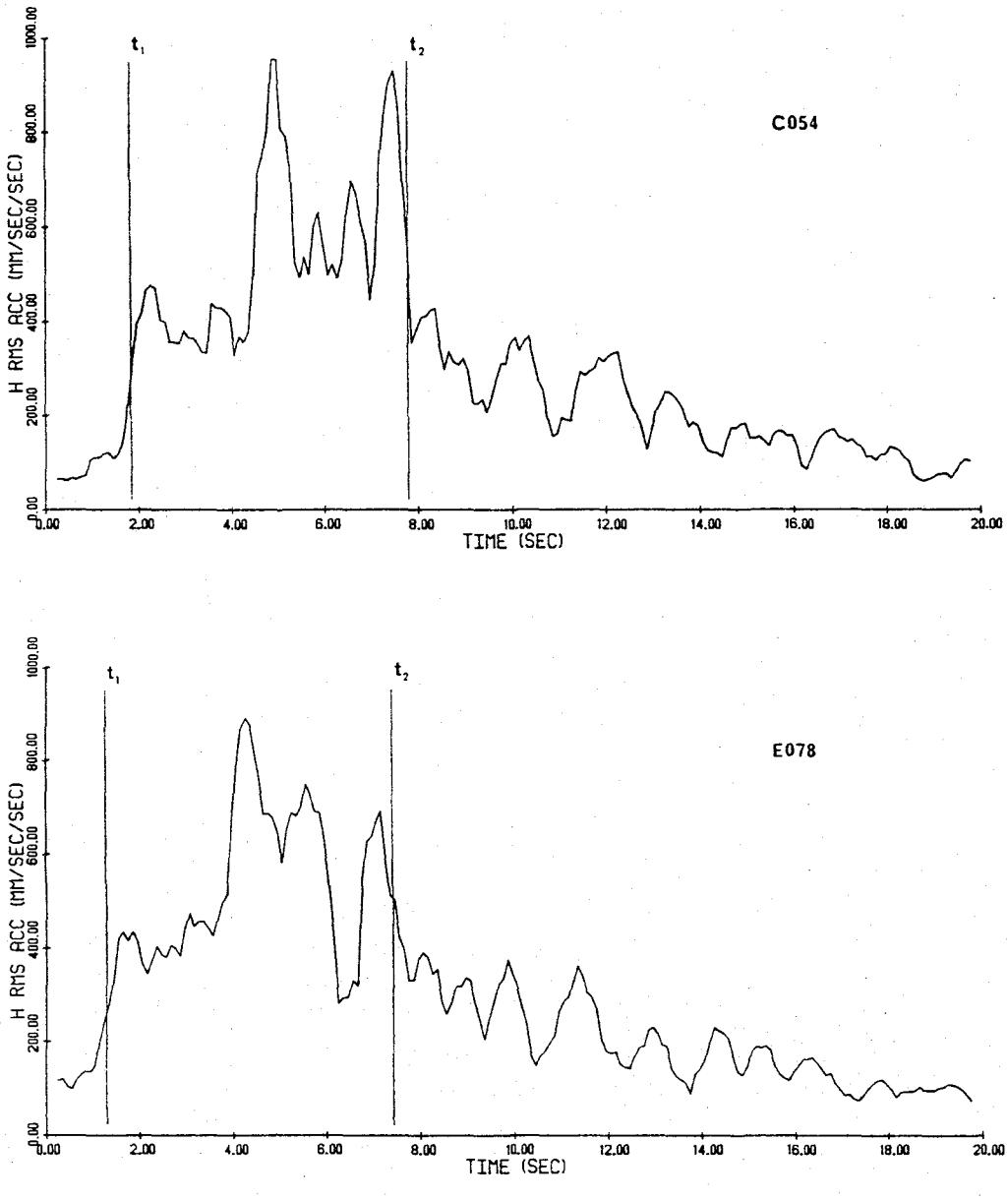

Figure 11 - Horizontal moving time window rms acceleration plots at 445 Figueroa (C054) and Water and Power Building (E078)

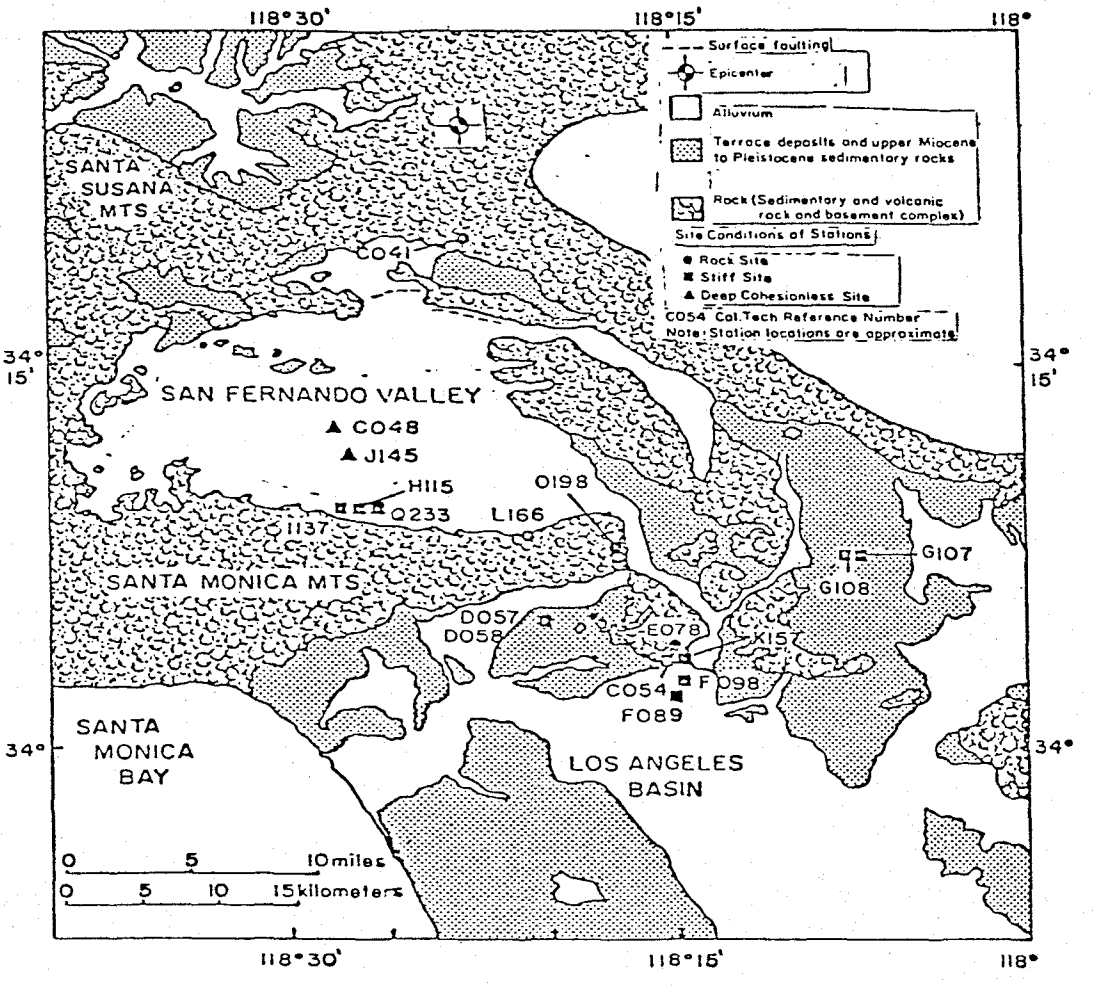

Figure 12 -- Map of the Los Angeles area

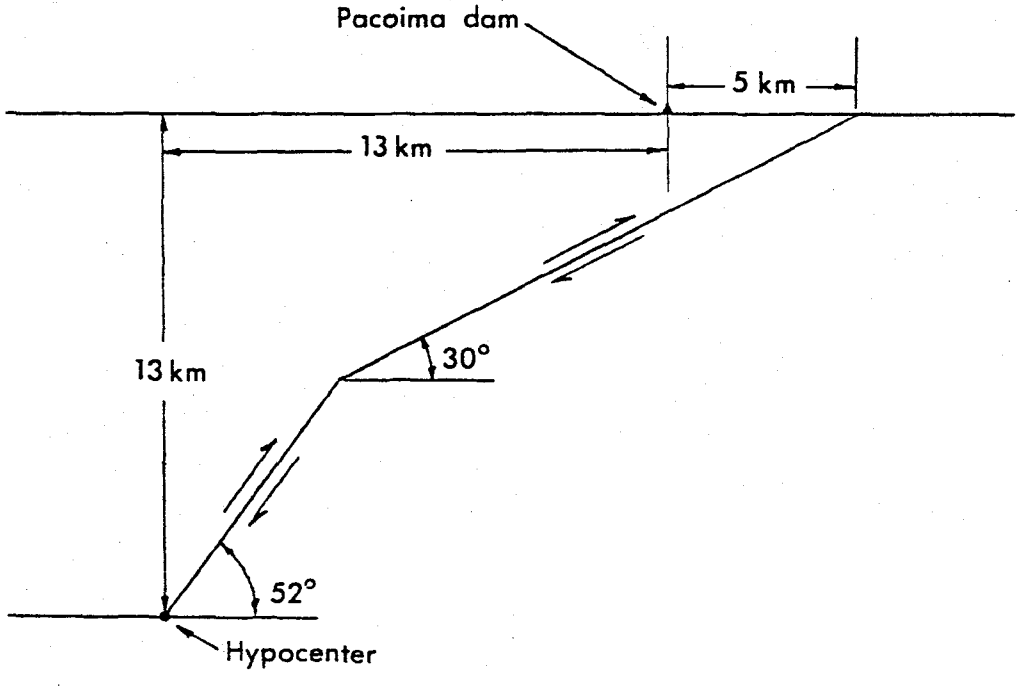

Figure 13 - Idealized fault plane geometry, 1971 San Fernando Earthquake (Bouchon, 1978)

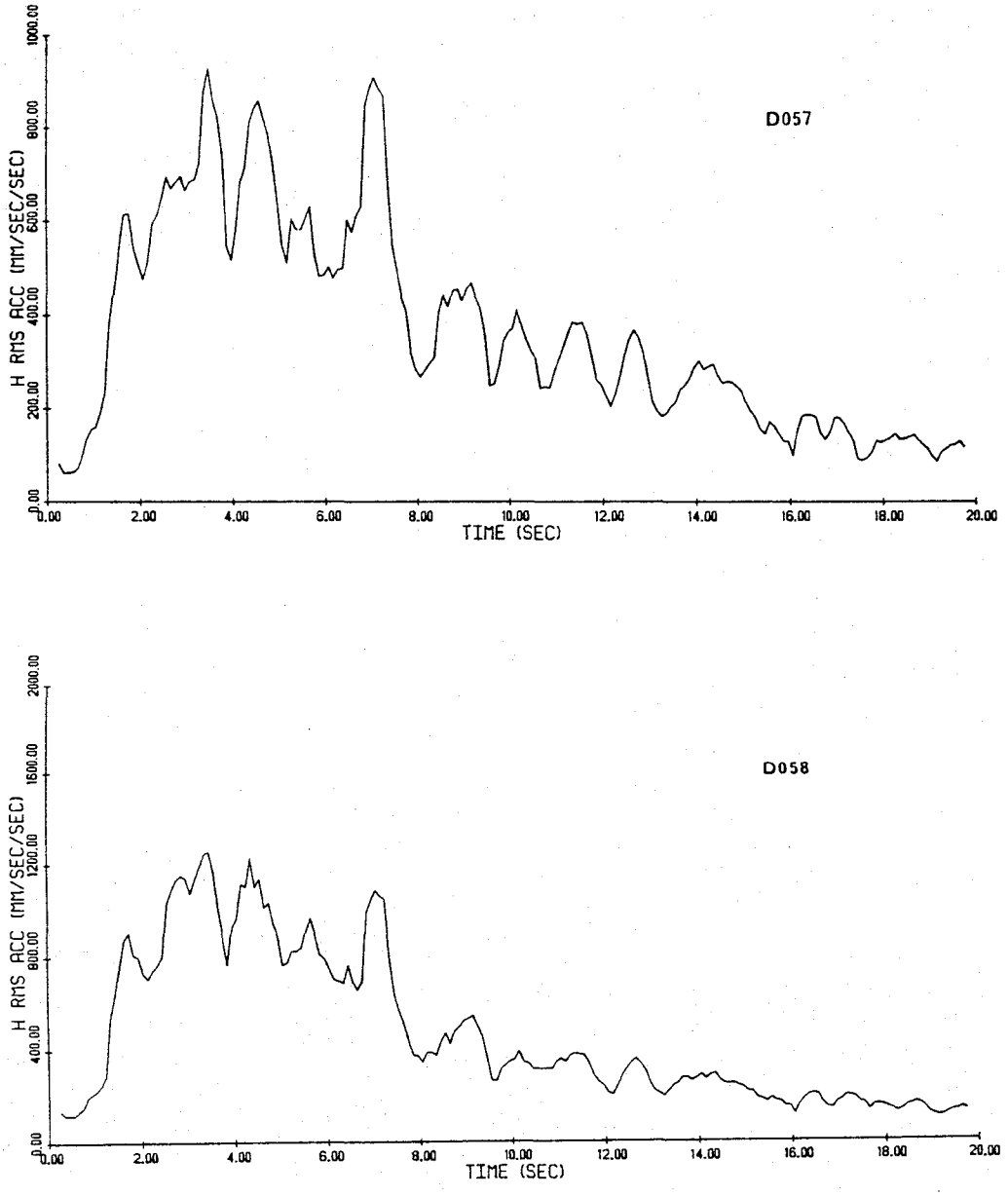

Figure 14 - Horizontal moving time window rms acceleration plots at Hollywood Storage Basement (D057) and P.E. Lot (D058)

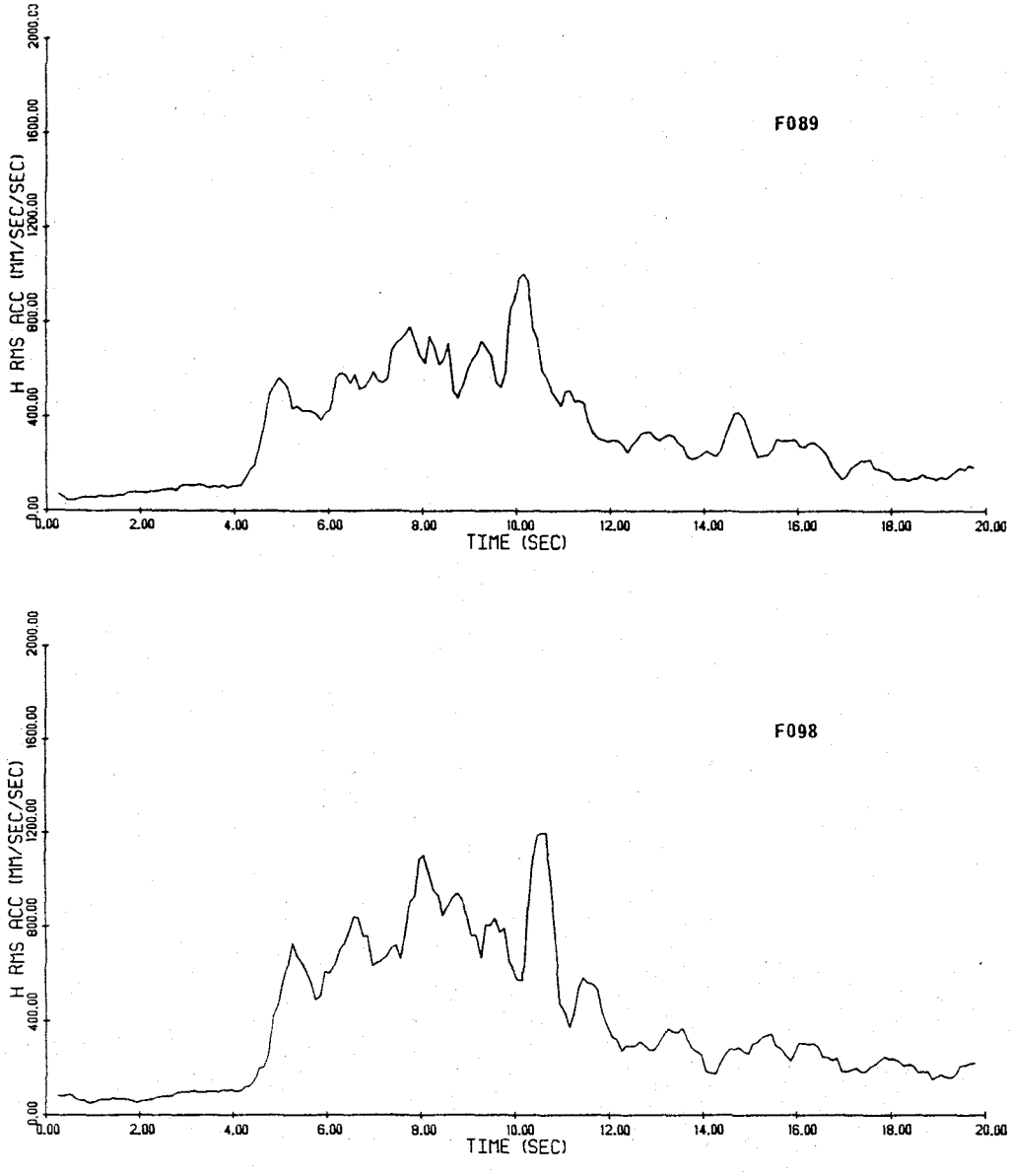

Figure 15 - Horizontal moving time window rms acceleration plots at 808 S. Olive Street (F089) and 646 S. Olive Street (F098)

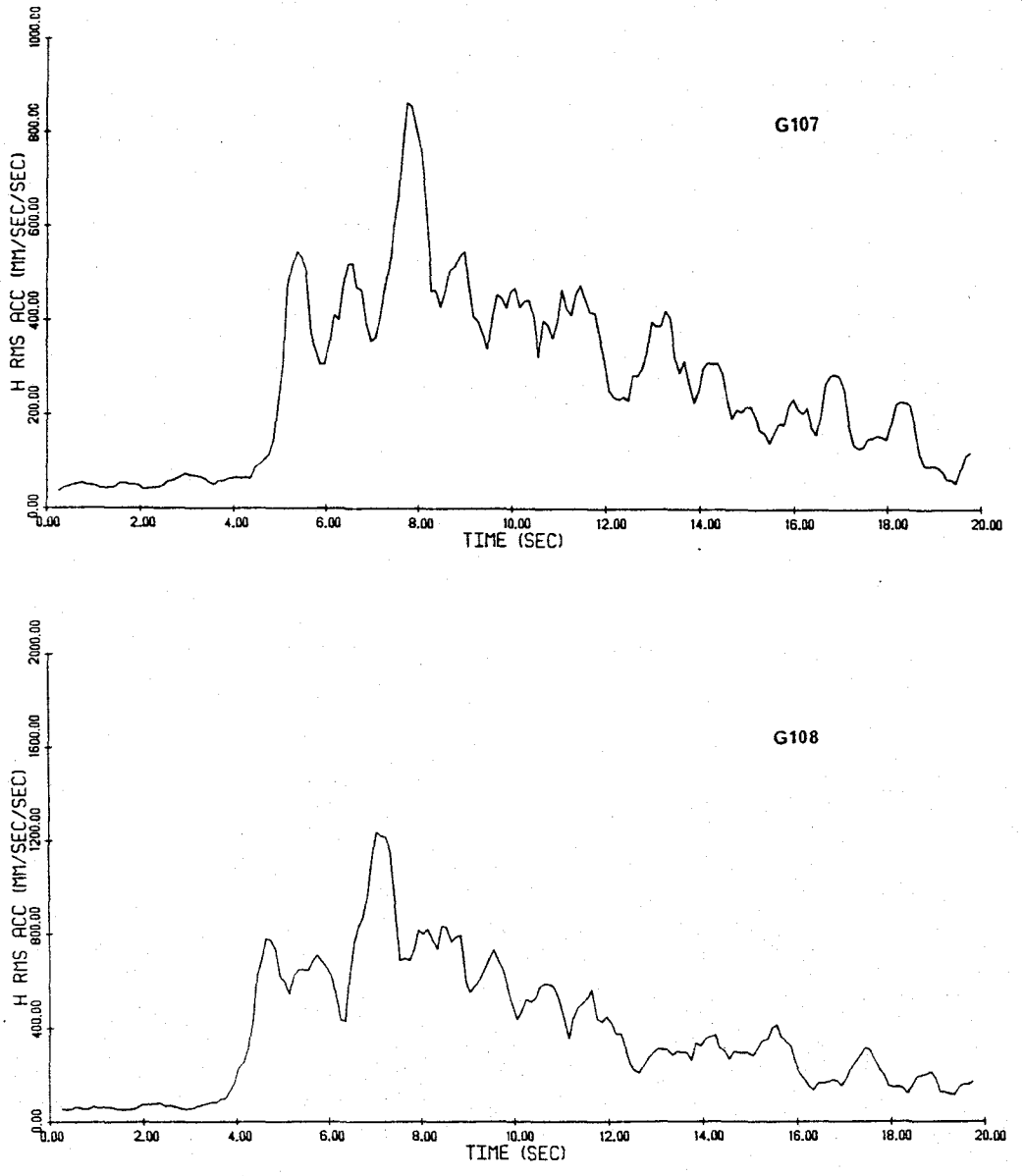

Figure 16 - Horizontal moving time window rms acceleration plots at Caltech Athenaeum (G107) and Caltech Millikan Library (G108)

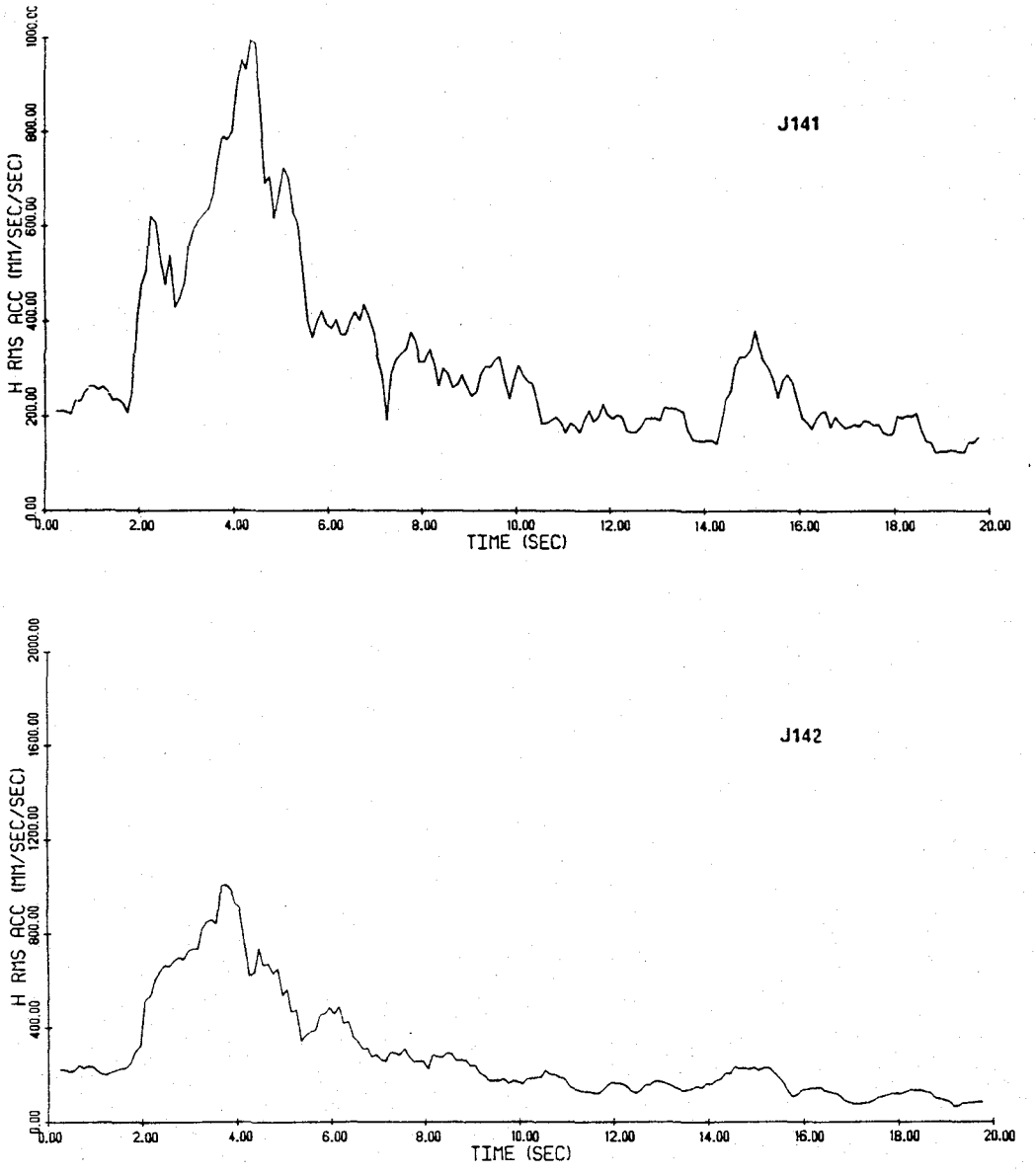

Figure 17 - Horizontal moving time window rms acceleration plots at Lake Hughes Station 1 (J141) and Station 4 (J142)

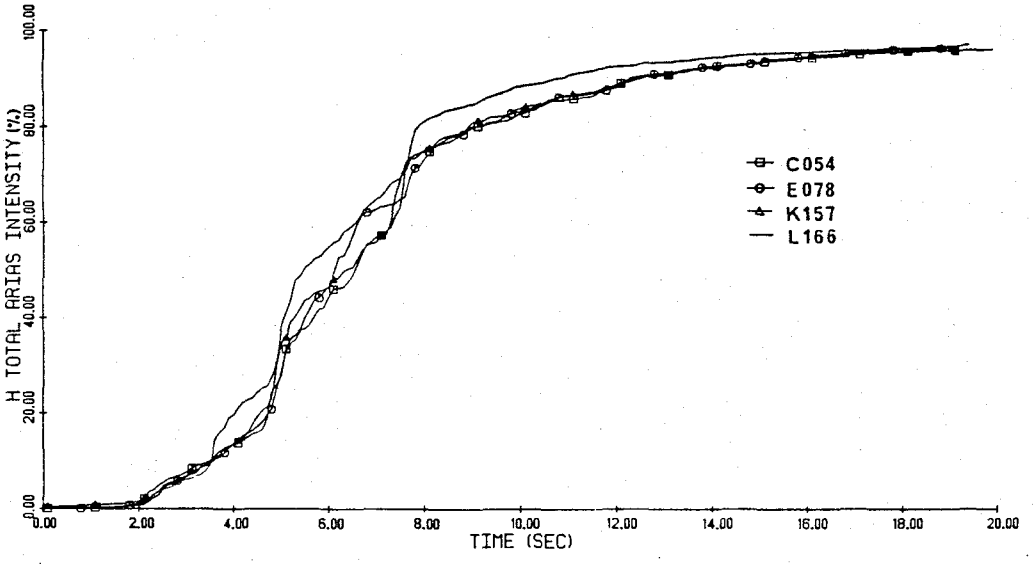

Figure 18 - Horizontal Husid plots at selected sites south of the fault, San Fernando Earthquake

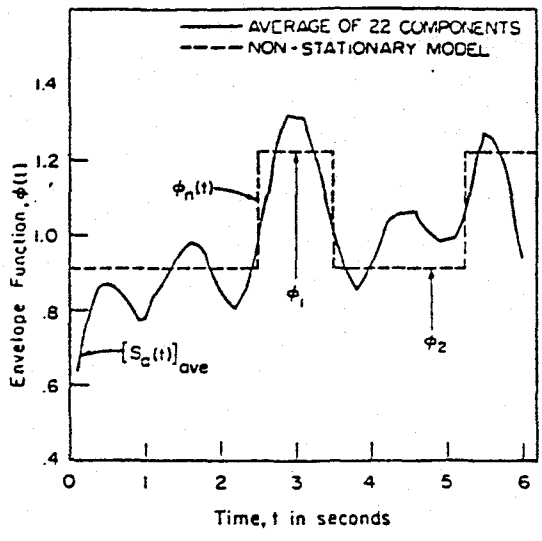

Figure 19a - Normalized average moving time window rms acceleration from 22 components, San Fernando Earthquake

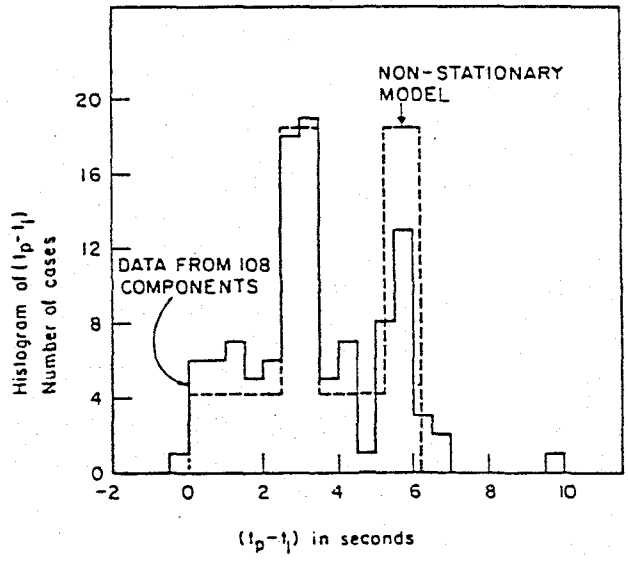

Figure 19b - Empirical and predicted histograms of the time of peak acceleration, San Fernando Earthquake

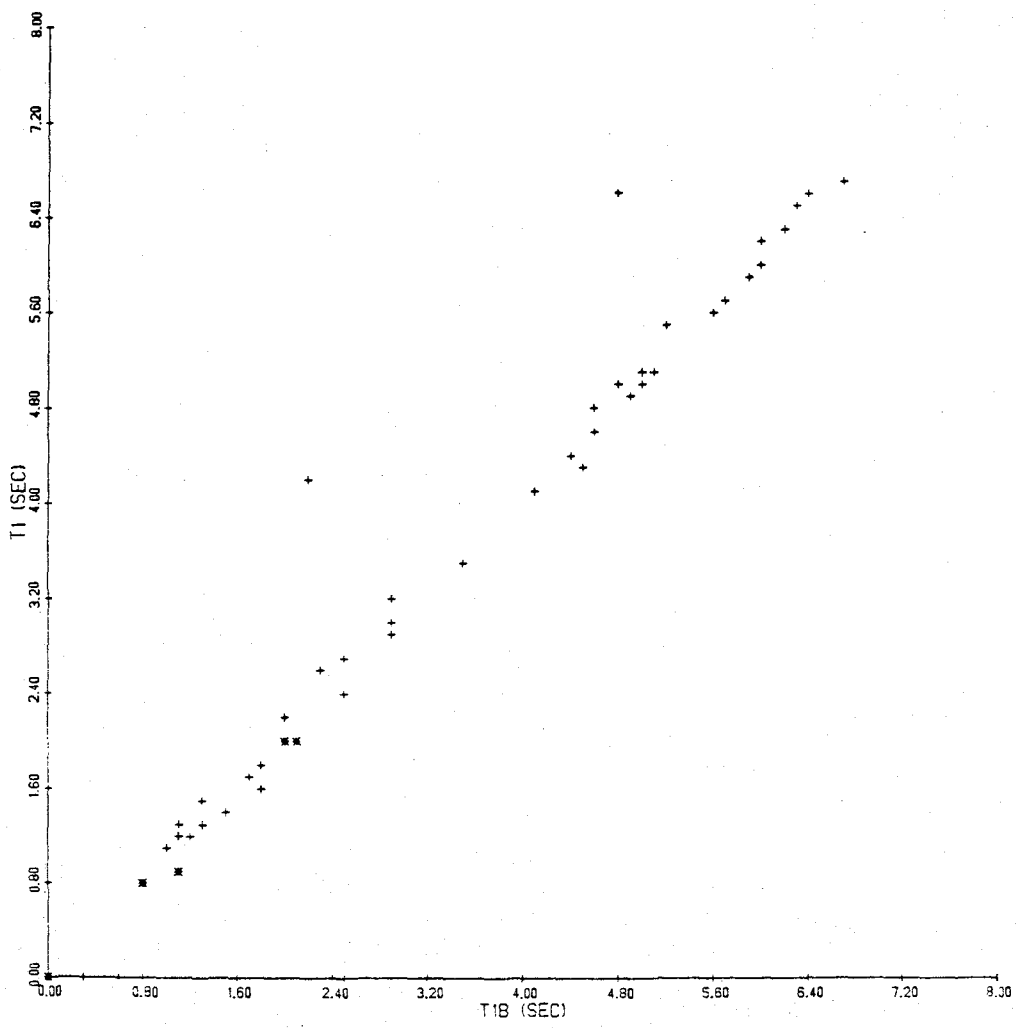

Figure 20 - t_1 versus t_{1B} , San Fernando Earthquake
* - site north of epicenter + - site south of epicenter

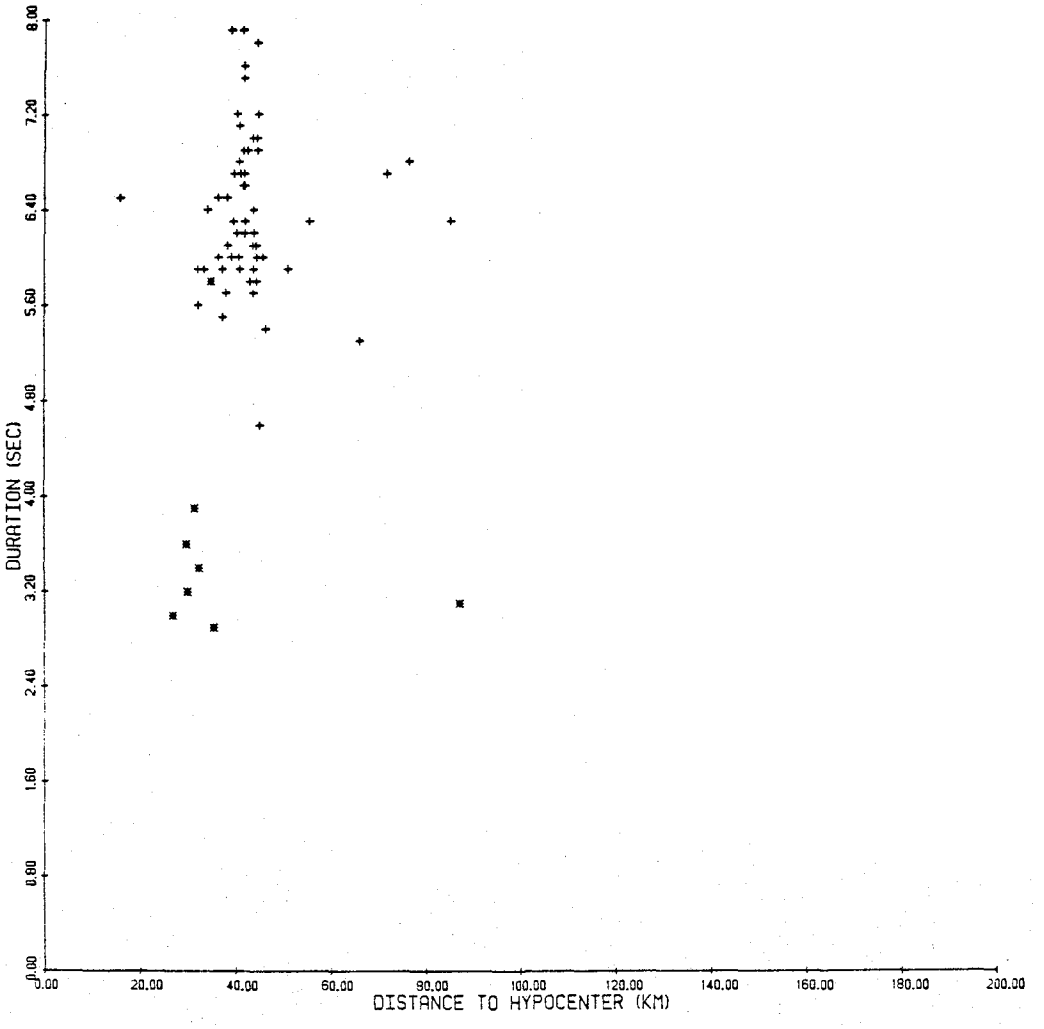

Figure 21 - Duration, Δ, versus distance to the hypocenter, San Fernando Earthquake
* - site north of epicenter + - site south of epicenter

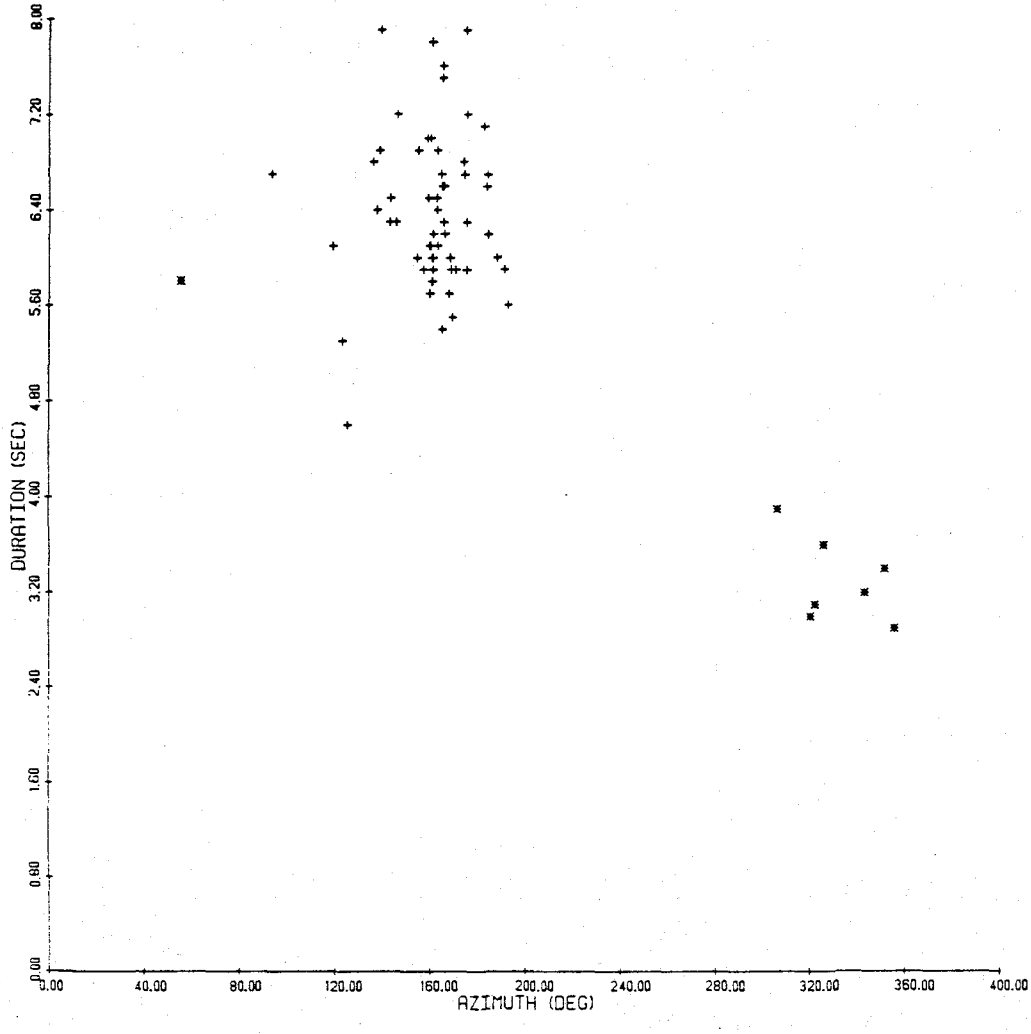

Figure 22 - Duration, Δ, versus azimuth from the epicenter, San Fernando Earthquake
* - site north of epicenter + - site south of epicenter

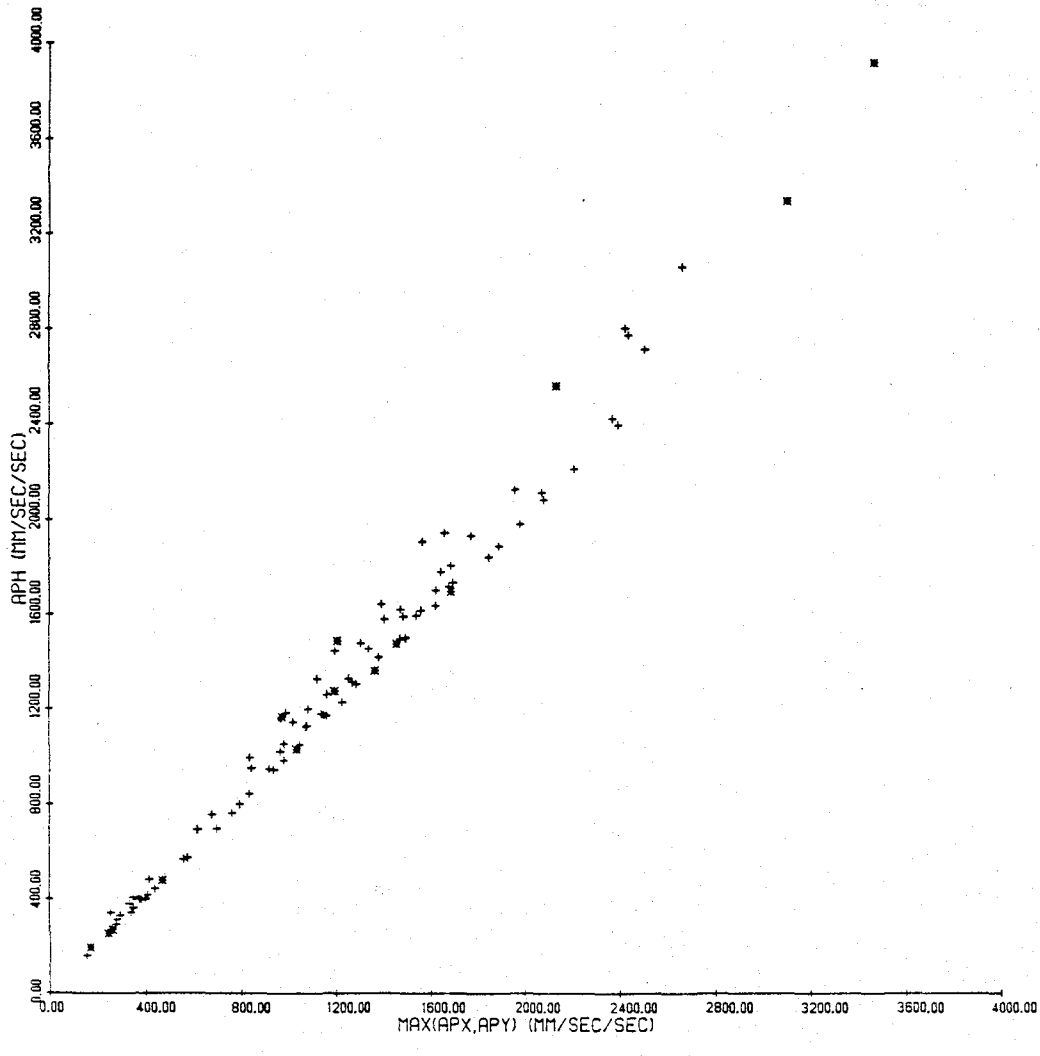

Figure 23 - a_{pH} versus the maximum of the horizontal components, a_{pX} and a_{pY}, San Fernando Earthquake
* - site north of epicenter + - site south of epicenter

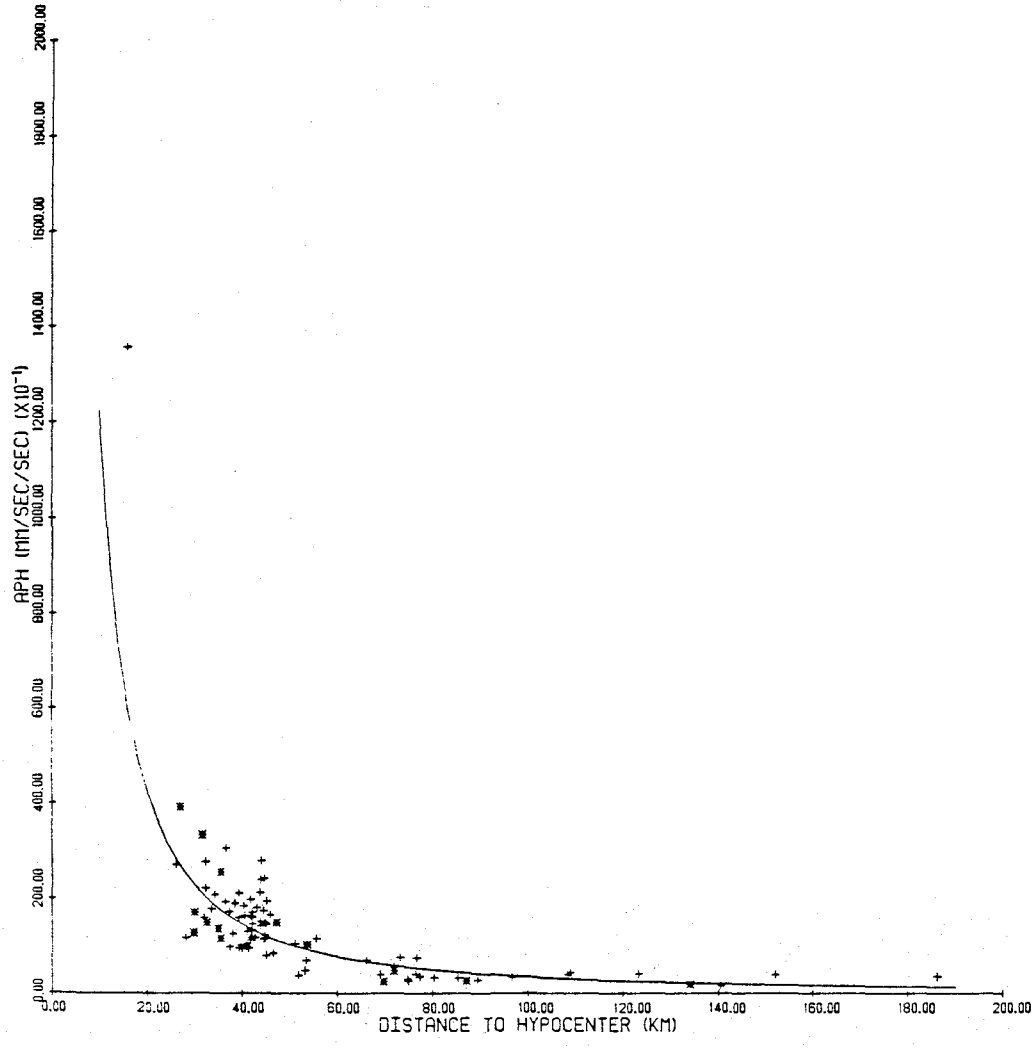

Figure 24 - a_{PH} versus distance to the hypocenter, San Fernando Earthquake
* - site north of epicenter + - site south of epicenter

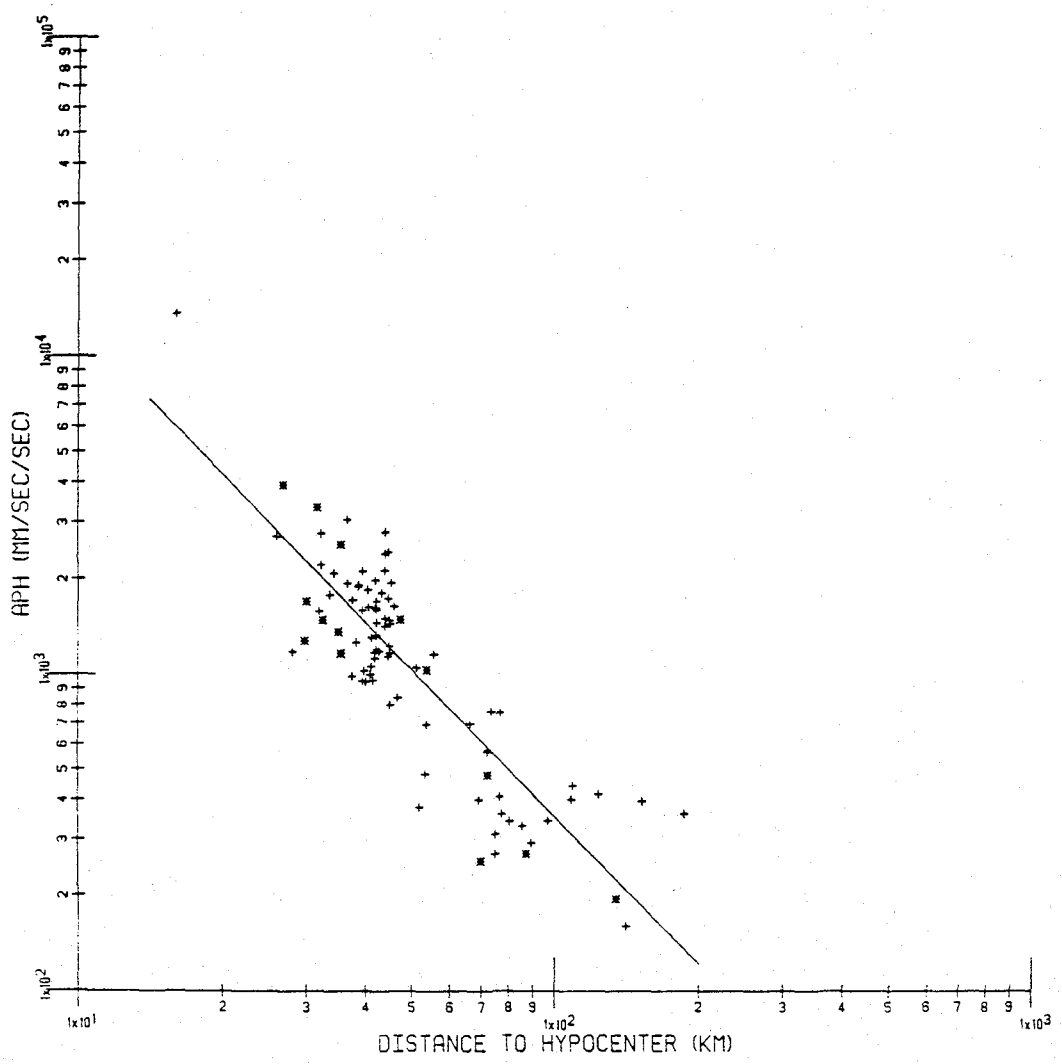

Figure 25 - a_{PH} versus distance to the hypocenter, San Fernando Earthquake
* - site north of epicenter + - site south of epicenter

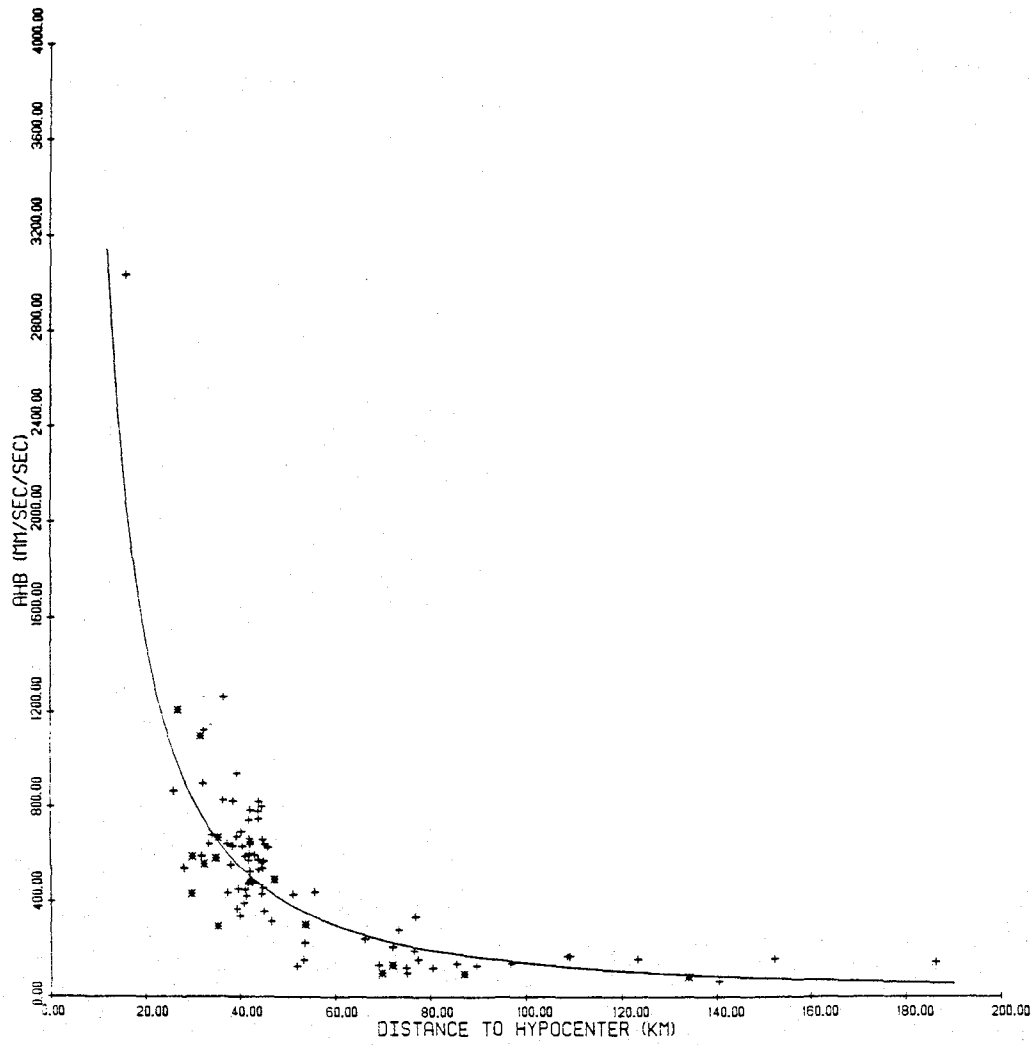

Figure 26 - $\bar{a}_{HB}$ versus distance to the hypocenter, San Fernando Earthquake
* - site north of epicenter + - site south of epicenter

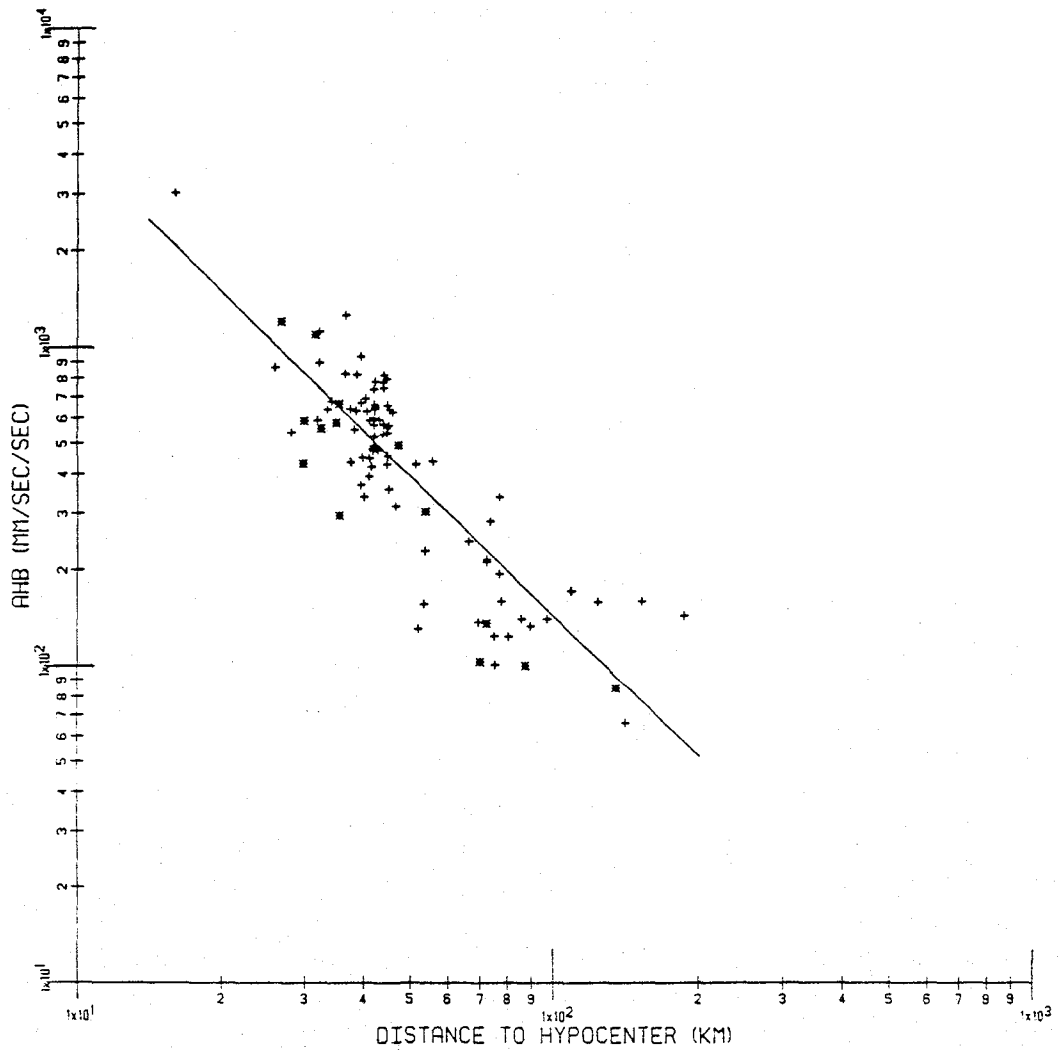

Figure 27 - $\bar{a}_{HB}$ versus distance to the hypocenter, San Fernando Earthquake
* - site north of epicenter + - site south of epicenter

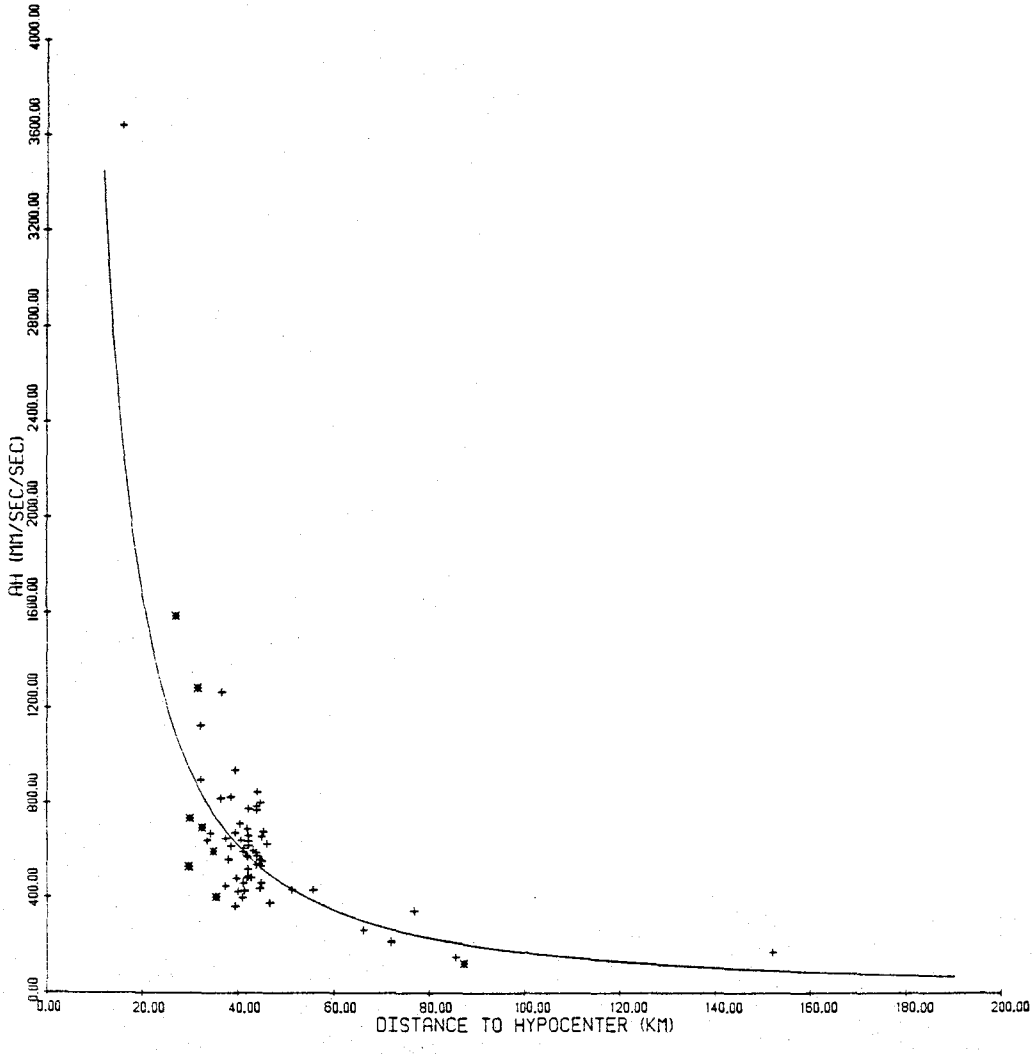

Figure 28 - $\bar{a}_H$ versus distance to the hypocenter, San Fernando Earthquake
* - site north of epicenter + - site south of epicenter

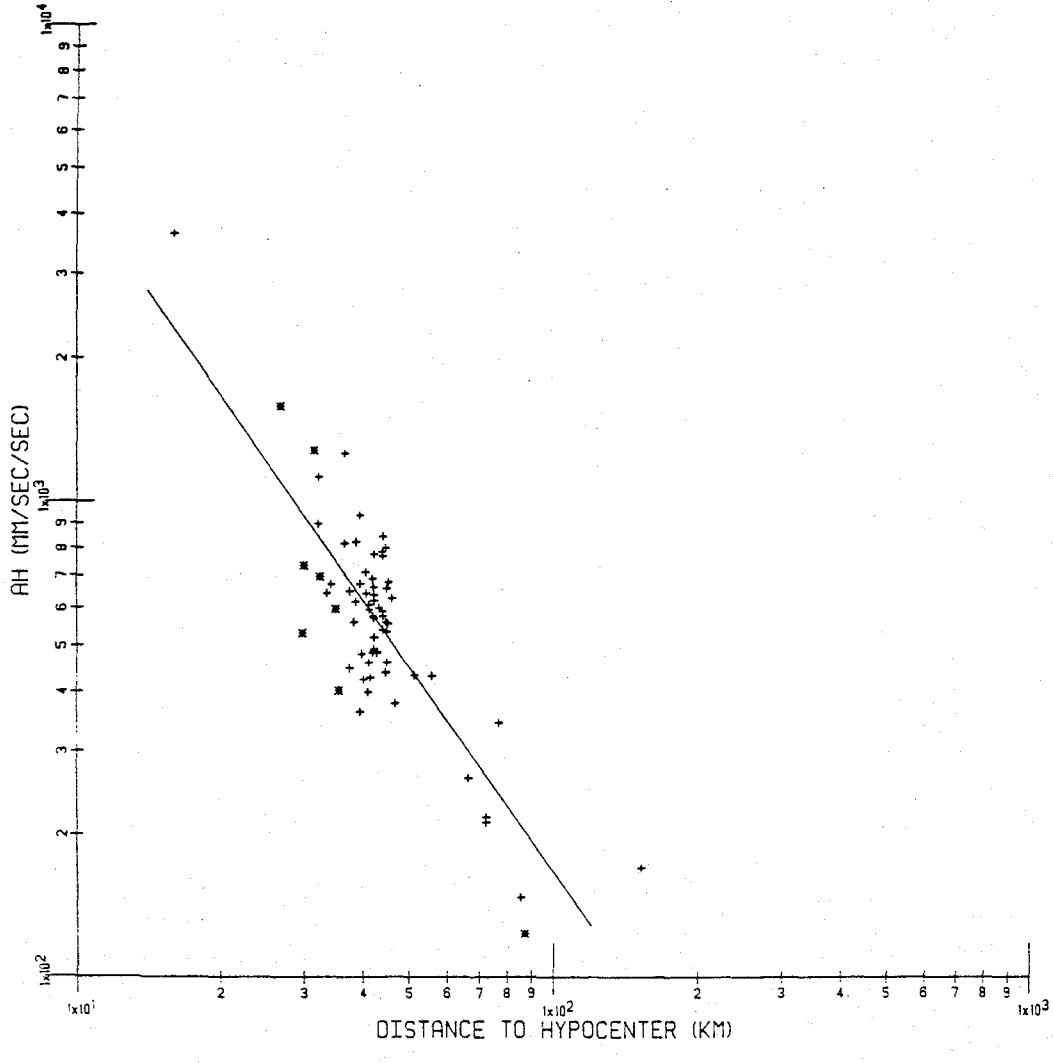

Figure 29 - $\bar{a}_H$ versus distance to the hypocenter, San Fernando Earthquake
* - site north of epicenter + - site south of epicenter

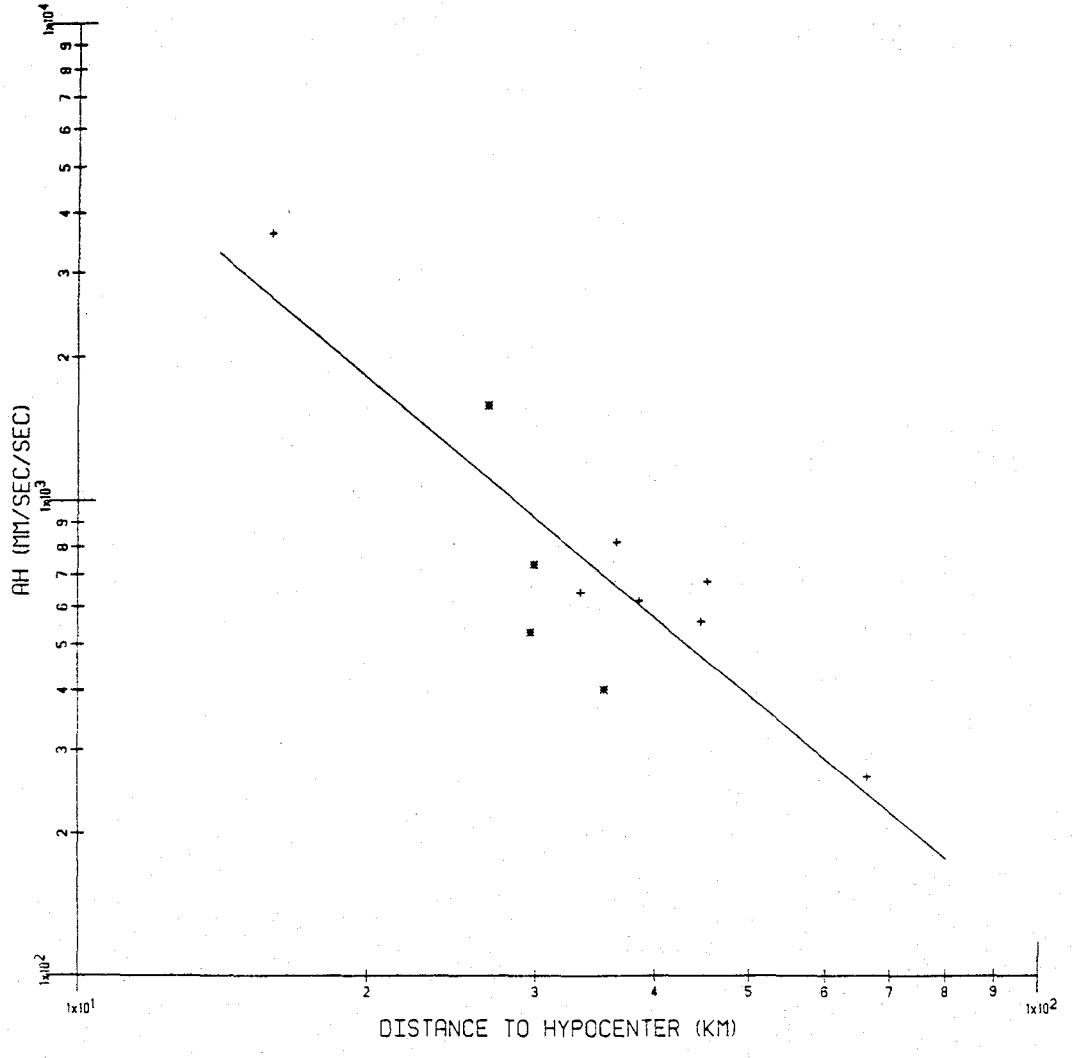

Figure 30 - $\bar{a}_H$ versus distance to the hypocenter, rock sites, San Fernando Earthquake
* - site north of epicenter + - site south of epicenter

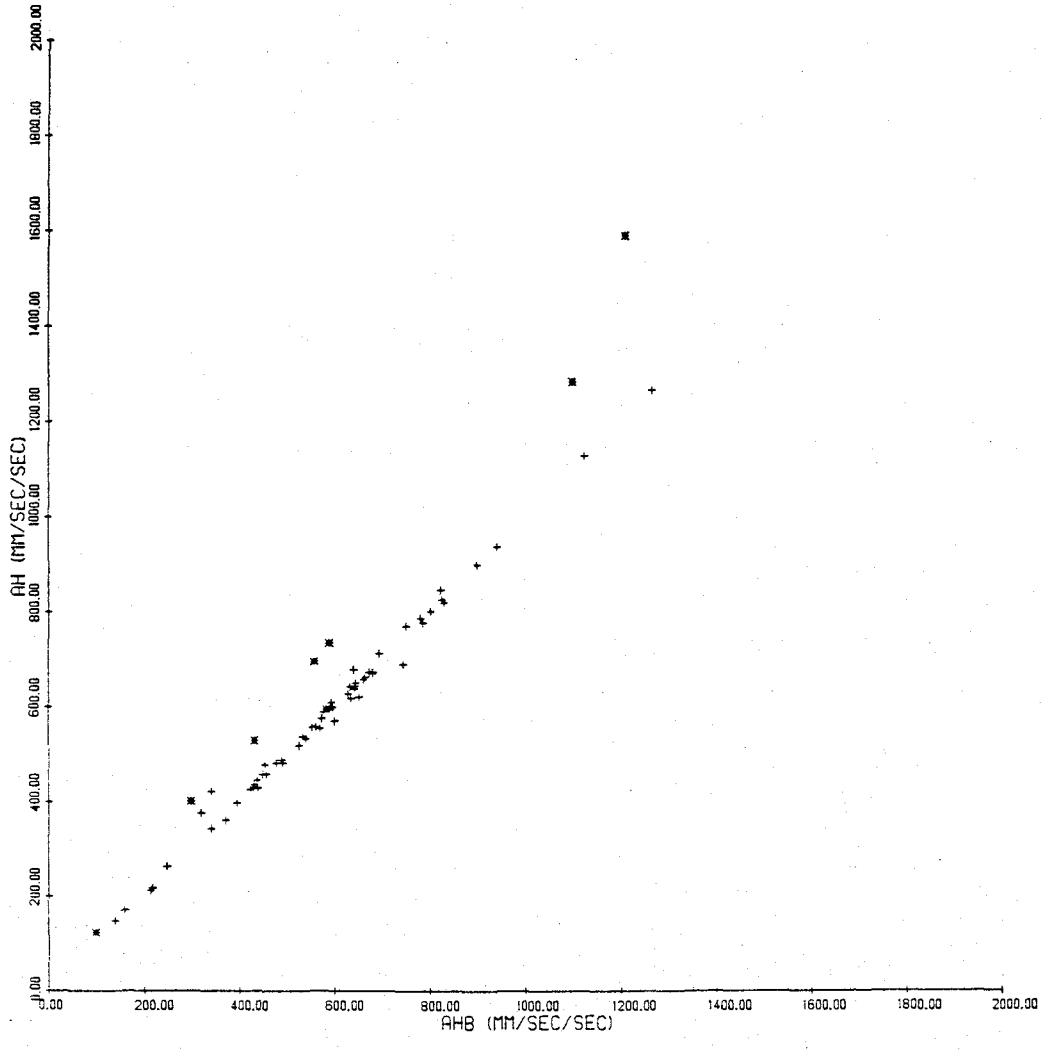

Figure 31 - $\bar{a}_H$ versus $\bar{a}_{HB}$, San Fernando Earthquake
* - site north of epicenter + - site south of epicenter

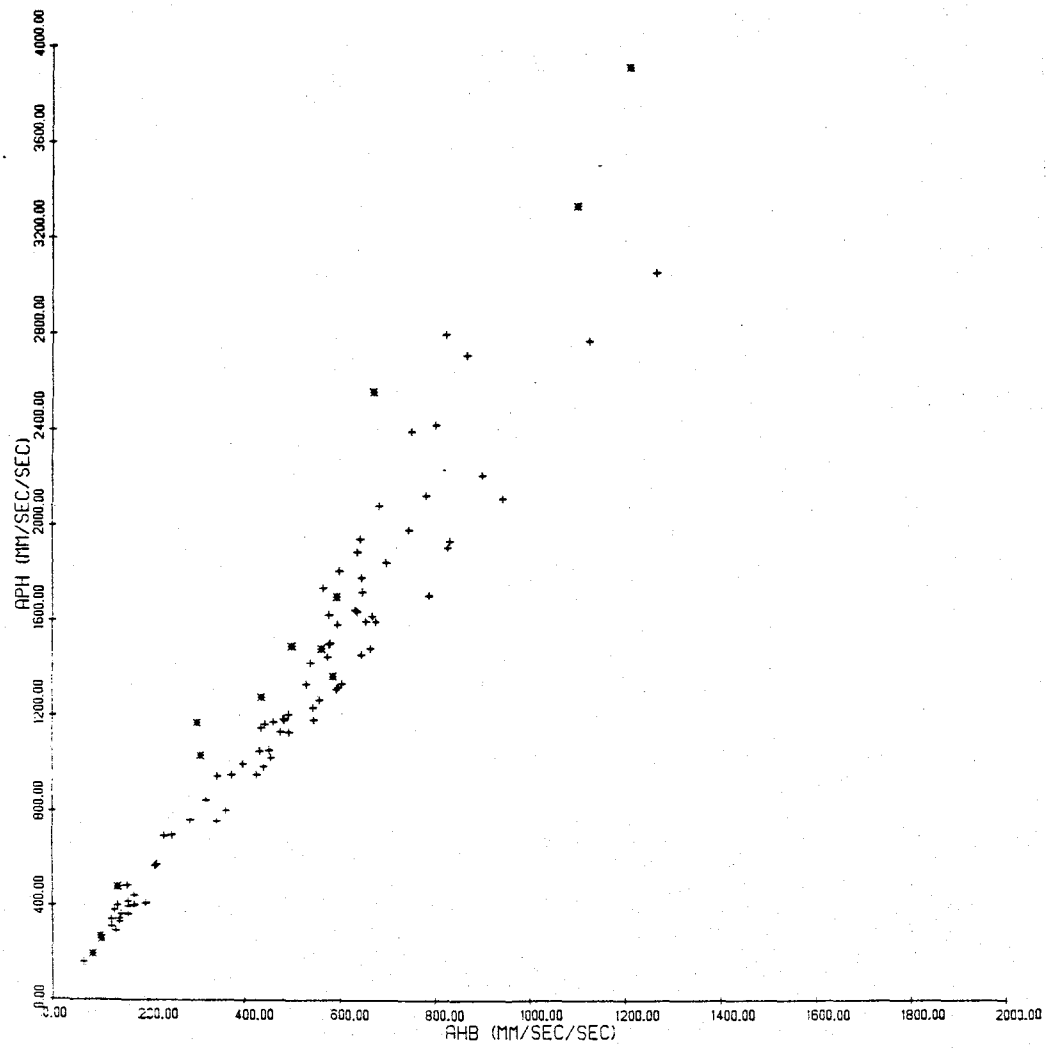

Figure 32 - a_{PH} versus $\bar{a}_{HB}$, San Fernando Earthquake
* - site north of epicenter + - site south of epicenter

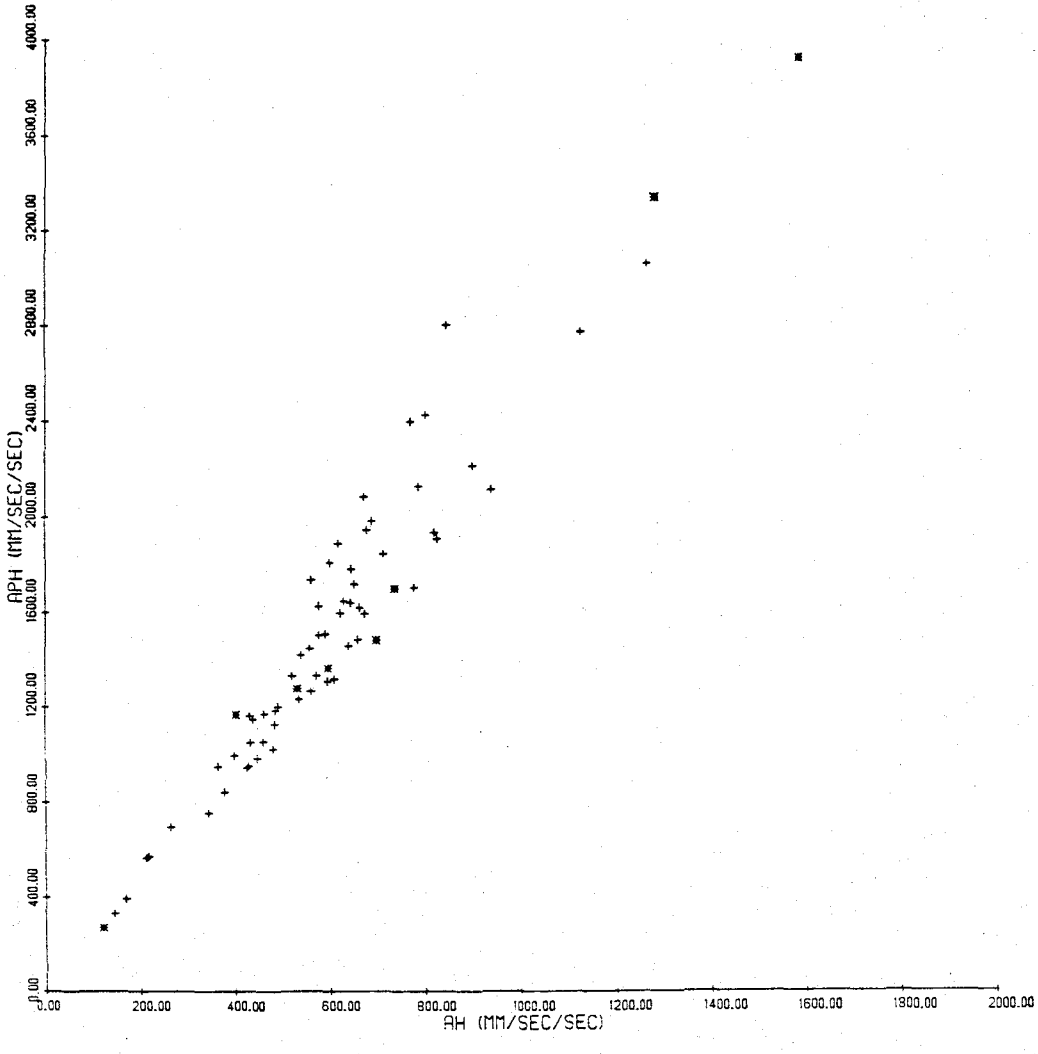

Figure 33 - a_{pH} versus $\bar{a}_H$, San Fernando Earthquake
* - site north of epicenter + - site south of epicenter

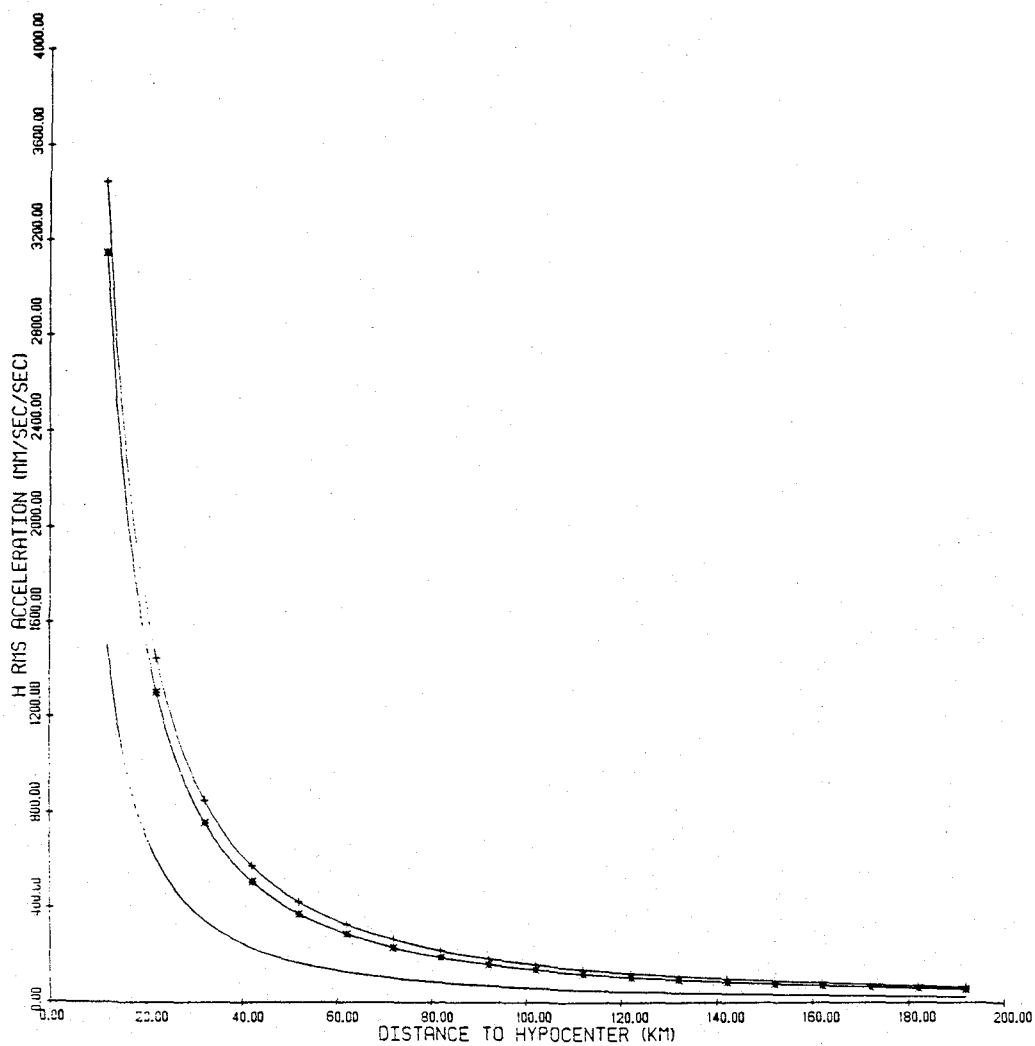

Figure 34 - Horizontal rms acceleration versus distance to the hypocenter, San Fernando Earthquake
+ - $\bar{a}_H$ * - $\bar{a}_{HB}$ - - Hank's rms acc

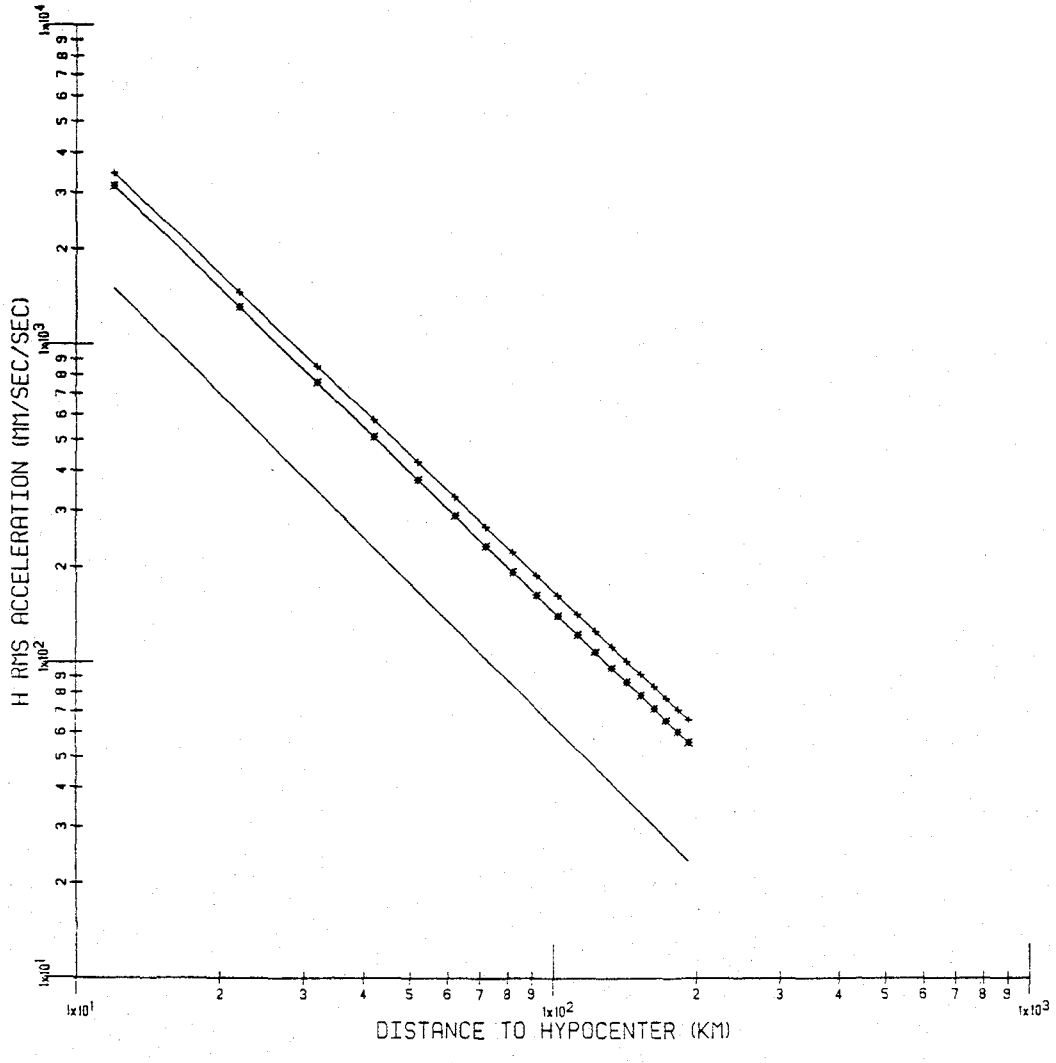

Figure 35 - Horizontal rms acceleration versus distance to the hypocenter, San Fernando Earthquake
+ - $\bar{a}_H$ * - $\bar{a}_{HB}$ - - Hank's rms acc

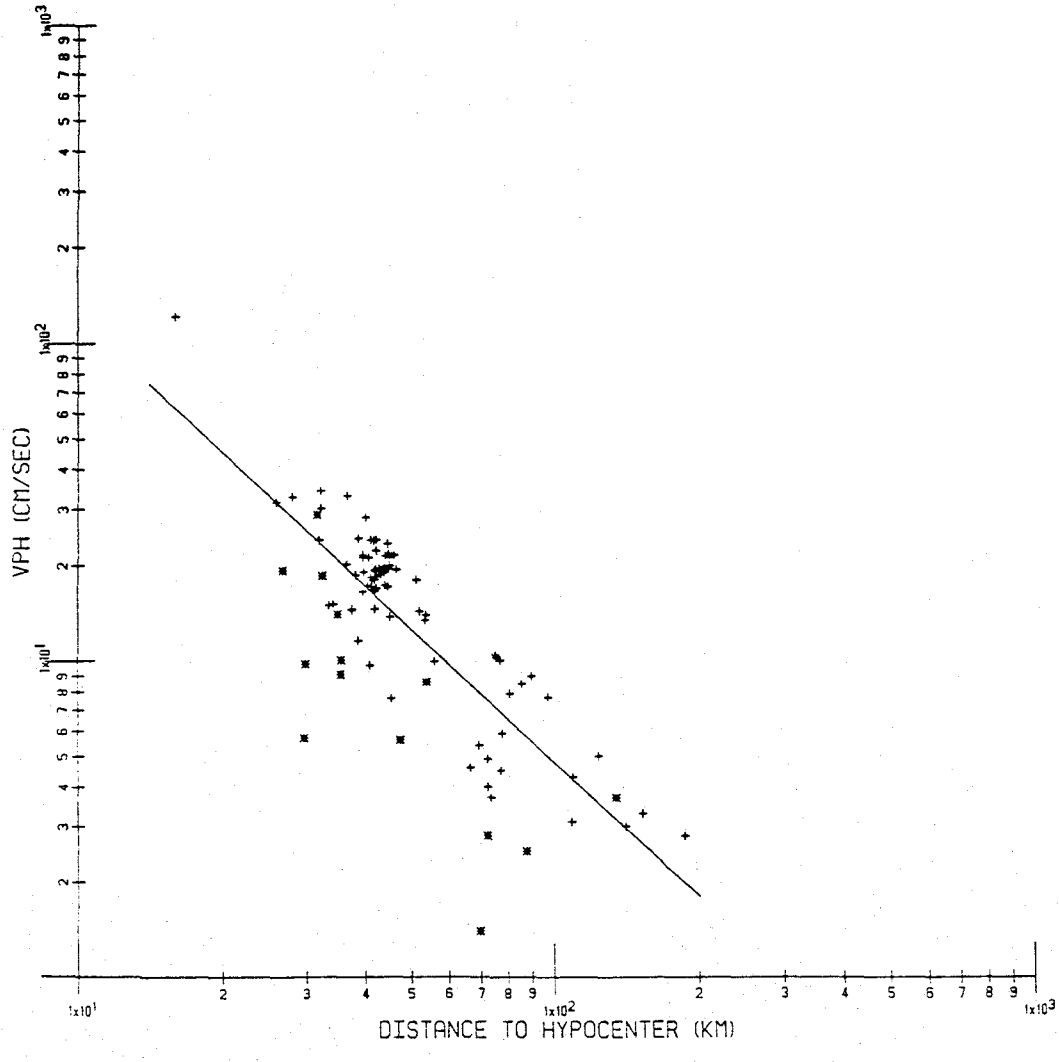

Figure 36 - v_{PH} versus distance to the hypocenter, San Fernando Earthquake
* - site north of epicenter + - site south of epicenter

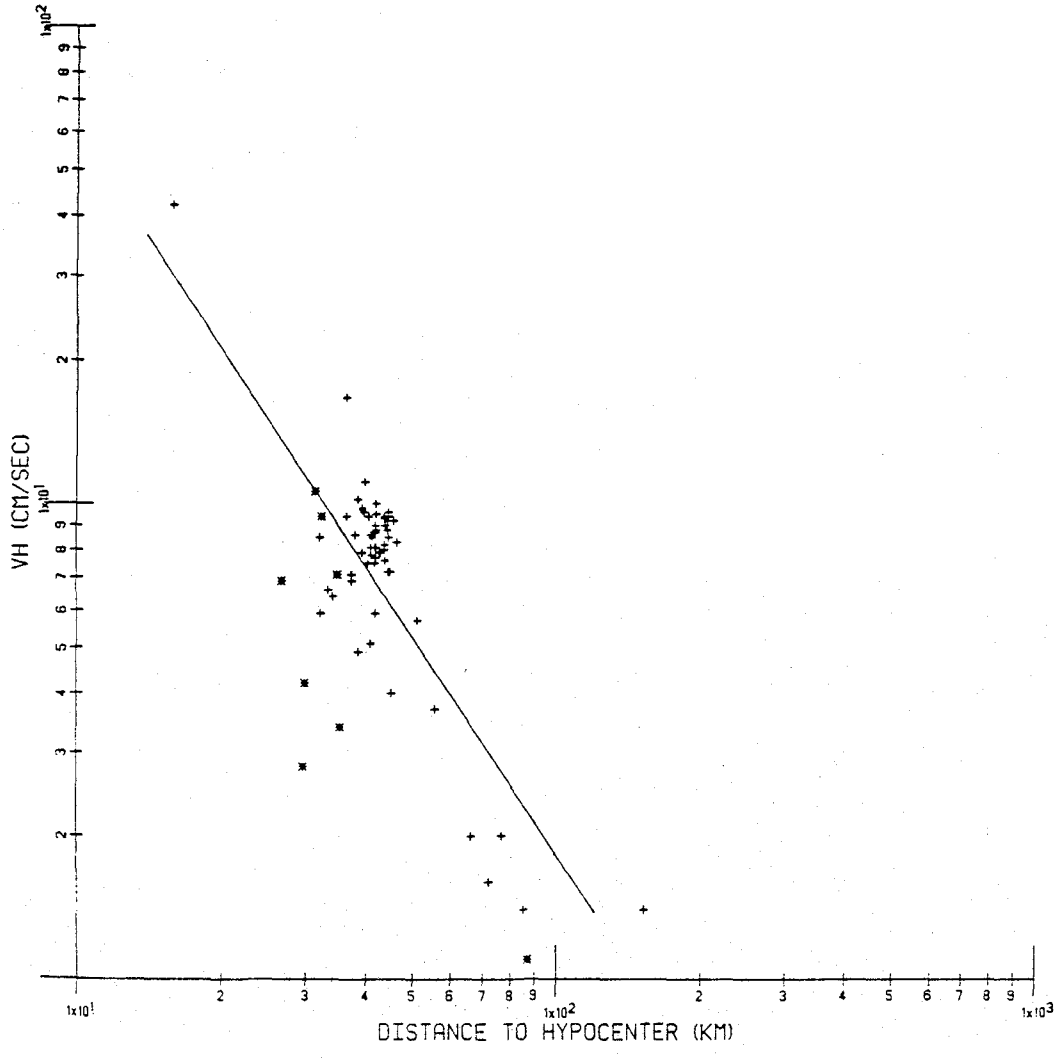

Figure 37 - $\bar{v}_H$ versus distance to the hypocenter, San Fernando Earthquake
* - site north of epicenter + - site south of epicenter

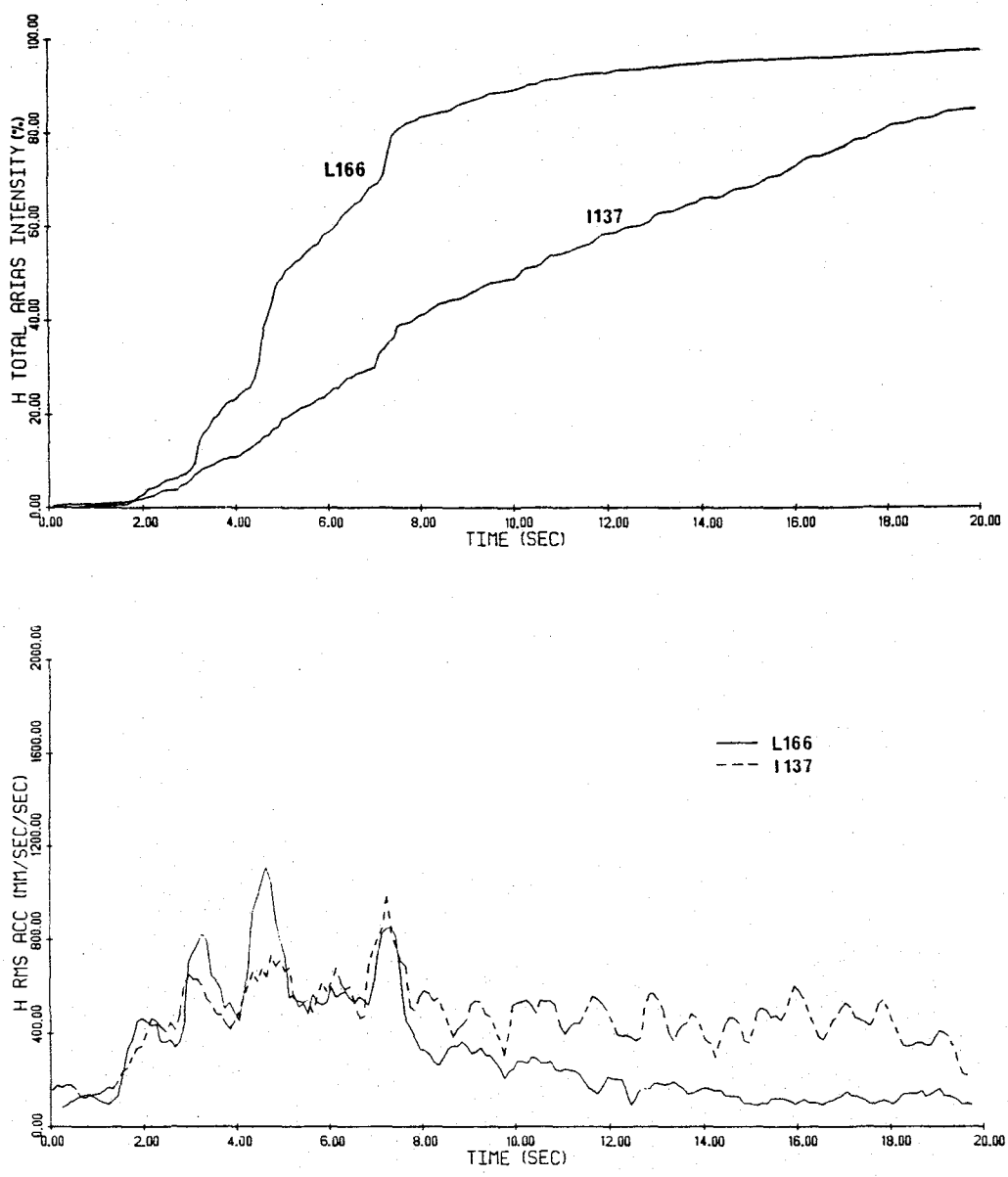

Figure 38 - Horizontal Husid and moving time window rms acceleration plots, L166 and I137

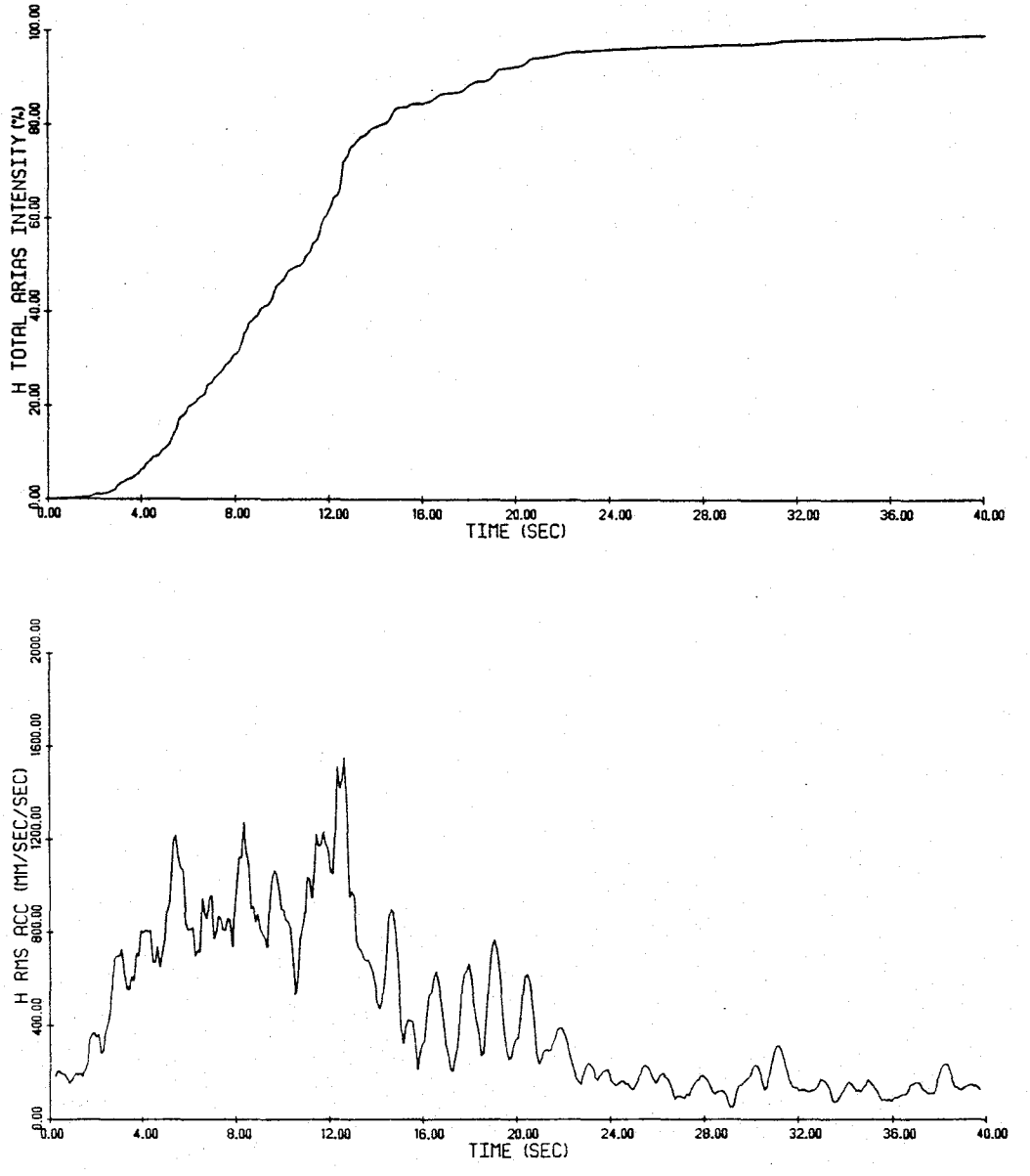

Figure 39 - Horizontal Husid and moving time window rms acceleration plots, 8244 Orion Boulevard (C048)

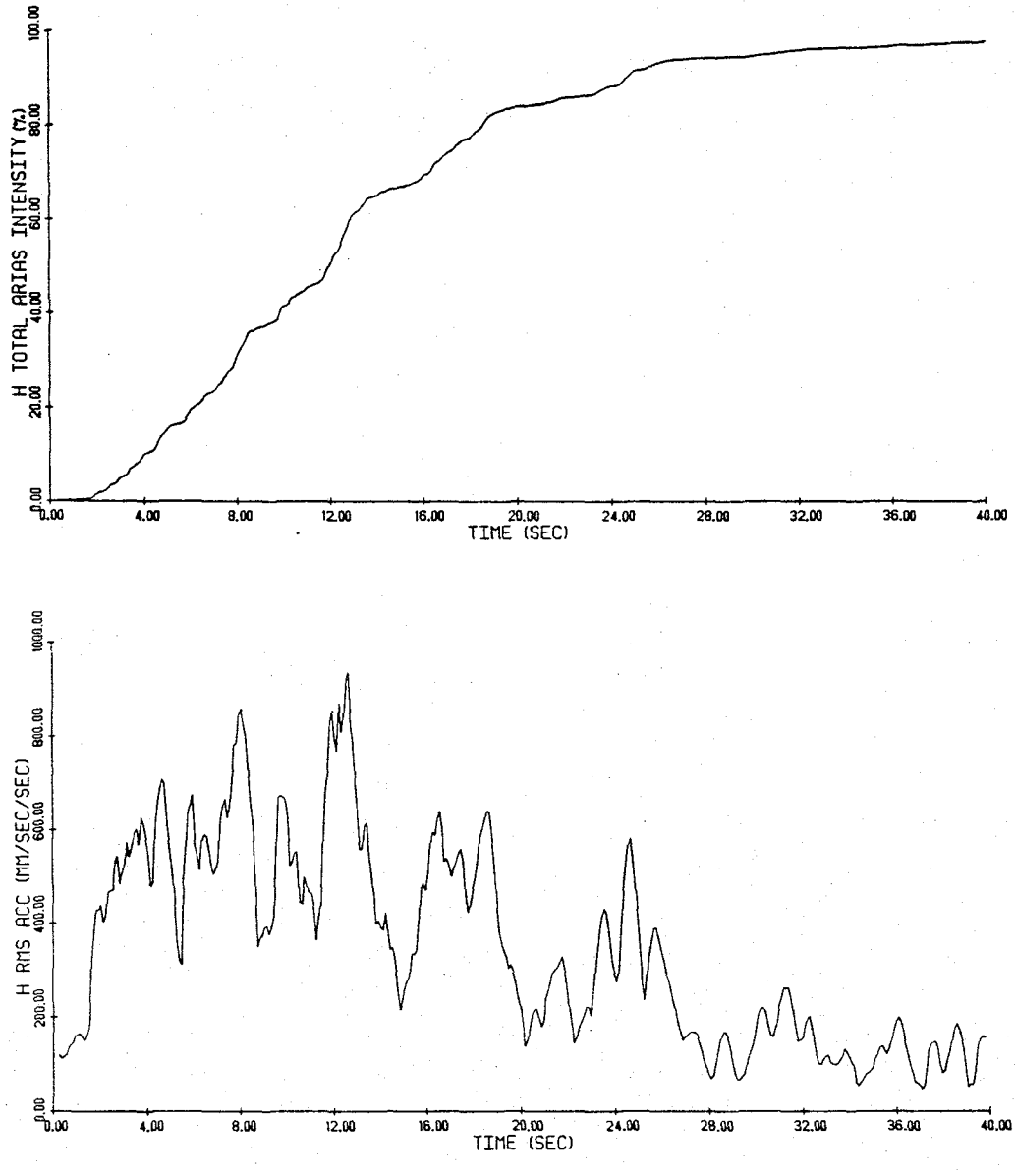

Figure 40 - Horizontal Husid and moving time window rms acceleration plots, 15107 Vanowen Street (J145)

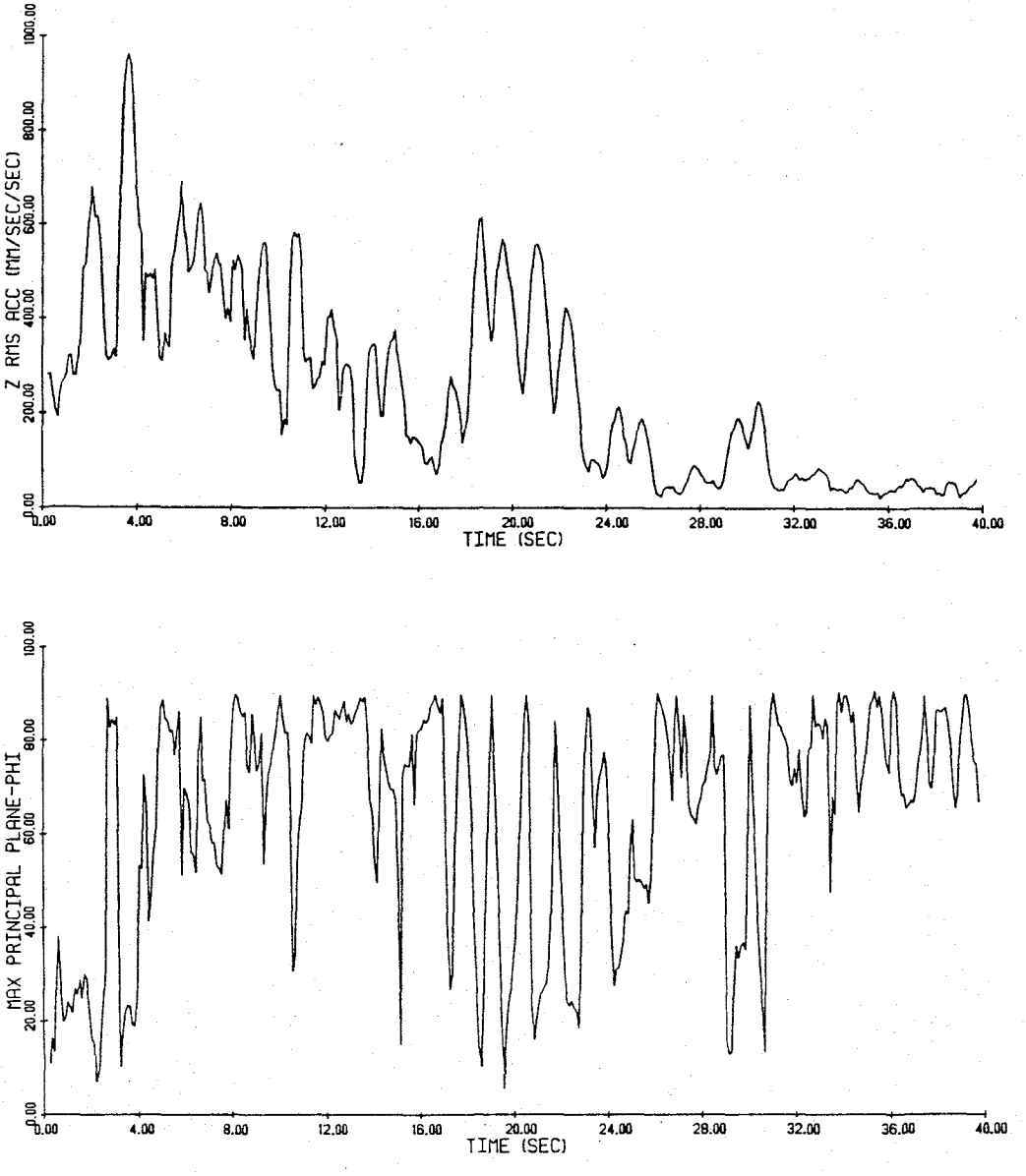

Figure 41 - Vertical moving time window rms acceleration and maximum principal plane phi plots, 8244 Orion Boulevard (C048)

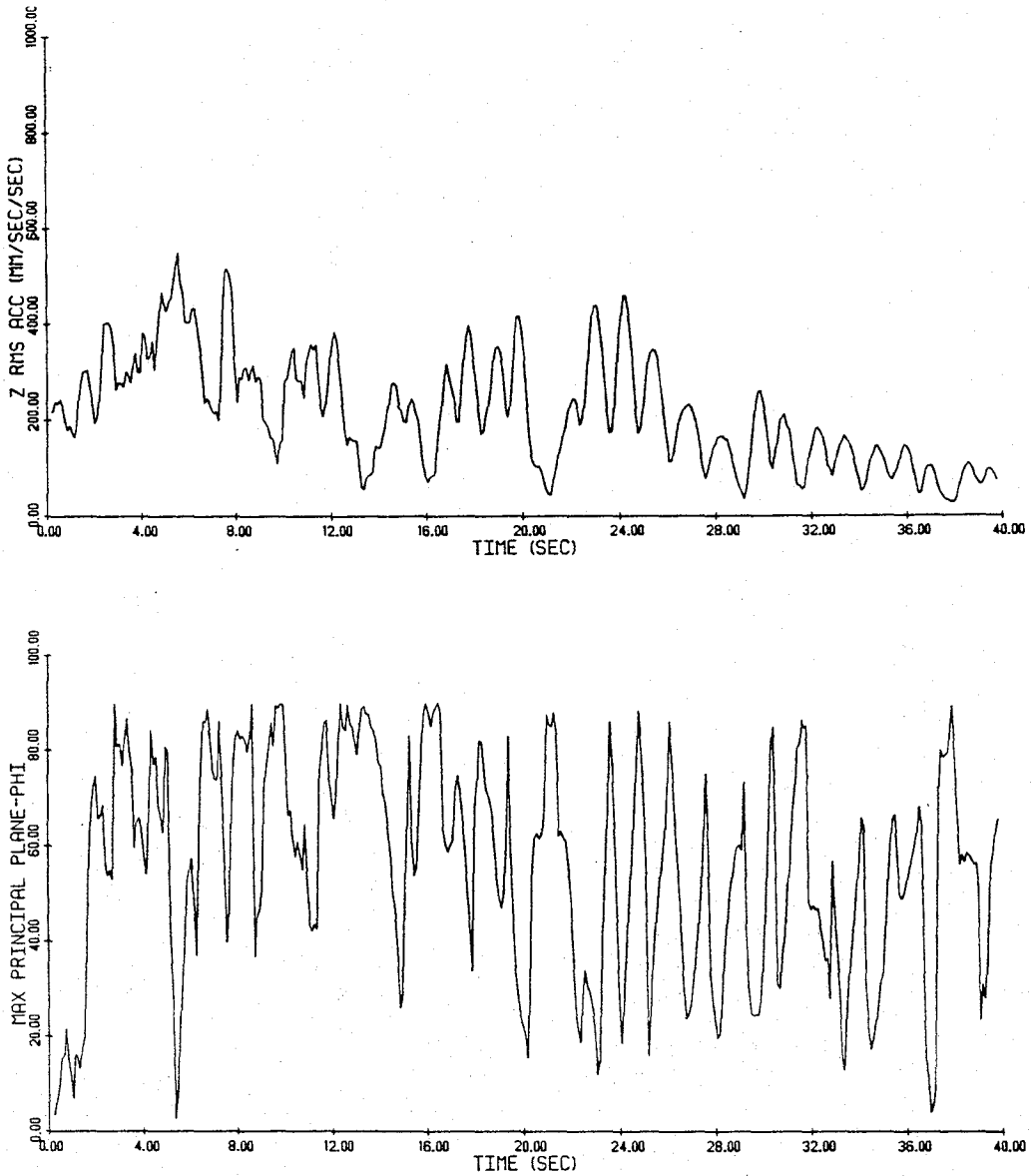

Figure 42 - Vertical moving time window rms acceleration and maximum principal plane phi plots, 15107 Vanowen Street (J145)

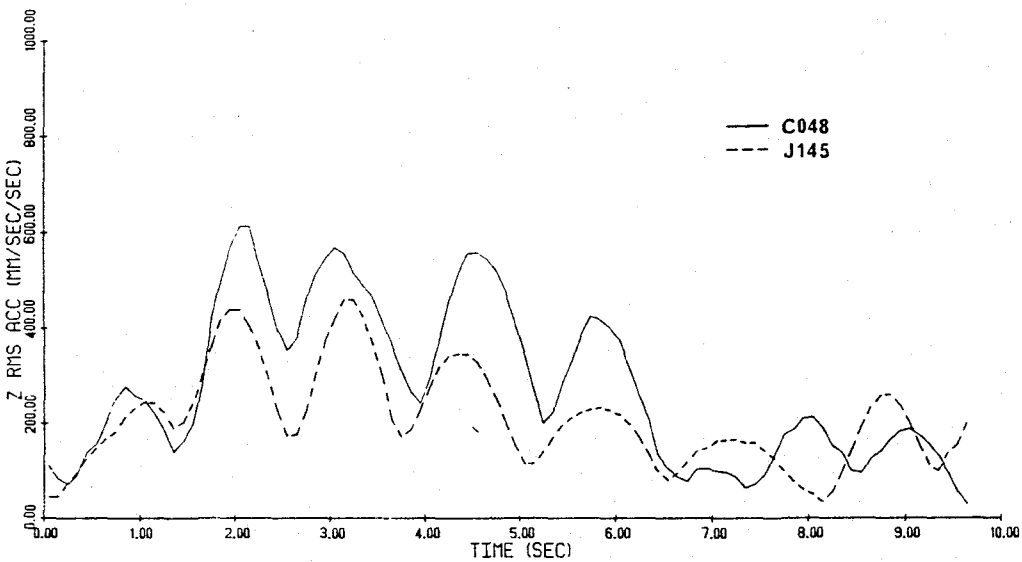

Figure 43 - Vertical moving time window rms acceleration plots, C048 and J145

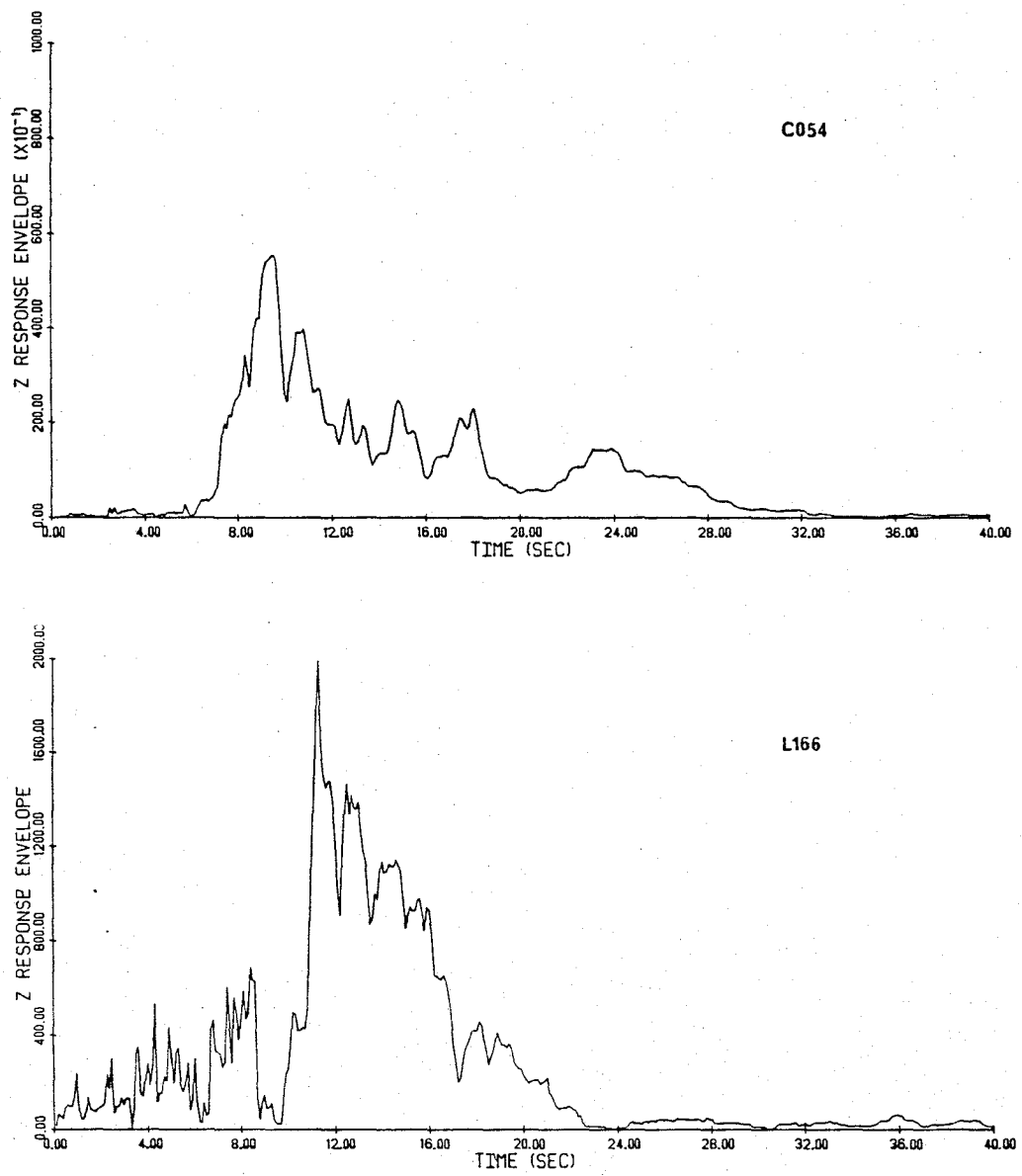

Figure 44 - 0.4 Hz vertical response envelope plots at 445 Figueroa Street (C054) and 3838 Lankershim Boulevard (L166)

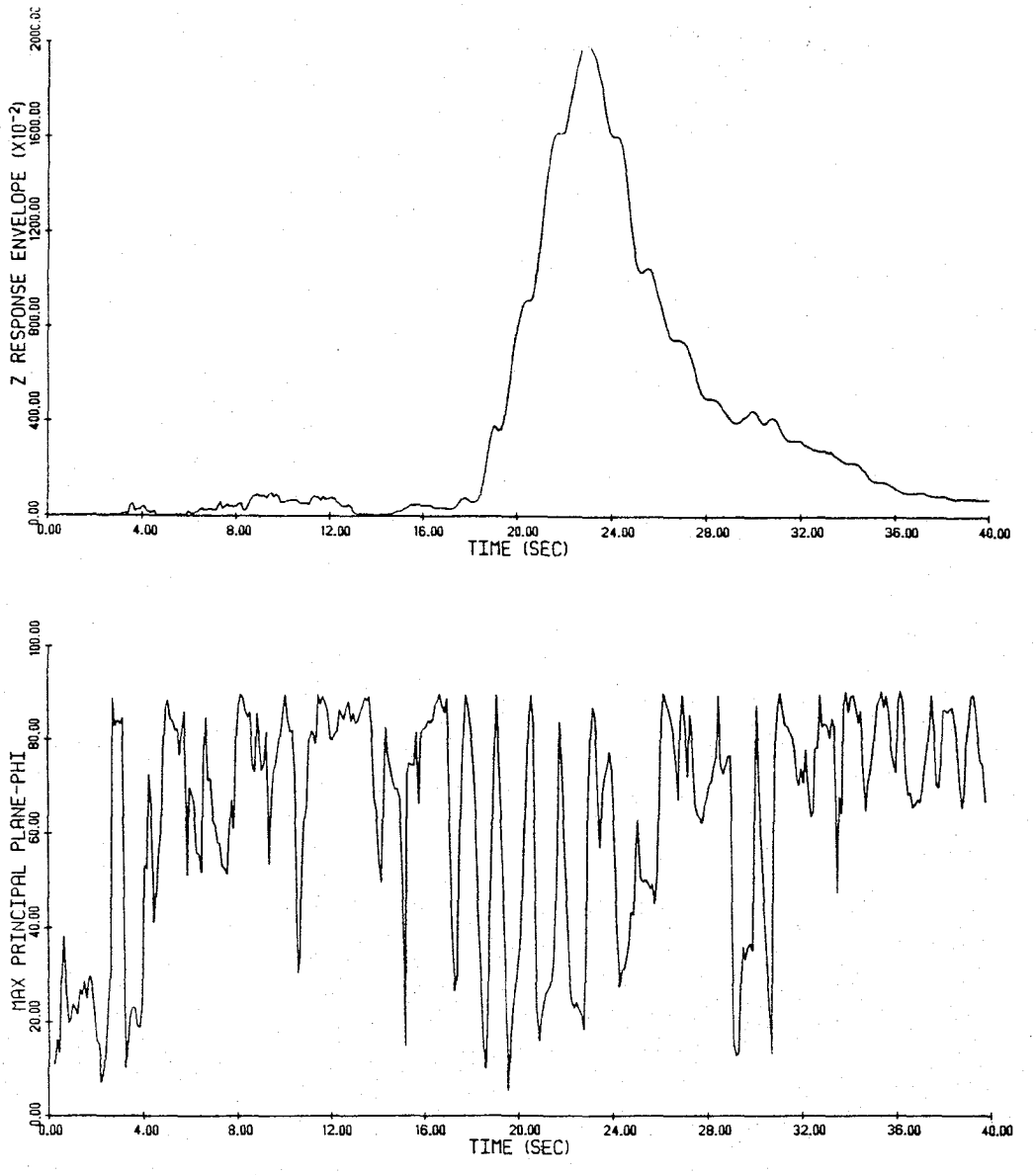

Figure 45 - 0.4 Hz vertical response envelope and maximum principal plane phi plots, 8244 Orion Boulevard (C048)

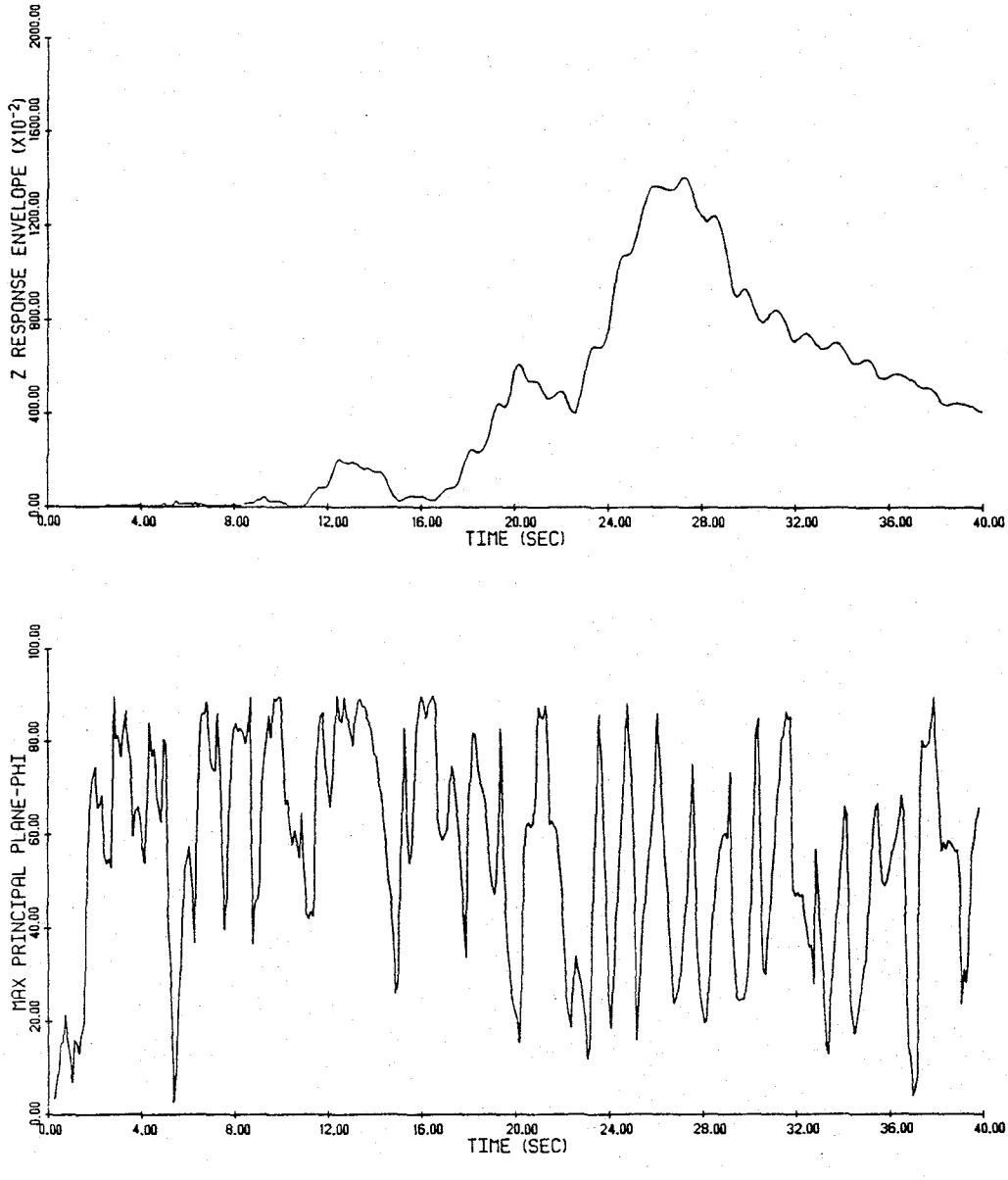

Figure 46 - 0.4 Hz vertical response envelope and maximum principal plane phi plots, 15107 Vanowen Street (J145)

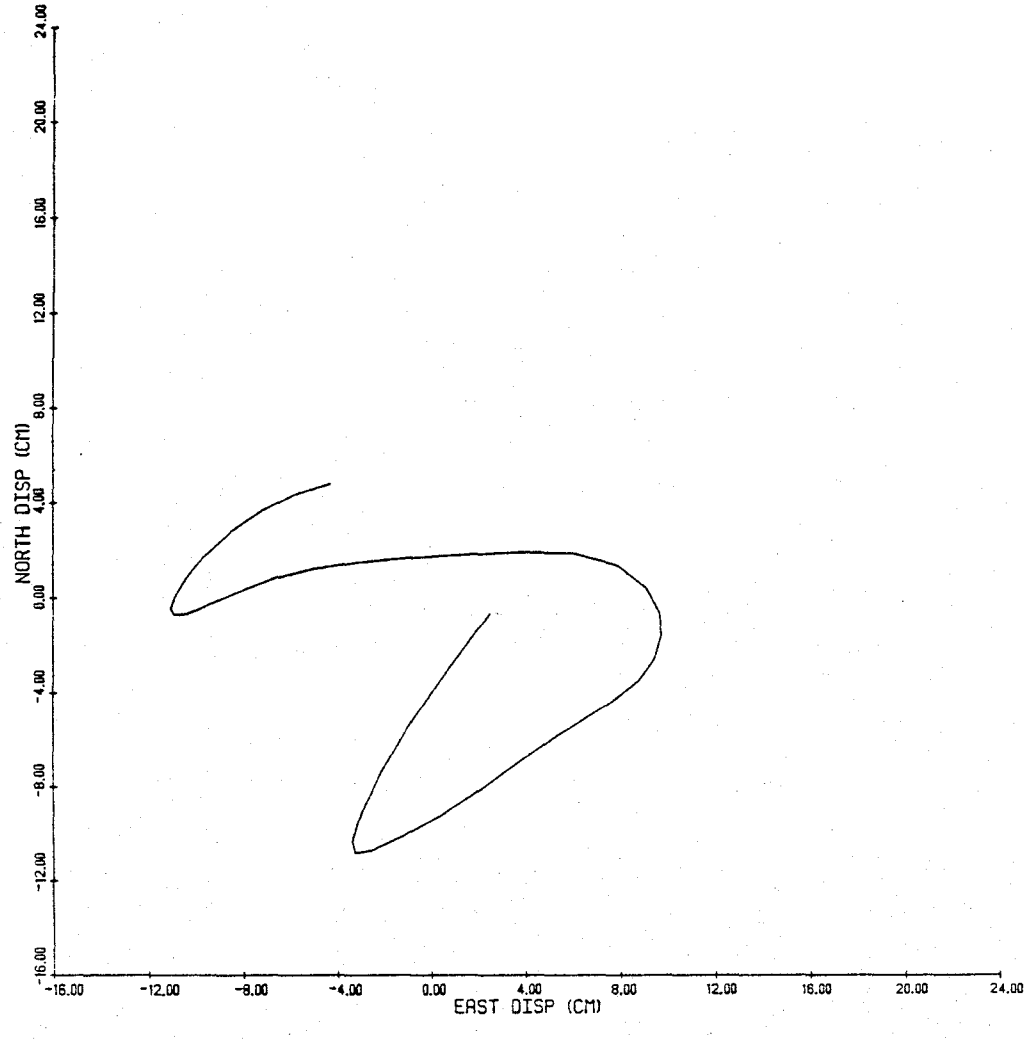

Figure 47 - Ground displacement between 18.5 and 22.5 seconds, north-east plane, 8244 Orion Boulevard (C048)

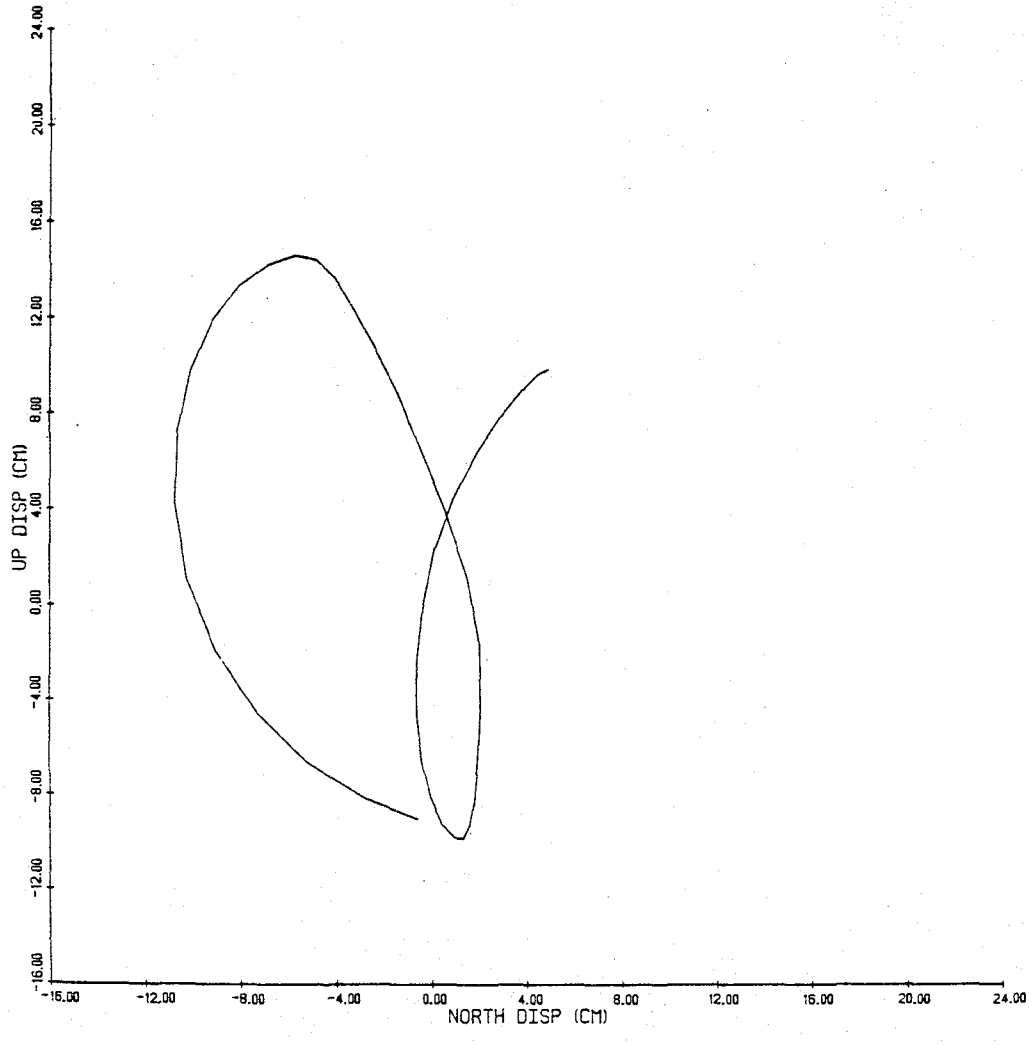

Figure 48 - Ground displacement between 18.5 and 22.5 seconds, up-north plane, 8244 Orion Boulevard (C048)

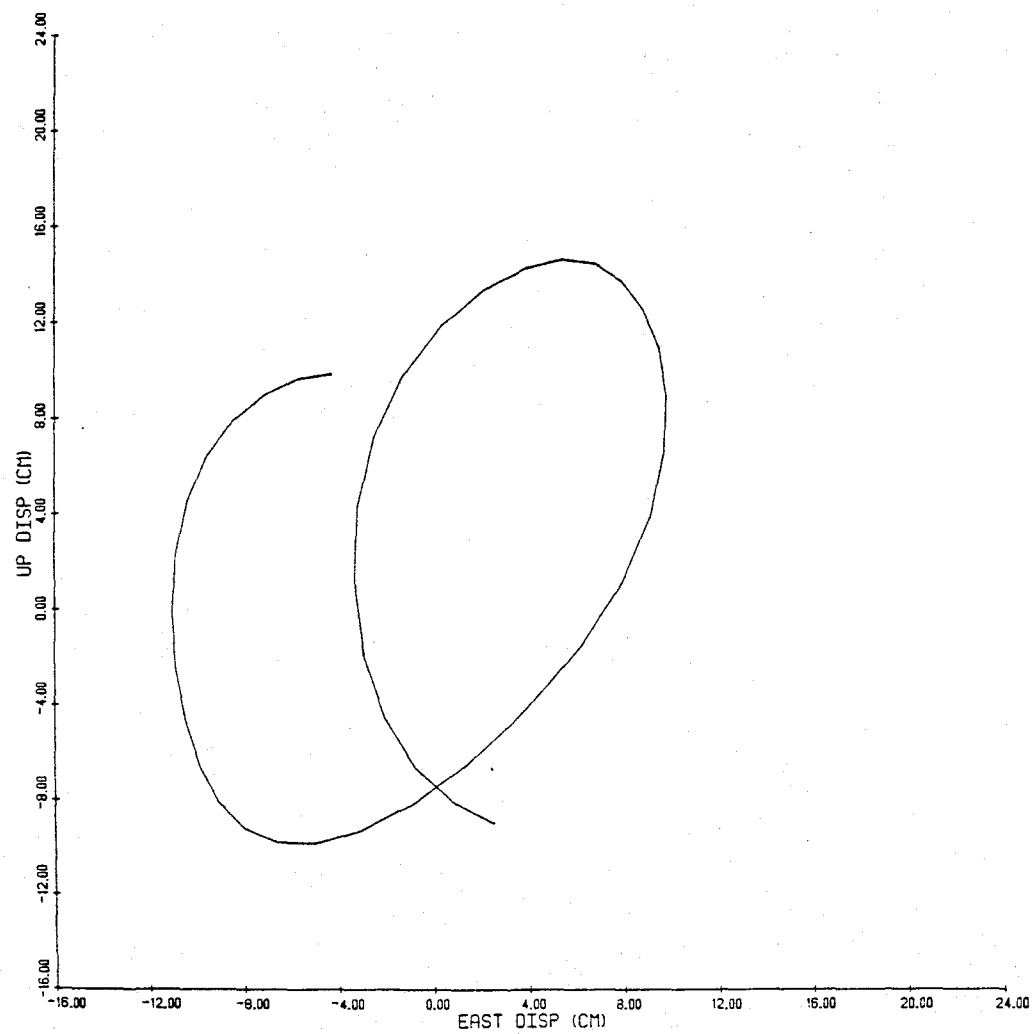

Figure 49 - Ground displacement between 18.5 and 22.5 seconds, up-east plane, 8244 Orion Boulevard (C048)

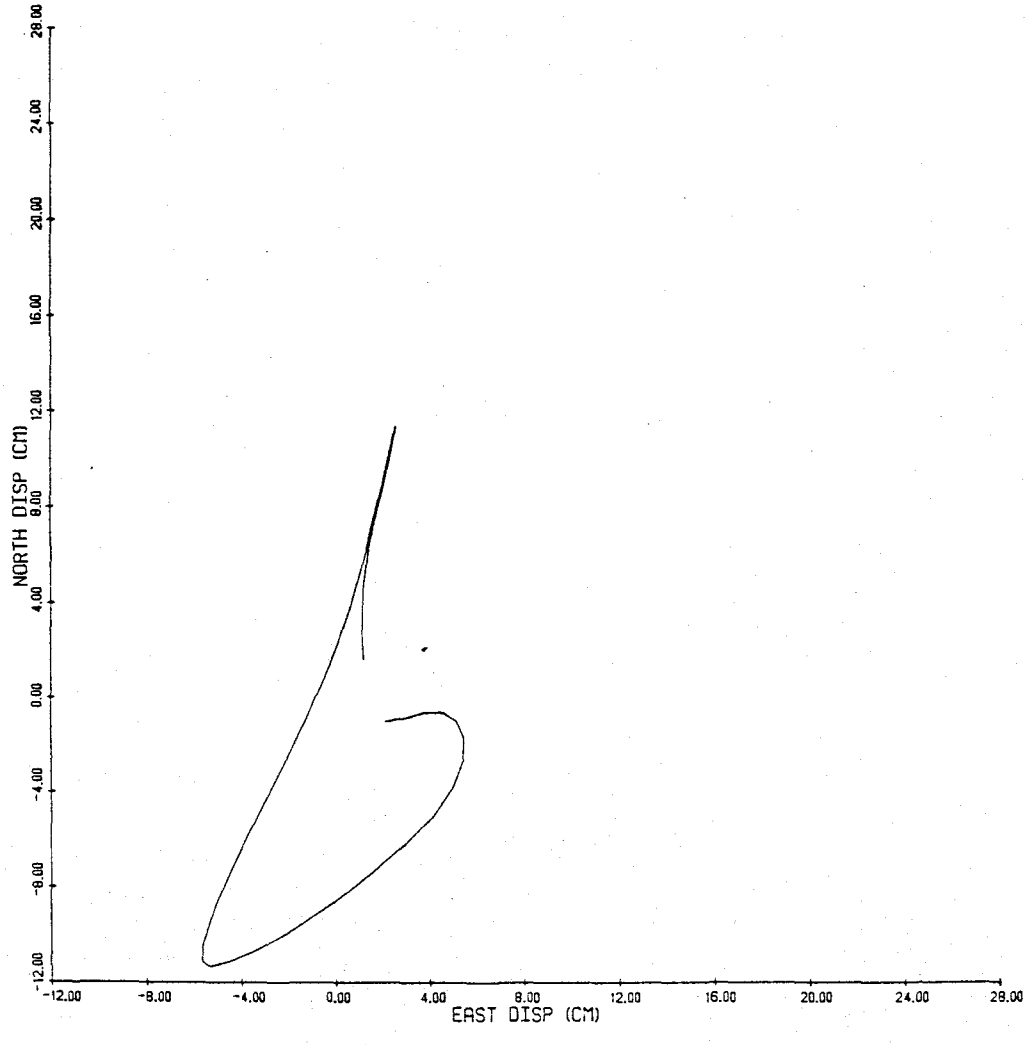

Figure 50 - Ground displacement between 23.0 and 27.0 seconds, north-east plane, 15107 Vanowen Street (J145)

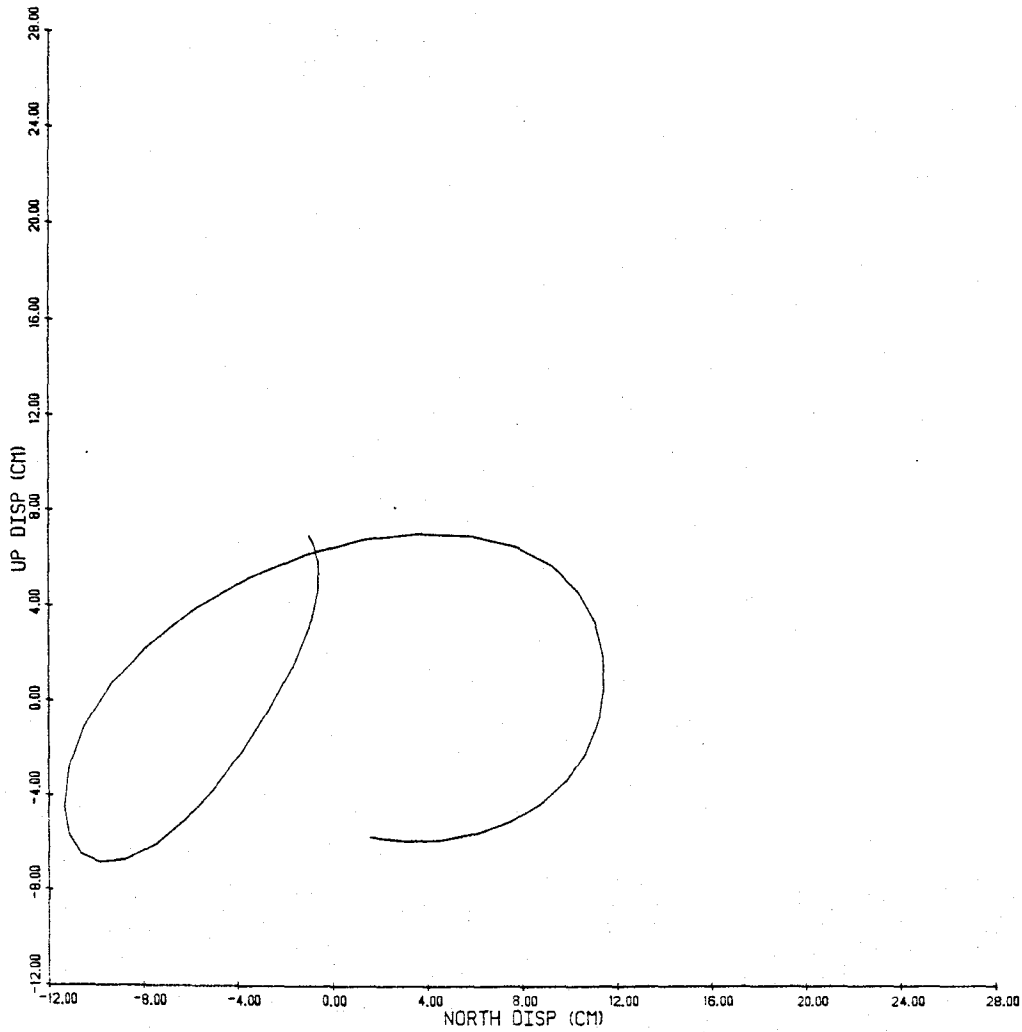

Figure 51 - Ground displacement between 23.0 and 27.0 seconds, up-north plane, 15107 Vanowen Street (J145)

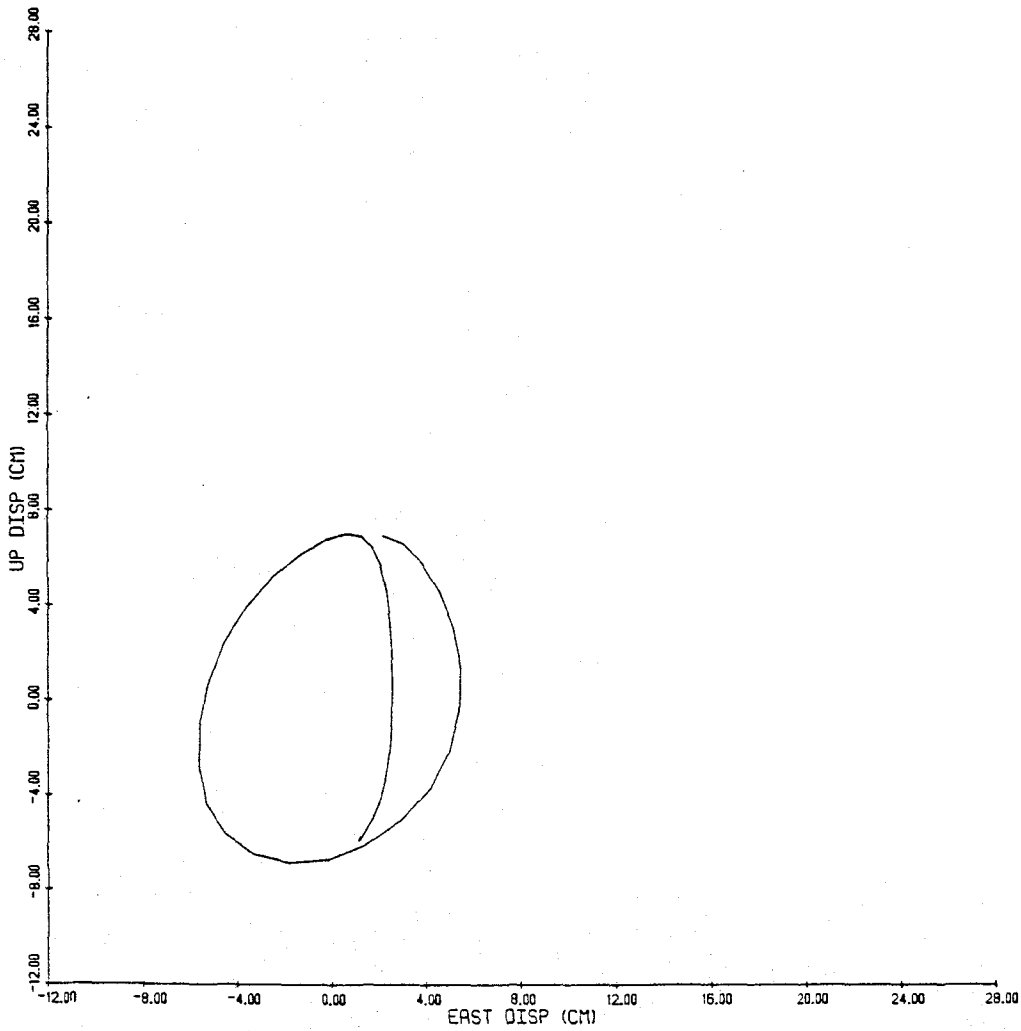

Figure 52 - Ground displacement between 23.0 and 27.0 seconds, up-east plane, 15107 Vanowen Street (J145)

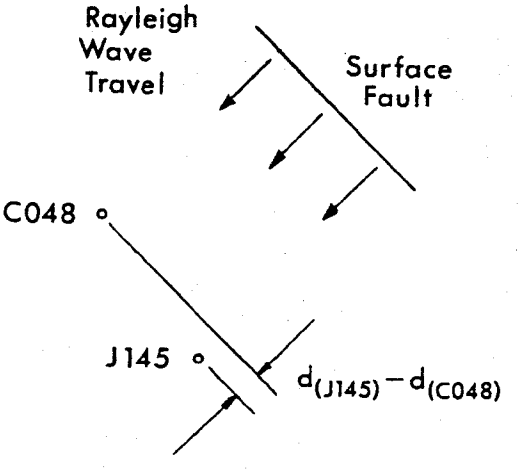

Figure 53 - San Fernando Rayleigh Wave Model

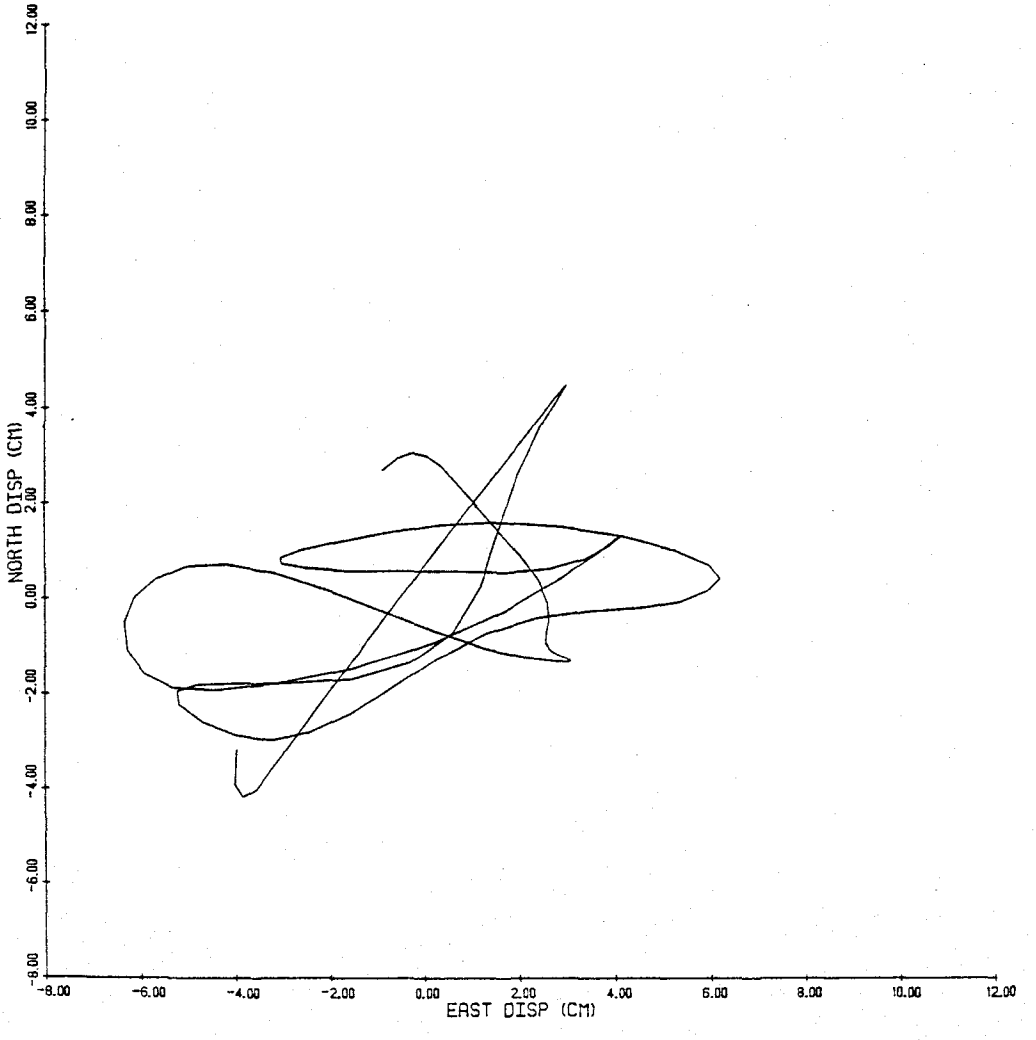

Figure 54 - Ground displacement between 20.0 and 30.0 seconds, north-east plane, 15910 Ventura Boulevard (I137)

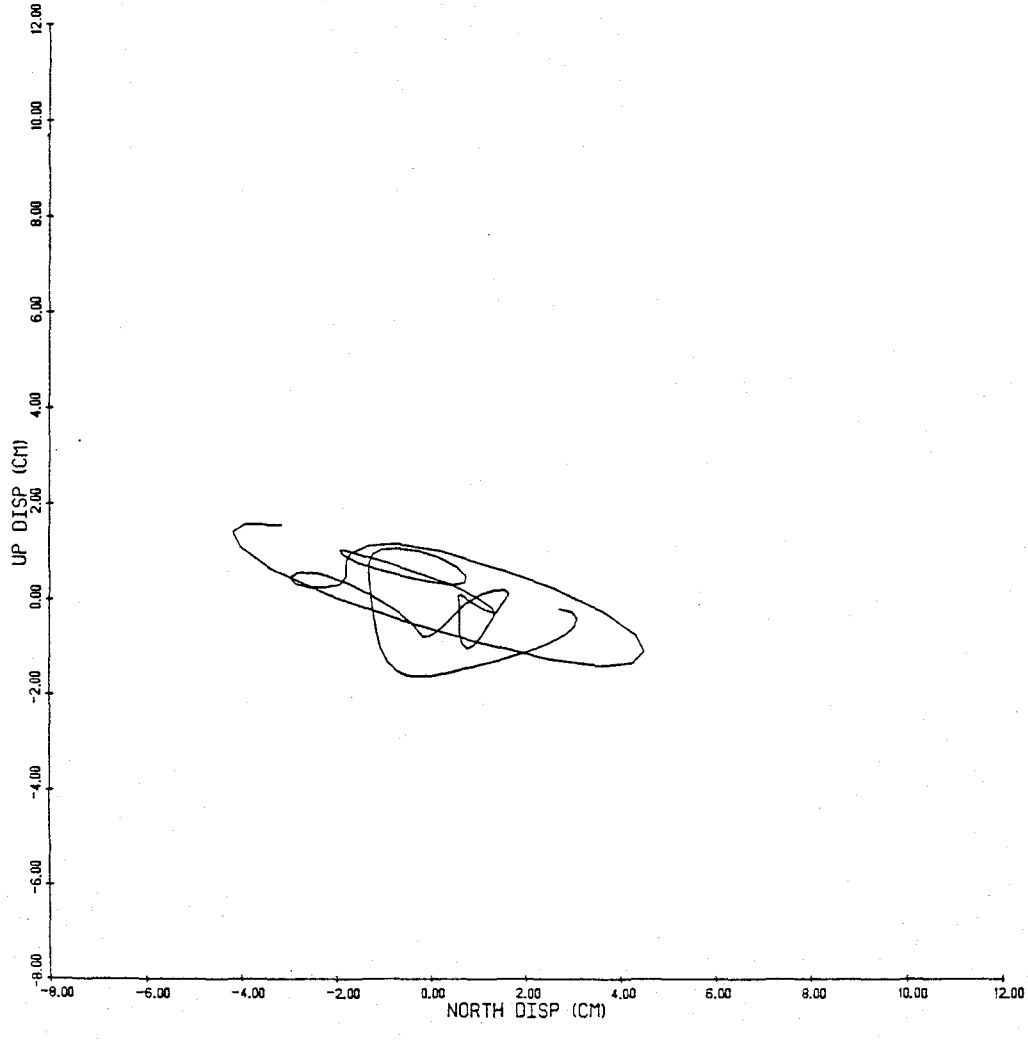

Figure 55 - Ground displacement between 20.0 and 30.0 seconds, up-north plane, 15910 Ventura Boulevard (I137)

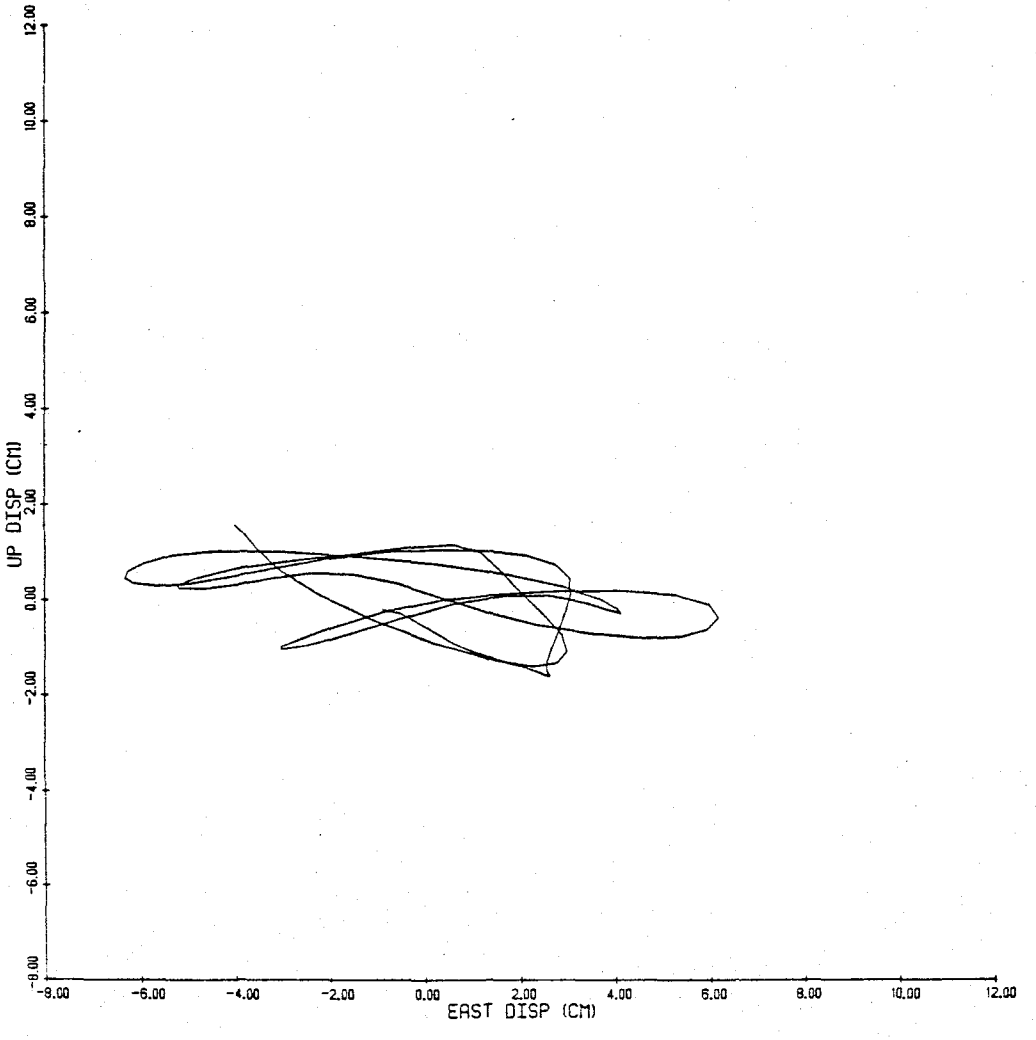

Figure 56 - Ground displacement between 20.0 and 30.0 seconds, up-east plane, 15910 Ventura Boulevard (I137)

APPENDIX 1 - COMPUTER PROGRAM DESCRIPTION

The program written to accomplish the time domain techniques has the following basic functions:

1) Read data - Caltech accelerogram data is read making it available for processing. Optionally the user may have such information as distance and direction from epicenter to the station, total record duration, Arias Intensity, peak acceleration, velocity, and displacement and their times of occurance for each component printed.

2) Display data - Causes the accelerogram data to be processed. Both graphical and numerical results are produced. The options available are described below:

- a) Husid plot
  - 1) x acceleration
  - 2) y acceleration
  - 3) z acceleration
  - 4) horizontal plane acceleration
- b) Moving time window rms acceleration
  - 1) x acceleration
  - 2) y acceleration
  - 3) z acceleration
  - 4) horizontal plane acceleration
- c) Principal planes of ground motion
  - 1) phi maximum plane
  - 2) theta maximum plane
  - 3) phi minimum plane
  - 4) theta minimum plane
- d) Response envelope
  - 1) x acceleration
  - 2) y acceleration
  - 3) z acceleration
- e) Acceleration
  - 1) x acceleration
  - 2) y acceleration
  - 3) z acceleration

The first component read is assigned to be x while the second is y. The third or vertical component is z. The plane formed by x and y is the horizontal plane.

3) Processing length - Defines what length of the record is to be considered.

4) Time window calculations - Determines the duration, rms acceleration, peak acceleration and its time of occurance, average phi and theta of the maximum principal plane, and

the equivalent frequency of the individual components and the horizontal plane for a specified portion of the accelerograms.

5) Stop execution - Terminates program execution.

The most significant feature of the program is that all possible results are displayed graphically to facilitate their interpretation.

APPENDIX 2 - ATTENUATION OF RMS ACCELERATION WITH DISTANCE TO THE EPICENTER

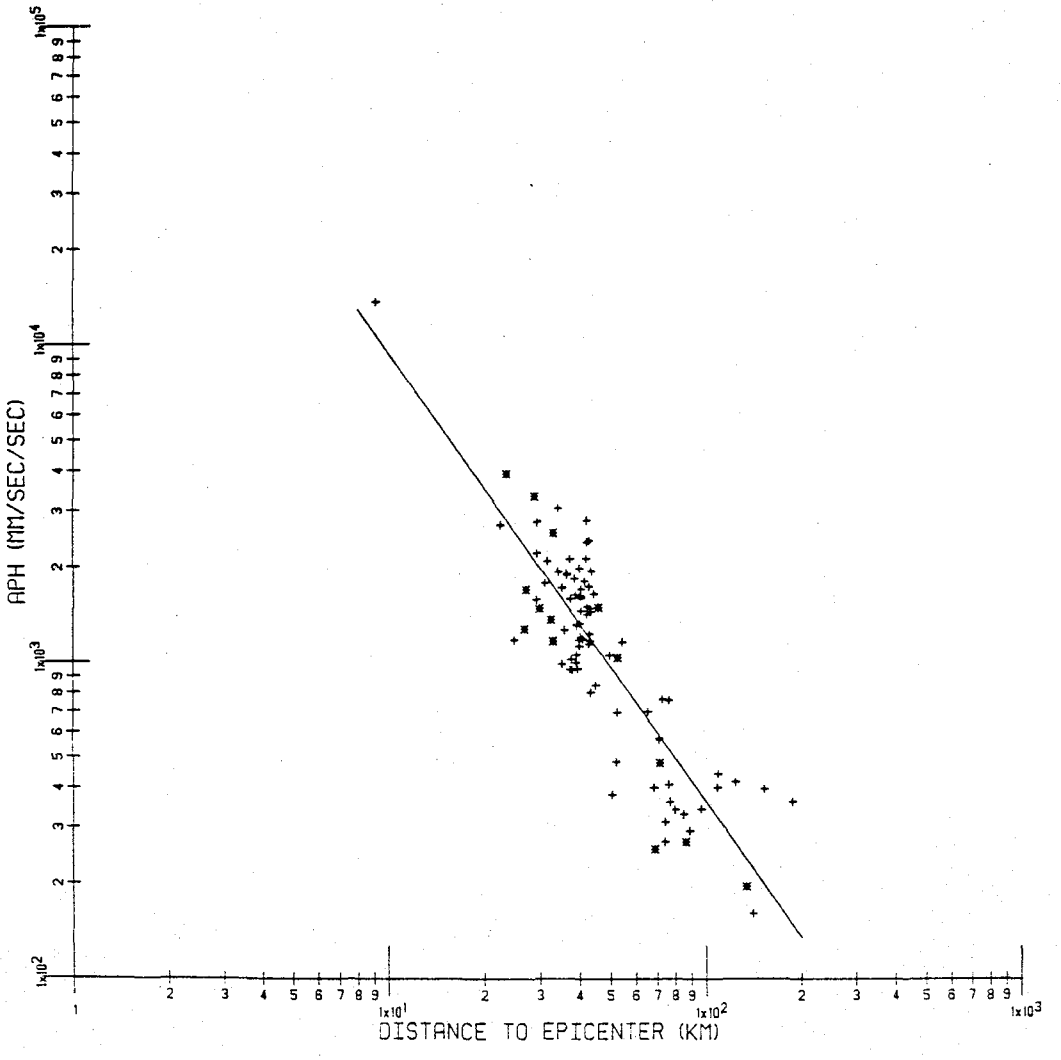

a_{PH} versus distance to the epicenter, San Fernando Earthquake

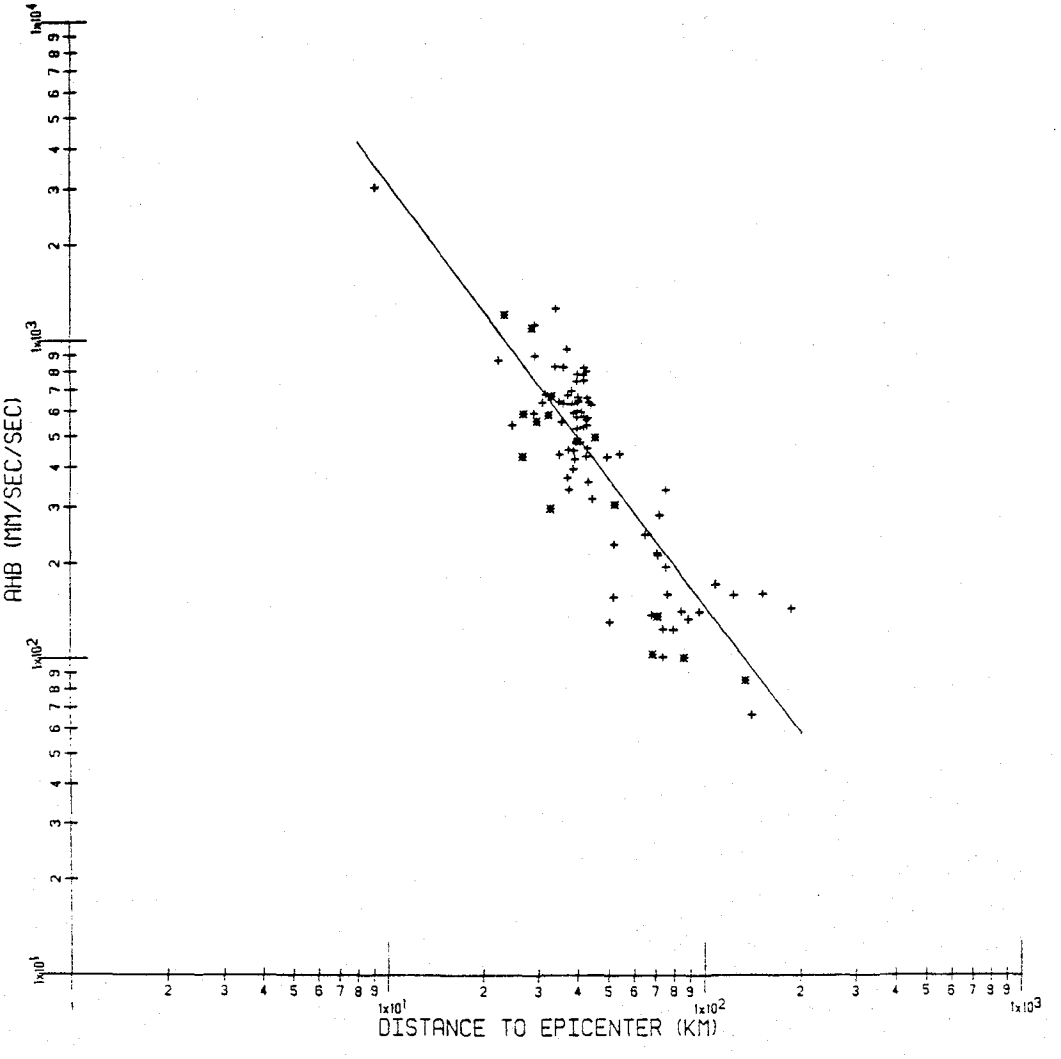

$\bar{a}_{HB}$ versus distance to the epicenter, San Fernando Earthquake

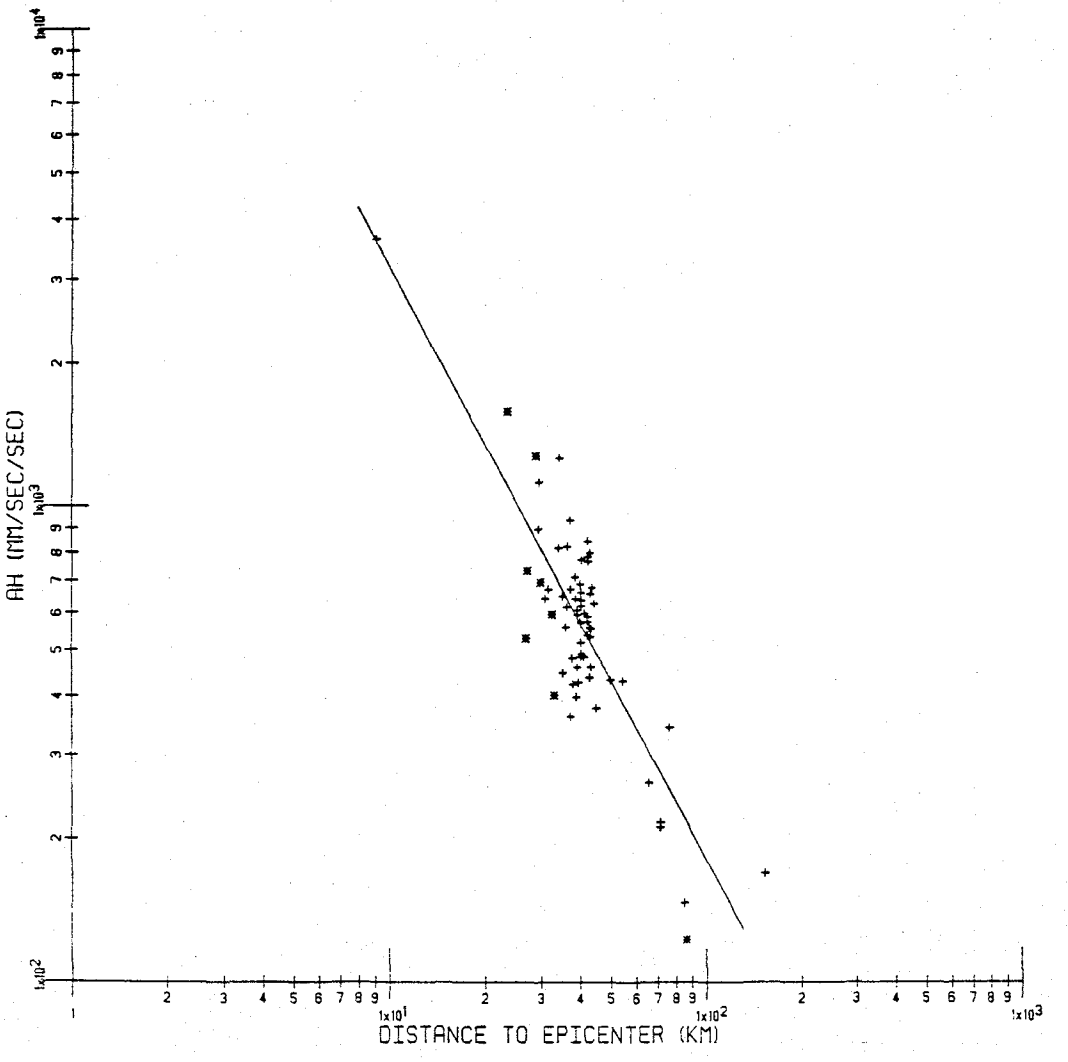

$\bar{a}_H$ versus distance to the epicenter, San Fernando Earthquake

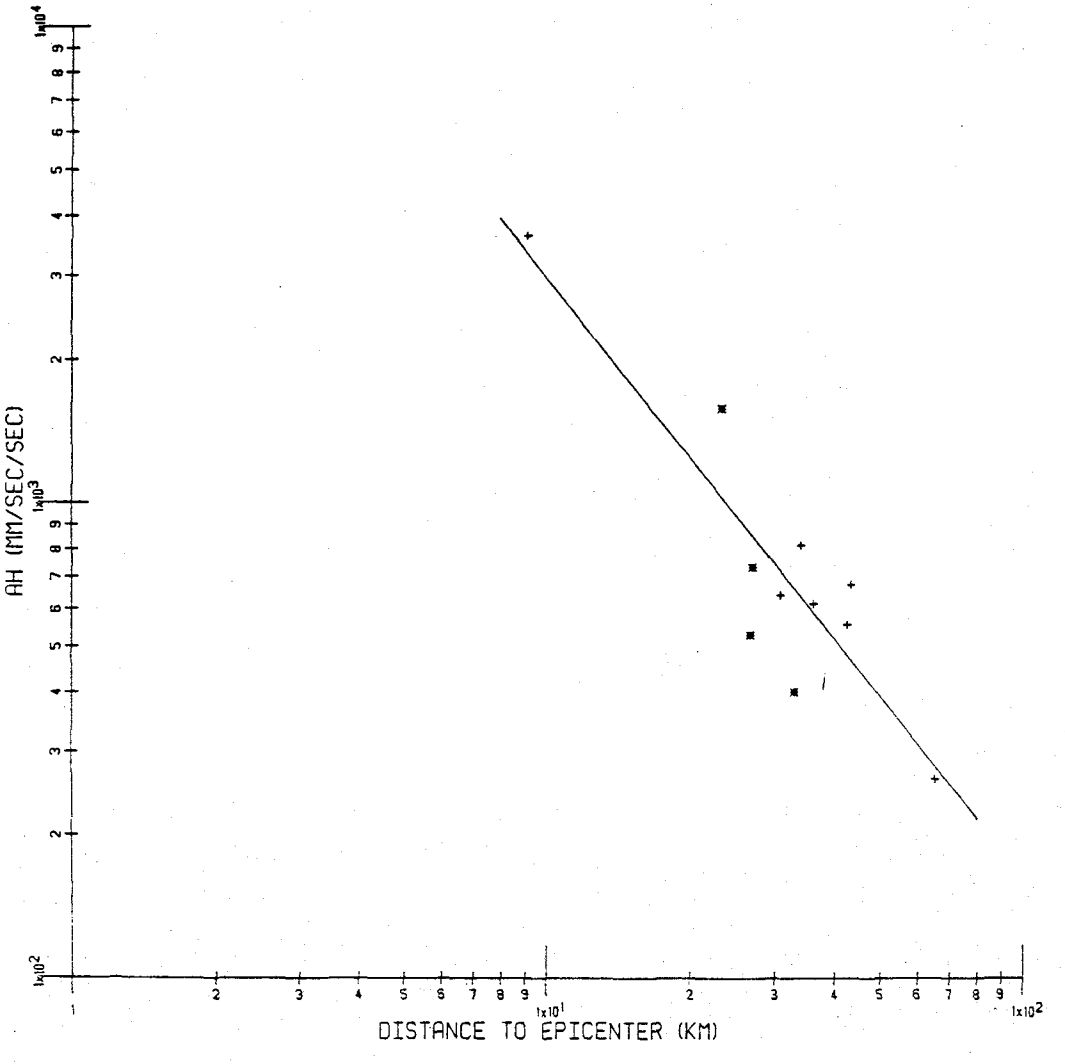

$\overline{a}_H$ versus distance to the epicenter, rock sites, San Fernando Earthquake

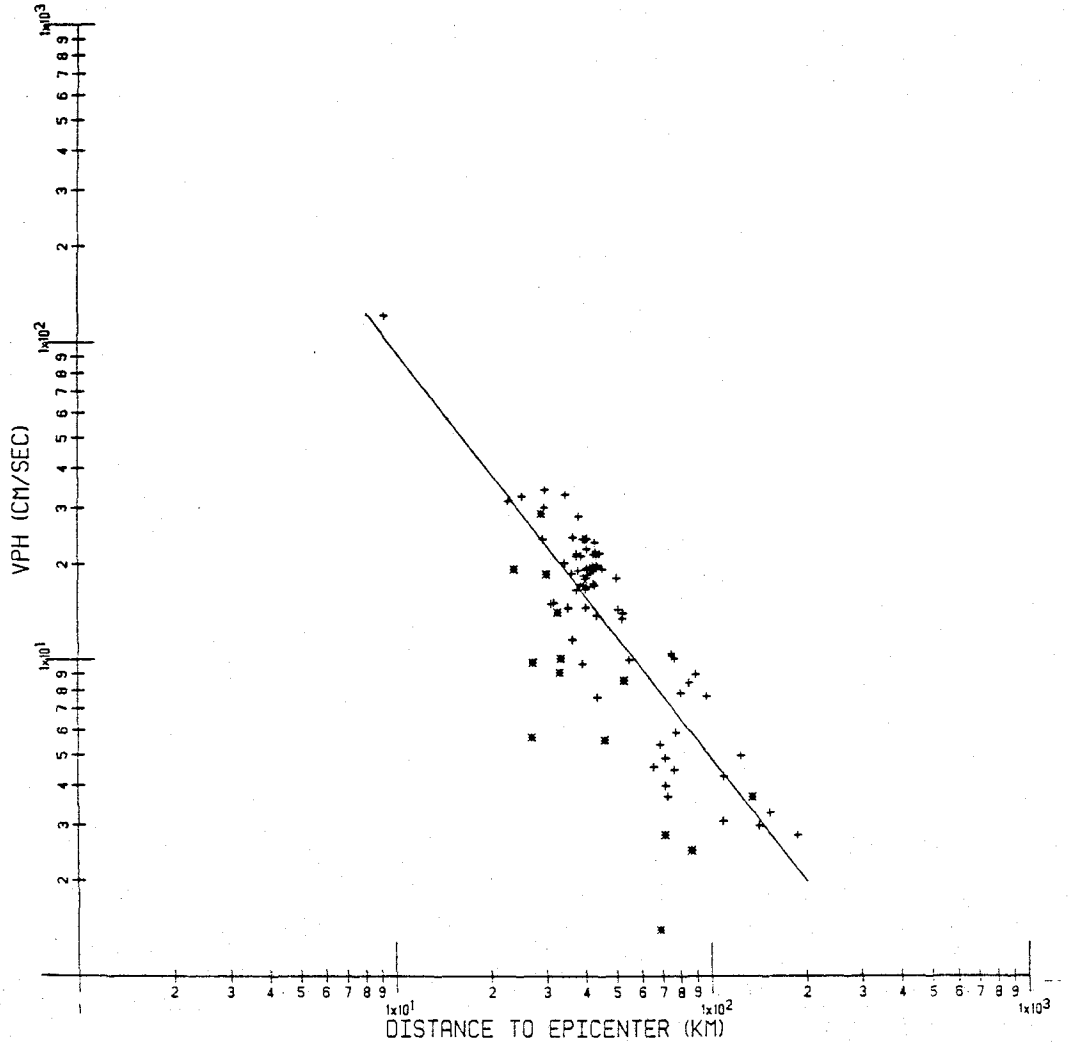

v_{PH} versus distance to the epicenter, San Fernando Earthquake

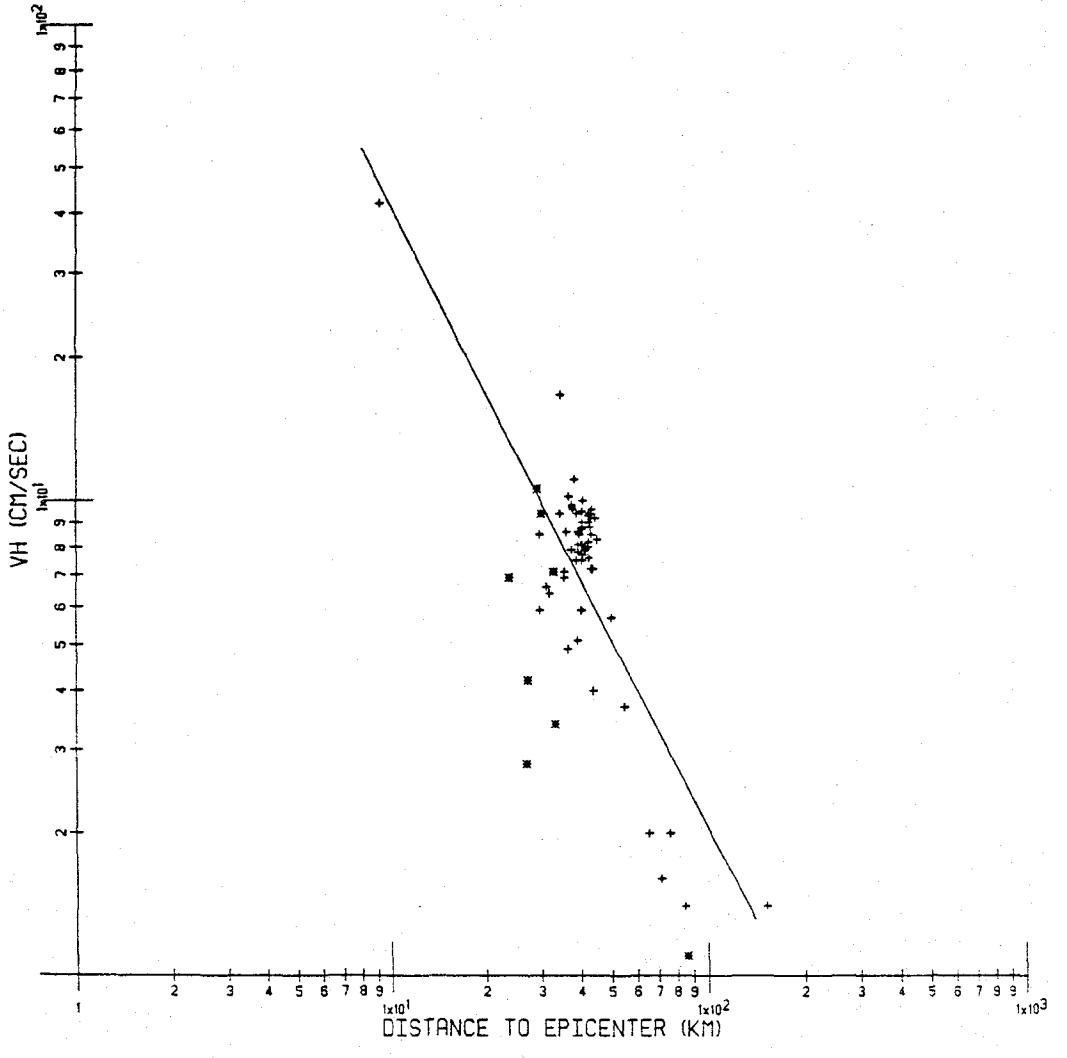

$\overline{v_H}$ versus distance to the epicenter, San Fernando Earthquake